

Distribution agreement

In presenting this thesis or dissertation as a partial fulfillment of the requirements for an advanced degree from Emory University, I hereby grant to Emory University and its agents the non-exclusive license to archive, make accessible, and display my thesis or dissertation in whole or in part in all forms of media, now or hereafter known, including display on the world wide web. I understand that I may select some access restrictions as part of the online submission of this thesis or dissertation. I retain all ownership rights to the copyright of the thesis or dissertation. I also retain the right to use in future works (such as articles or books) all or part of this thesis or dissertation.

Signature:

Allyson E. Koyen

Date

**Elucidating and Targeting EZH2 and HELZ
in the DNA Damage Response in Small Cell Lung
Cancer**

Allyson E. Koyen
Doctor of Philosophy
Graduate Division of Biological and Biomedical
Sciences Cancer Biology

David Yu, M.D., Ph.D., Thesis Advisor

Paul Doetsch, Ph.D., Committee Member

Xingming Deng, Ph.D., Committee Member

Ya Wang, Ph.D., Committee Member

Wei Zhou, Ph.D., Committee Member

Taofeek Owonikoko, M.D., Ph.D., Committee Member

Accepted:

Lisa A. Tedesco, Ph.D.
Dean of the James T. Laney School of Graduate Studies

Date

**Elucidating and Targeting EZH2 and HELZ
in the DNA Damage Response in Small Cell Lung Cancer**

By

Allyson E. Koyen

B.S., Carnegie Mellon University, 2012

Advisor: David S. Yu, M.D., Ph.D.

An Abstract of

A dissertation submitted to the Faculty of the
James T. Laney School of Graduate Studies of Emory University

in Partial fulfillment of the requirements of the degree of

Doctor of Philosophy

in Cancer Biology

2020

Abstract

Small cell lung cancer (SCLC) is a highly aggressive malignancy with poor outcomes associated with resistance to the first line treatment of cisplatin with etoposide (EP). Targeting proteins critical to the repair of EP mediated DNA damage is a promising strategy for overcoming acquired EP resistance in SCLC. In this thesis, we performed synthetic lethal siRNA screens in EP resistant SCLC cells, and identified EZH2 and HELZ as two of the most promising mediators of cisplatin and etoposide resistance, respectively. We show that EZH2 has a non-catalytic and PRC2 independent role in stabilizing DDB2 to promote nucleotide excision repair (NER) and governs cisplatin resistance in SCLC. EZH2 complexes with DDB1-DDB2 and promotes DDB2 stability by impairing its ubiquitination independent of methyltransferase activity or PRC2, thereby facilitating DDB2 localization to cyclobutane pyrimidine dimer (CPD) crosslinks to govern their repair. Furthermore, targeting EZH2 for depletion with DZNep strongly sensitizes SCLC cells and tumors to cisplatin. Our findings reveal a non-catalytic and PRC2-independent function for EZH2 in promoting NER through DDB2 stabilization, suggesting a rationale for targeting EZH2 beyond its catalytic activity for overcoming cisplatin resistance in SCLC. Further, we show that HELZ, a previously uncharacterized putative RNA helicase, is a novel mediator of etoposide and DSB resistance, and that HELZ promotes homologous recombination, genomic instability, and the resolution of DNA-RNA hybrids. HELZ localizes to DSB sites in a PARP1 dependent manner. Depletion of HELZ induces DSB hypersensitivity and impairs proper formation of RAD51 foci in HR. Lower levels of HELZ are associated with better patient outcomes in cancers. Taken together, our data define roles for EZH2 and HELZ in the DDR and implicate them as highly relevant therapeutic targets that have the potential to synergize with EP therapy and impact patient outcome in SCLC.

**Elucidating and Targeting EZH2 and HELZ
in the DNA Damage Response**

By

Allyson E. Koyen

B.S., Carnegie Mellon University, 2012

Advisor: David S. Yu, M.D., Ph.D.

A dissertation submitted to the Faculty of the
James T. Laney School of Graduate Studies of Emory University
in Partial fulfillment of the requirements of the degree of
Doctor of Philosophy
in Cancer Biology

2020

ACKNOWLEDGEMENTS

There are many people who made this dissertation possible. I want to take the opportunity to thank them:

Thank you to my advisor Dr. David Yu for letting me be a part of your lab, for your time, energy, patience and example as I waded through the sea of endless failures and occasional successes. Thank you for letting me be creative and listening to my ideas but also challenging me to be a more meticulous scientist, and for supporting and encouraging our team, which gave me the confidence to strive for things far greater than I thought I was capable of.

Thank you to my teammates in the Yu lab--it has been a huge motivation to work alongside so many intelligent and driven people during my tenure. Thank you for being there to answer my many questions and help me think about science in new ways. It has been my privilege to have you as my teammates and many of you have played essential roles in shaping me into the scientist I am today.

To my thesis committee, thank you for taking the time and energy out of your busy schedules to help me improve my dissertation work. Thank you to the Cancer Biology program and GDBBS. I am proud to call myself a member of this outstanding community.

To my family, and especially to my parents, thank you for not only supporting but encouraging my decision to pursue a Ph.D. in cancer biology, and for being there for me every single day of the process, from providing a listening ear over the phone, sending a care package my way, or making an impromptu weekend trip possible so we could walk the beach together in the Florida sunshine.

Thank you to my friends who helped me get away from the lab to make fun memories and to help me remember that there is more to life than work.

Thank you most of all to my husband Jason. Coming home to you, Simba, and the bliss of our life in Inman Park (and now onto our next adventure in the Bay area) has helped me find the resilience necessary to complete this degree. Thank you for being the most supportive partner I could have asked for, especially all those tough times when you encouraged me to go back to the lab on all those evenings and weekends and making me coffees for the road. I love you.

TABLE OF CONTENTS

Chapter 1: Introduction	1
1.1: Small Cell Lung Cancer	1
Figure 1.1: Inherent and Acquired Resistance	5
Figure 1.2: Synthetic Lethality	8
1.2: The DNA Damage Response	12
1.3: Nucleotide Excision Repair	14
Figure 1.3: NER Pathway Overview	19
1.4: Double Strand Break Repair	20
1.5: Homologous Recombination	21
Figure 1.4: HR Pathway Overview	23
1.6: Genomic Instability	24
1.7: EZH2	25
Figure 1.5: Domain Map of EZH2	27
Figure 1.6: Overview of EZH2 Functions	29
1.8: EZH2 in Cancer	30
1.9: EZH2 in the DDR	31
1.10: RNA Helicases	31
1.11: RNA Helicases in the DDR	32
1.12: HELZ	33
Figure 1.7: Domains and Motifs of HELZ	35
1.13: Scope of Dissertation	36
Chapter 2: EZH2 has a Non-Catalytic and PRC2 Independent Role in Stabilizing DDB2 to Promote Nucleotide Excision Repair	37
2.1 Author Contributions and Reproducibility Statement	37
2.2 Abstract	39
2.3 Introduction	40
2.4 Materials and Methods	42

2.5 Results	56
2.6 Discussion	95
2.7 Acknowledgements	99
2.8 Funding.....	100
2.9 Conflict of Interest	100
Chapter 3: RNA Helicase HELZ Promotes Homologous Recombination Repair to Maintain Genomic Stability	101
3.1 Author Contributions.....	101
3.2 Abstract	102
3.3 Introduction	103
3.4 Materials and Methods	105
3.5 Results	115
3.6 Discussion	141
3.7 Acknowledgements	145
3.8 Funding.....	145
3.9 Conflict of Interest	145
Chapter 4: Discussion	146
4.1 Summary of Key Results and Remaining Questions	146
4.2 The Utility of Phenotypic Screens	149
4.3 Non-Catalytic Functions of Enzymes in the DDR	152
4.4 Linking RNA Processing to the DDR	154
4.5 Translational Applications	155
References	159

LIST OF FIGURES

Chapter 1: Introduction	1
Figure 1.1. Inherent and Acquired Resistance	5
Figure 1.2. Synthetic Lethality.....	8
Figure 1.3. The Nucleotide Excision Repair Pathway	19
Figure 1.4. The Homologous Recombination Repair Pathway	23
Figure 1.5. Domain Map of EZH2.....	27
Figure 1.6. Overview of EZH2 Functions	29
Figure 1.7. Domains and Motifs of HELZ	35
Chapter 2: EZH2 has a Non-Catalytic and PRC2 Independent Role in Stabilizing DDB2 to Promote Nucleotide Excision Repair	37
Figure 2.1. A siRNA Screen Targeting Nuclear Enzymes Identifies Genes that mediate Cisplatin Resistance in SCLC.....	58
Figure 2.2. Bioinformatic Analysis of Cisplatin Sensitization Hits	60
Figure 2.3. EZH2 Mediates Cisplatin Resistance in SCLC	64
Figure 2.4. EZH2 Mediates Cisplatin Resistance and is Overexpressed in SCLC	66
Figure 2.5. EZH2 Localizes to and Promotes Repair of UV-Induced CPD Lesions.....	69
Figure 2.6. EZH2 Localizes to and Promotes Repair of UV-Induced CPD Lesions, 2	71
Figure 2.7. EZH2 Interacts with and is Epistatic with DDB1-DDB2 in Sensitizing SCLC cells to Cisplatin and UV	75
Figure 2.8. EZH2 Interacts with and is Epistatic with DDB1-DDB2 in Sensitizing SCLC cells to Cisplatin and UV, 2	77
Figure 2.9. EZH2 Promotes the Stability of DDB2 Independent of its Catalytic Activity and PRC2	82
Figure 2.10. EZH2 Promotes the Stability of DDB2 Independent of its Catalytic Activity and PRC2, 2	85
Figure 2.11. DDB2 Functions Downstream of EZH2 in NER and in Mediating Cisplatin Resistance in SCLC	88
Figure 2.12. EZH2 Depletion with DZNep Sensitizes SCLC to Cisplatin <i>in vitro</i> and <i>in vivo</i> and a Model for EZH2 in NER.....	92
Figure 2.13. EZH2 Depletion with DZNep Sensitizes SCLC to Cisplatin <i>in vitro</i>	94

Chapter 3: RNA Helicase HELZ Promotes Homologous Recombination Repair to Maintain Genomic Stability	101
Figure 3.1. A siRNA Screen Targeting Nuclear Enzymes Identifies Genes that mediate Etoposide Resistance in SCLC	118
Figure 3.2. Bioinformatic Analysis of Etoposide Sensitization Hits	120
Figure 3.3. HELZ mediates DSB resistance in Cancer.....	122
Figure 3.4. HELZ localizes to and promotes repair of DNA DSBs through the HR pathway ..	126
Figure 3.5. HELZ localizes to and promotes repair of DNA DSBs	128
Figure 3.6. HELZ promotes Genomic Stability.....	131
Figure 3.7. HELZ promotes Genomic Stability, 2.....	133
Figure 3.8. HELZ interacts with HR proteins PRP19 and DDX1 and promotes DNA-RNA hybrid resolution	136
Figure 3.9. High HELZ Expression is associated with poor outcome in cancers and model for HELZ in HR	139

Chapter 1: Introduction

1.1 Small Cell Lung Cancer

Small cell lung cancer, also known as oat cell lung cancer, is a subtype of lung cancer, representing approximately 15 percent of all lung cancer cases. [1]. SCLC can occur throughout the lung, including in the central, bronchial and hilar regions, and rarely in a peripheral nodule. It can also occur as a submucosal growth. SCLC is characterized by its unique pathology, with cells that are round to spindle in shape, and smaller in size relative to other cancer cells, with a scant cytoplasm, a high rate of proliferation, with an average mitotic rate of 80 mitoses per mm^2 , and with a tendency to be accompanied by the presence of necrosis [2]. When confirming its diagnosis using immunohistochemistry, SCLC will stain positive for the neuroendocrine markers synaptophysin, chromogranin A, CD56, thyroid transcription factor 1 and MIB-1 [2]. A leading cause of SCLC is through mutations that occur progressively over time when lung tissue is exposed to cigarette smoke, a highly mutagenic carcinogen. The disease rarely presents in nonsmokers. Indeed, the incidence of SCLC has been declining in the U.S. over the past two decades, likely due to the decrease in smoking. Exposure to second hand smoke, radon, asbestos, and other carcinogenic air pollutants can also lead to SCLC [3].

In terms of its molecular features, SCLC possesses many of the classical characteristics of cancers, including gain of function mutations or amplifications in oncogenes and proto oncogenes, loss of function of tumor suppressors, and alteration in the expression of

caretaker genes. In detail, SCLC exhibits a high mutational load [4]. Perhaps the most distinctive feature is the biallelic inactivation of the tumor suppressor genes *TP53* and *RB* [5]. To a lesser extent, mutations are also common in the tumor suppressors *CREBBP*, *PTEN*, *EP300* and oncogene *PIK3CA* [4, 6-8]. Amplification is often found in oncogenic transcription factors including *MYC* family members, as well as *SOX2*, and the growth factor receptor *FGFR1* [4, 7, 8]. Indeed, one analysis found amplifications in *SOX2* in 27% and *RLF-MYCL1* fusion in 9% of samples examined [6]. Yet another found amplification in the mTOR pathway member *RICTOR* in 10% of cases analyzed [8]. Genomic rearrangements have identified at the *TP73* locus, a *TP53* homolog, resulting in the generation of the oncogenic variant *TP73Δex2/3* [5]. Inactivating mutations in the tumor suppressive *NOTCH* family are also common, as one comprehensive study found these in about 25 percent of cases in their analysis. [5]. Hotspot mutations commonly occur in oncogenes *KRAS* and *EGFR* [4, 6, 7, 9]. One study uniquely comparing differences between SCLC to NSCLC found the transcriptional silencer *EZH2* and DNA repair gene *PARP1* to be aberrantly expressed in SCLC [10]. On a cellular level, SCLC is thought to be of neuroendocrine origin, however, the cell of origin in patients has not been fully elucidated. Studies in mouse models have suggested that neuroendocrine cells and/or their stem-like precursors are indeed the cells of origin for SCLC [11].

Small cell lung cancer is well characterized as a highly aggressive malignancy. 70 percent of patients that first present in the clinic already have metastatic disease [12]. Common sites of metastasis include the liver, adrenal glands, bones, bone marrow, and brain, as well as regional metastasis to other areas of the lung and neighboring lymph node. It is not

uncommon for SCLC to progress in a widespread fashion. Only a minority of patients who present with disease that has not progressed are fortunate to have their disease managed with surgical resection of the primary tumor, local radiation, and periodic chemotherapy. Those with advanced SCLC will rapidly succumb to their disease. Indeed, the five year survival rate is quite poor, at <7% with a median survival of 24 months [1]. This is attributed to the fact that (1) metastatic disease is difficult to treat, and (2) SCLC quickly becomes resistant to the available therapeutic regimen.

Treatment for small cell lung cancer consists primarily of a combination of chemotherapy, a platinum agent (cisplatin or its less cytotoxic analog, carboplatin) and etoposide (EP). In Japanese patients, irinotecan is used in the place of etoposide, as the patients respond better [13]. Although EP is initially effective, with response rates close to 70%, the response is transient, as the majority of patients eventually develop resistance to EP and succumb to the disease [2]. Unfortunately, treatment options for advanced SCLC are limited. There have been very few developments in this area since the 1980s. The FDA-approved second line treatment is topotecan, a highly toxic topoisomerase inhibitor with substantial side effects and transient responses occurring in only 25% of patients [14]. The FDA has very recently approved immunotherapy for advanced SCLC in the form of monoclonal antibodies targeting the PD1/PDL1 checkpoint. [15]. Though this form of immunotherapy has had an impact on patient outcomes, success has been marginal. Incorporation of atezolizumab into the first line regimen has resulted in a slight increase in median survival of advanced patients from 10.3 to 12.3 months [15]. With respect to other drug classes, there are currently no other FDA approved targeted therapies for small cell lung cancer.

There are a number of proposed therapeutic targets and drugs under clinical investigation for SCLC. These include the RNA polymerase II inhibitor lurbinectedin and the multi-tyrosine kinase inhibitor anlotinib [16]. Many targeted therapies have already been tested and failed to be impactful, including inhibitors targeting tyrosine kinases (EGFR, c-KIT, IGFR), the NOTCH pathway (DLL3), angiogenesis (VEGF, MMPs, RET), apoptosis promoters (BCL family), the PI3K/AKT/mTOR pathway and immune checkpoint inhibitors (CTLA-4) [9, 17]. The transcription factors associated with SCLC, such as myc family members and sox, are difficult to target due to the lack of binding pockets on transcription factors [18]. Increased efforts are being made to further characterize SCLC into subtypes based on a common molecular signature to help better define appropriate targets and direct treatment plans [19]. However, many of these failed and newly proposed strategies do not take into account why the first-line therapeutic regimen of EP is initially so effective, or how resistance develops on a molecular level. As such, this biology must be studied and leveraged to design more effective therapeutic regimens.

Functionally, etoposide and platinum promote cytotoxicity by damaging cellular DNA. High levels of DNA damage can either impair cell proliferation, promoting apoptosis, or, when left unrepaired, lead to mutagenesis, strand breaks, and genomic instability that make actively proliferating cancers increasingly difficult to treat (Fig. 1.1).

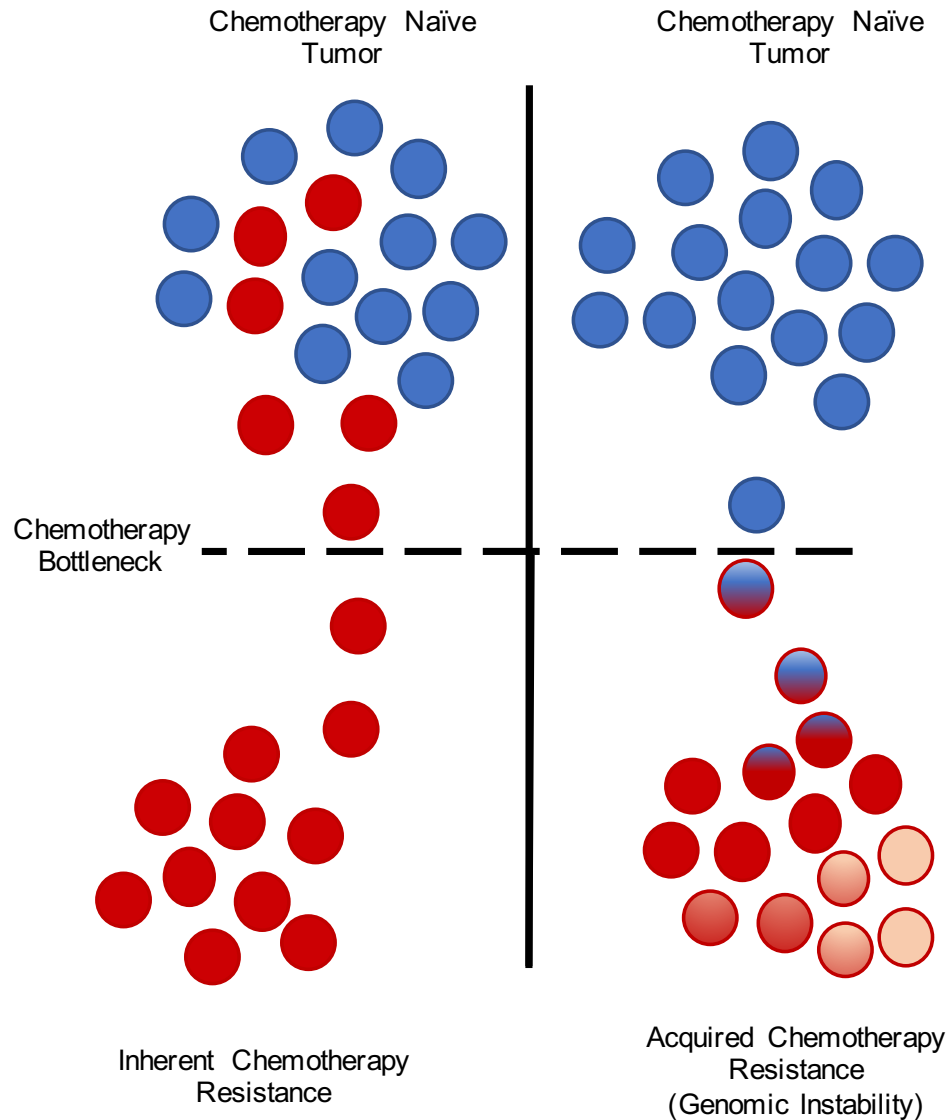


Fig. 1.1. Model of Inherent and Acquired Chemotherapy Resistance that occurs in Cancer. Adapted from McClelland et al. *Endocrine Related Cancer* (2017) [20]. Chemotherapy resistance is hypothesized to fall in to two categories: inherent or acquired. Tumors are composed of cells that are molecularly heterogeneous. Inherently resistant tumors possess subpopulations of cells inherently capable of resisting chemotherapy treatment. Such tumors will respond, where the majority of the cells are sensitive to the chemotherapy, and thus die off, shrinking the tumor. However, the chemotherapy resistant

cells will survive and provide a foundation for tumor recurrence, which has been selected by the chemotherapy treatment, providing a bottleneck that is selecting for chemotherapy resistant cells. Thus, recurrent tumors are usually more resistant to further rounds of chemotherapy. This bottleneck becomes more complicated during the treatment of tumors with genomic instability. Unrepaired damage via chemotherapy can induce genomic instability, where the tumor has a chance to develop chemotherapy resistant colonies through acquired mutations and chromosomal aberrations. This is known as acquired resistance. On top of this, once a genome becomes unstable, a tumor can continue to acquire mutations favorable to its survival, making the cancer increasingly difficult to treat.

How cancers respond to DNA damage plays an important role in determining if they will be sensitive to chemotherapy. It is speculated that the aberrant activation of the DNA damage response pathways can promote resistance to cisplatin and etoposide. To this end, one approach that may hold promise for SCLC treatment is targeting genes that are synthetically lethal with EP. Synthetic lethality describes the process where deficiencies in the expression of two genes together (or the deficiencies generated by drugs, such as EP), lead to cell death, and where deficiencies in only one of these genes or the drug treatment alone do not (Fig. 1.2). Thus, genes that are synthetically lethal with EP likely play roles in the DDR.

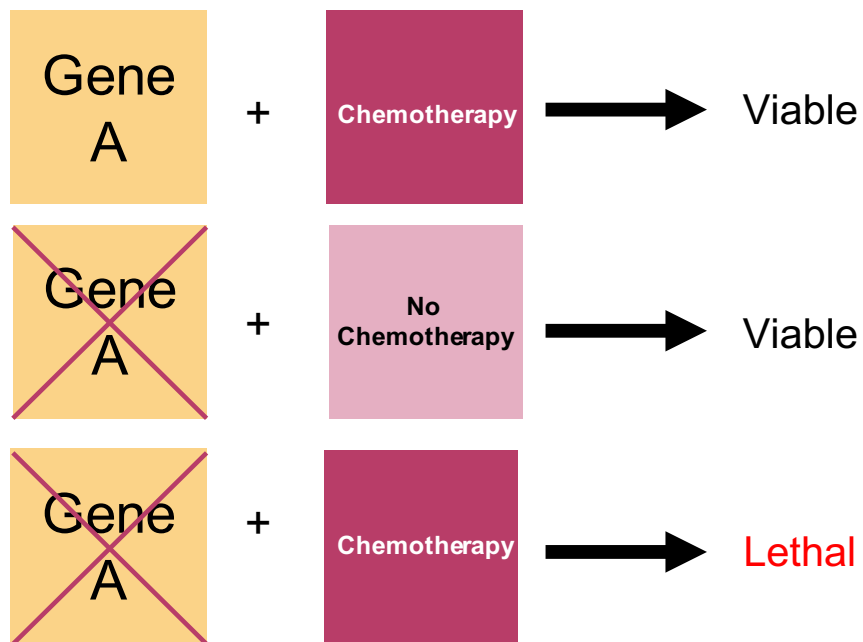


Fig. 1.2. Model of Synthetic Lethality.

Synthetic lethality describes cellular cytotoxicity or organismal death that occurs when two genes are deficient in expression at the same time, but not when either gene is deficient alone. Synthetic lethality can also be studied in the context of drugs. In this thesis, we utilized synthetic lethality as a model to understand interactions occurring between genes and EP chemotherapy. EP treatment alone is not capable of inducing cytotoxicity in resistant SCLC. Gene A, which is hypothetically responsible for mediating EP resistance in SCLC will not induce cytotoxicity on its own when depleted. It is only in the specific

context, when Gene A is depleted and EP chemotherapy is applied, that synthetic lethality occurs. Thus, synthetic lethality can be used to screen through a library of genes with potential interactions with EP. If synthetic lethality is achieved, the gene of interest is likely involved in a pathway related to the mediation of chemotherapy resistance. Knowledge of drug-gene synthetic lethal interactions can be used to design therapy combinations to treat cancer.

Platinum based chemotherapy is one of the most effective and widely used treatments for cancer. Functionally, cisplatin generates crosslinks throughout the cell, including its primary target, DNA [21]. These platinum based DNA crosslinks cause helix distortions that interfere with DNA replication and transcription, triggering apoptosis [22]. The primary lesion formed on DNA are intrastrand crosslinks, but other lesions can be formed including monofunctional adducts, protein-DNA crosslinks, and interstrand crosslinks between complimentary strands of DNA, which are most lethal to the cell but occur more rarely (2%) [21, 23]. Repairing cisplatin induced DNA damage primarily involves nucleotide excision repair, which processes intrastrand crosslinks. Cisplatin lesion repair can also involve the fanconi anemia pathway [24], which is responsible for processing interstrand crosslinks; double strand break repair pathways, because interstrand crosslink repair results in the formation of a double strand break; mismatch repair, which is triggered by base mismatches that occur from cisplatin mediated helix distortions, and translesion bypass mechanisms, which ensure replication fork continuity without repair of the actual damage [25]. The mismatch repair pathway can only correct base mismatches on DNA, and cannot resolve the cisplatin crosslinks themselves. The persistence of cisplatin crosslinks causes the hyperactivation of the MMR pathway which can lead to the induction of double strand breaks [25]. Bypass mechanisms enable DNA damage tolerance and include pathways such as translesion synthesis, occurring via the employment of specialized DNA polymerases that lack proofreading activity and are capable of processing modified nucleotides [26], and template switching, which is poorly understood but seemingly dependent on homologous recombination factors [27, 28].

The cellular mechanism of cisplatin resistance is not fully elucidated, but it is known to involve pleiotropic genomic alterations, including but not limited to modifications to DNA damage response pathway, decreased cisplatin uptake and accumulation, through processes that result in aberrant localization of membrane transporters and changes in the endocytosis pathway, and alterations in factors that regulate the cellular detoxification of cisplatin, such as heat shock proteins [29].

Etoposide is one of the most effective and prescribed anticancer drugs in the world. Functionally, it targets type IIA topoisomerase activity. Topoisomerases are enzymes that regulate DNA topological orientation by ensuring proper DNA winding. [30] They are involved in DNA replication, transcription, chromatin remodeling, and DNA repair [31]. During these processes, DNA can become wound too tightly or loosely. Topoisomerases correct these errors by cutting the DNA backbone to allow DNA relaxation, and then they rejoin the broken DNA back together. Type II topoisomerases are ATP dependent enzymes that function to cut both strands of DNA to promote duplex relaxation. Type IIA topoisomerases are an evolutionarily conserved class of topoisomerases that form double strand breaks with a four-base pair overhang [32]. This class includes DNA Gyrase, Topoisomerase IV and Topoisomerase II α and β . Etoposide functions by binding to and stabilizing a transient state in the catalytic cycle of IIA topoisomerases, where the topoisomerase is bound to DNA after it has been cleaved but before it is rejoined. This is known as the cleavage complex [33]. The generation of cleavage complexes in the cell can stall the DNA replication fork and transcriptional machinery. Further, they can result in permanent double permanent strand breaks, which if left unresolved, can lead to apoptosis

mediated cytotoxicity, or if propagated, can lead to mutagenesis, chromosomal breaks and rearrangements and thus, genomic instability.

Underlying mechanisms of etoposide resistance have mostly been attributed to decreases in type II topoisomerases. Overexpression or the presence of a single nucleotide polymorphism (SNP309 (T/G)) in MDM2, a protein that promotes topoisomerase instability, confers resistance to type II topoisomerase inhibitors, including etoposide [1]. A number of mediators of etoposide resistance have been identified in SCLC. One group reported that targeting DNA polymerase β mediated etoposide resistance while overexpressing the neuroendocrine transcription factor NKX2.2 promoted etoposide sensitivity in SCLC [2]. Another group identified that the transcriptional silencing of SLFN11 via EZH2 mediates etoposide resistance in SCLC [3]. SLFN11 functionally impairs checkpoint maintenance and homologous recombination by destabilizing RPA coating of ssDNA, which helps promote sensitivity of cells to DNA damaging agents such as etoposide [4]. SLFN11 could be increasingly silenced due to the aberrant overexpression of EZH2 that occurs in SCLC.

1.2 The DNA Damage Response

The DNA damage response (DDR) describes the biological infrastructure of a number of pathways that together are responsible for maintaining the integrity of the genome so that it can be replicated and passed to a daughter cell in an uncompromised fashion. The DNA

damage response involves three key steps, including the detection, signaling of and repair of DNA damage. When DNA damage is left unrepaired, one of two main outcomes will occur: the triggering of programmed cell death (apoptosis) or, more problematically, the propagation of unrepaired DNA damage that can lead to mutagenesis, double strand breaks and resulting chromosomal rearrangements, genomic instability and cancer. One of the most common DNA damaging agent the human body encounters through the environment is exposure to UV light, which damages DNA by crosslinking nucleotides together, impairing DNA replication. Ionizing radiation, which is widely used in the treatment of cancer, causes DNA damage, mainly double strand breaks, which are difficult to repair, and thus, highly cytotoxic. Other common assaults on the genome involve exposure to highly mutagenic carcinogens, such as tobacco, and even biological processes that occur naturally, such as the increased exposure to endogenous reactive oxygen species as a function of the aging process, or the DNA mismatches and topoisomerase mediated strand breaks that occasionally occur during DNA replication.

One of the universal markers of DNA damage is the phosphorylation of histone variant H2A.X on chromatin (γ H2AX) [34]. This modification functions as a nucleation signal that recruits and stabilizes the DDR signaling network at sites of DNA damage. Phosphorylation of γ H2AX is generated by the ATM/ATR kinases. ATM is activated by the MRN (MRE-11, Rad50, and NBS1) complex, the global sensor of double strand breaks, which are highly lethal [35]. ATR becomes active when replication fork stalling occurs, which happens, in part, when DNA lesions interfere with the replication machinery. Upon

its activation, γ H2AX signaling is amplified, spreading up to megabases away from the lesion, and recruiting the DDR network with it. This accumulation results in the formation of visible nuclear foci.

Another universal feature of the DDR is the general flow of signal transduction. Damage is recognized by DNA damage sensors (MRN, RPA, PARP, Ku), then, signals are transmitted to transducers (ATM, ATR, DNAPKs, the 9-1-1 complex, ATRIP), usually kinases that, in turn, signal to the DDR effectors (Chk1, Chk2, p53, p21, CDC25, Bax), which directly control cell fate by signaling either (1) the repair of DNA damage, (2) the arrest of the cell cycle, in part to allow additional time for DNA repair, or, if damage is overwhelming or irreparable, (3) programmed cell death (apoptosis). [36].

The main DNA repair pathways include DNA-lesion reversal, the simple and direct reversal of small DNA lesions, occurring without DNA backbone incision [37]; mismatch repair, the detection of mismatched nucleotides on complementary strands of DNA that arise mostly from replication and recombination errors [38]; base excision repair, the correction of smaller forms of damage occurring within a single nucleotide that do not distort the DNA helix structure [39]; nucleotide excision repair, the removal of larger, helix distorting lesions on DNA [40]; trans-lesion bypass mechanisms, maneuvering around bulky lesions to ensure the continuity of DNA replication [26]; non-homologous end joining, the re-ligation of a double strand break back together; homologous recombination, the exchange and recombination of DNA between sister chromatids in response to a double strand break [41]; the fanconi anemia pathway, the network responsible for the removal of

crosslinks between strands of DNA [24]; and ATM/ATR-mediated upstream checkpoint signaling, which coordinates the response to DNA damage with cell cycle arrest [42, 43].

1.3 Nucleotide Excision Repair

Nucleotide excision repair (NER) is a cut and patch DNA repair pathway involving the removal of helix-distorting lesions, including crosslinks and bulky base adducts that can destabilize the complementary pairing of bases [44]. It is arguably the most versatile of the DDR pathways, as it is capable of removing the widest range of DNA lesions. Common NER lesions include cyclopyrimidine dimers (CPDs) and pyrimidine-pyrimidone (6-4) photoproducts 6-4PPs, which are the dominant lesions generated on DNA upon exposure to UV light, as well as cisplatin intrastrand crosslinks, which are the primary lesions formed on DNA that is exposed to cisplatin [23]. Lesion repair ensures that the DNA replication machinery is able to continue its processing during S phase of the cell cycle. NER has two main branches: global genome NER (GG-NER), which occurs throughout the genome, and transcription coupled NER (TC-NER), which is confined to areas of active transcription [23]. The general process for both mechanisms is similar. First, NER begins with a lesion recognition step, where molecules detect and verify the presence of a lesion. Next, DNA helix unwinding occurs and the single strand containing the lesion is stabilized. Exonucleases within this complex create nicks in the DNA on either side of the lesion, leading to the excision of approximately 22-32 nucleotide long segments [45]. Lastly, using the intact strand as a template, DNA polymerase is recruited and fills in the gap left by the excision. (Figure 1.1).

The NER pathway is characterized but not fully understood. Loss of function mutations in the key players involved in NER result in xeroderma pigmentoum (XP), a rare skin disorder characterized by premature skin aging and sunlight sensitivity. Additionally, the loss of function of specific NER factors also results in other diseases including cockayne syndrome (CS), a rare disorder characterized by distinct features including small head size, short stature, failure to grow at a normal rate and and sunlight sensitivity; and trichothiodystrophy (TTD), a disorder of brittle hair coupled with neurological abnormalities [46].

Depending on where in the genome DNA damage occurs, NER lesions can be detected by two different sets of molecules (Figure 1.3). In TC-NER, in areas of active transcription, RNA polymerase II is responsible for detection, where it is stalled when it encounters an obstructing lesion [47]. RNA polymerase transiently interacts with the Cockayne syndrome protein CSB, UVSSA and USP7 during transcription. Upon stalling at a lesion, RNA polymerase affinity for CSB increases, facilitating the interaction with CSA. The CSA-CSB complex promotes RNA polymerase backtracking, which makes the DNA lesion accessible for repair, promoting the recruitment of the TFIIH complex [48]. Together, USP7, a deubiquitinating enzyme, and UVSSA, help promote the stability of CSB before it is ubiquitinated and degraded by the proteasome, thereby making the lesion accessible to the TFIIH complex.

In GG-NER, lesion recognition is not completely understood. XPC is considered the central molecule responsible for lesion recognition in GG-NER, where it binds the lesion directly and recruits TFIIH complex, which contains helicases to unwind and stabilize DNA to promote repair [49]. Lesion recognition through XPC is tightly regulated. For example, XPC functions in complex with its stabilizers CETN2 and RAD23B to recruit the TFIIH complex. Looking upstream, XPC must first gain affinity for the NER lesion, occurring through the activities of the E3 ubiquitination ligase complex CRL4^{DDB2}. CRL4^{DDB2} is composed of the heterodimer DDB1-DDB2, CUL4A and ROC1, which function together as the initial lesion recognition factor in GG-NER. [50] [51]. DDB2 binds to lesions by inserting a hairpin structure into the lesion directly and structurally extruding the lesion into its binding pocket, which results in the formation of a DNA kink that XPC can then bind to [50]. After recognition, the CRL4^{DDB2} complex functionally ubiquitinates a number of targets including DDB2, causing the CRL4^{DDB2} complex to fall off the lesion; histones H2A, H3 and H4, which may promote chromatin relaxation around the site of damage; and XPC, which enhances its binding for the lesion [52-54]. Studies have suggested that DDB2 is more adept at promoting resolution of CPD lesions than 6-4PPs [51, 55, 56].

The recruitment of the TFIIH complex is the point of convergence of the GG-NER and TC-NER pathways. Importantly, TFIIH is composed of 10 subunits, including the CAK subcomplex, and helicases XPB and XPD. When TFIIH binds to the lesion, the CAK core dissociates, activating the helicases (XPB and XPD), which unwind the duplex at the site of the lesion [57]. Short stretches of exposed ssDNA are then coated with RPA to promote

stabilization, and verified for damage by RPA together with XPA [58]. Structure specific exonucleases (XPF–ERCC1 and XPG) are then recruited, which generate dual incisions close to the site of damage, on the 5' and 3' side, respectively [59, 60]. The dual incision step is considered to be the “point of no return” step in the pathway. The PCNA complex is subsequently loaded at the 5' end of the incision, which then recruits polymerases (δ , κ or ϵ) perform repair synthesis across the gap, using the undamaged strand of DNA as a template [61, 62]. The residual nick is sealed by DNA ligase (I or 3) [63]. (Figure 1.3).

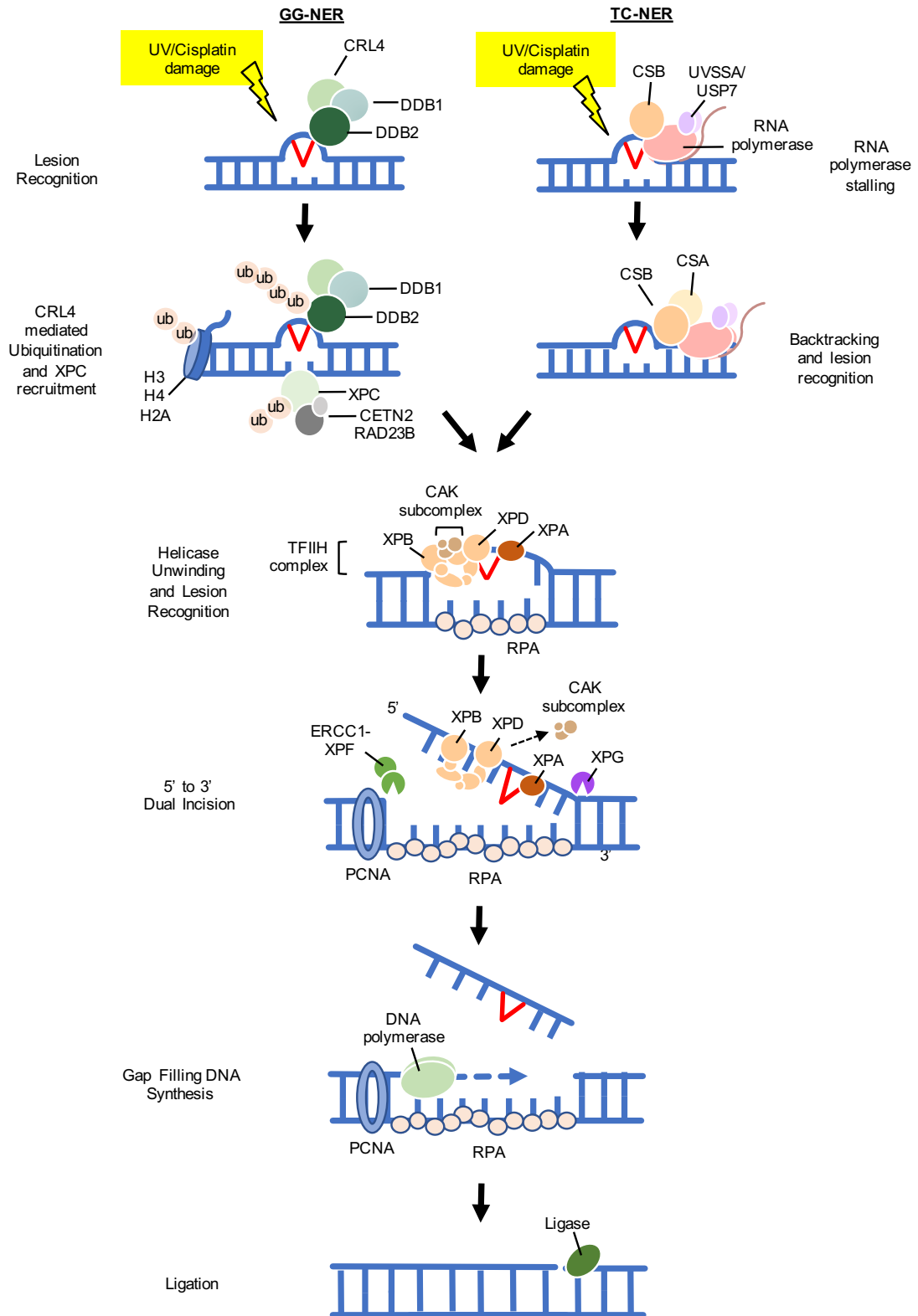


Figure 1.3: The Nucleotide Excision Repair Pathway. Adapted from Marteiijn et al. *Nature Reviews Molecular Cell Biology* (2014) [40]

1.4 Double Strand Break Repair

DNA double strand breaks (DSBs) are highly lethal lesions that must be repaired to ensure cell survival. DSBs can be artificially induced by ionizing radiation and treatment with topoisomerase inhibitors, such as etoposide and camptothecin, or they can occur naturally during DNA replication, when the replication fork encounters DNA repair intermediates and collapses. Induction of cellular DSBs is one of the most commonly used and effective anticancer strategies to promote cancer cell cytotoxicity. Local ionizing radiation is routinely used in the clinic. Further, drugs that target molecules that normally help clear DNA repair intermediates can be leveraged to promote DSB formation, thus targeting cancer. Perhaps one of the most well studied examples of this is the use of PARP inhibitors in BRCA deficient tumors. PARP proteins are key DNA damage sensors responsible for the detection of single strand breaks where they parylate chromatin at the site of the lesion, promoting its decondensation, and making the lesion accessible to DNA repair factors to process the lesion. PARP is proven to recruit many DDR factors to sites of DNA damage. BRCA proteins promote repair of DSB through the homologous recombination pathway. When PARP inhibitors are used on BRCA deficient tumors, PARP deficiency results in lesions that are unable to be detected or processed and, when these are encountered by the replication fork, these undetected lesions can result in the formation of double strand breaks. Because of deficiency in BRCA, which are proteins critical to the repair of DSBs, the DSBs are left unrepaired as well, which triggers apoptosis. Thus, PARP and BRCA deficiency are synthetically lethal in mediating cytotoxicity, which is a potent anticancer strategy [64].

Alternatively, when DSBs are left unrepaired, they can also lead to chromosomal rearrangements, genomic instability, and cancer.

The two main pathways of DSB repair include homologous recombination (HR) and non-homologous end joining (NHEJ), where NHEJ occurs more often and throughout the cell cycle, and HR, which requires the presence of a sister chromatid, takes place during S/G2 phase of the cell cycle. Recent studies have suggested additional pathways may also be involved in DSB repair, including alternative non homologous end joining (alt-NHEJ) and single strand annealing (SSA). NHEJ is error prone because the DSB is re-ligated back together quickly. However, it is the only DSBR pathway that operates during the G0 and G1 phases of the cell cycle. Other pathways are confined to the S/G2 phase of the cell cycle because they require ctIP mediated end resection, the chewing back of the 5' end of DNA at a DSB to generate 3' single stranded DNA tail, which is limited to S/G2 phases itself. Pathways requiring ctIP dependent end resection include alt-NHEJ, SSA and HR. Mechanistically, the SSA and alt-NHEJ pathways are induced depending on the type of homology that exists on either side of the DSB. SSA requires larger homologous repeats on either side of the DSB while alt-NHEJ makes use of regions of microhomology existing on either side of the DSB, respectively, to bridge DSB ends back together. Both pathways can result in deletion mutations between repeats.

1.5 Homologous Recombination

While all other DSB pathways are error prone, homologous recombination is the only DSB repair pathway capable of processing the lesion in an error free fashion. It accomplishes this by invading and replicating the sequence of an intact sister chromatid, using its sequence as a template to fill in the gap generated at the site of the DSB. Thus, error free repair of DSB is confined to S/G2 phases of the cell cycle, when a homologous donor is present [65]. (Figure 1.2). In detail, a DSB forms, and the Ku heterodimer (Ku70/80), an abundant nuclear complex with high affinity for blunt and sticky DNA ends, binds to the exposed DNA ends that are generated by the break [66]. The HR pathway begins when the DSB is recognized by the MRN complex (MRE11, Rad50, and NBS1). This is followed by the recruitment of ctIP and the initiation of end resection of the 5' DNA end of the break [67]. Together, MRN and ctIP generate a nick through endonuclease activity. This is also facilitated by the activity of BRCA1-BARD1. MRN and ctIP further serve to displace the Ku heterodimer [66]. Removal of Ku signals end resection of the DSB through the 3' to 5' exonuclease activity of MRN through Mre11, and the 5' to 3' exonuclease activities of EXO1 and the heterodimer BLM-DNA2. After end resection occurs, it generates single stranded DNA with a 3' overhang [68, 69]. RPA coats the ssDNA overhang to promote its stability. RPA is subsequently exchanged for RAD51 in coating the ssDNA, facilitated by BRCA2, BRCA1-BARD1, and PRP19 [70, 71]. After RAD51 is loaded, it performs a homology search and promotes strand invasion into the sister chromatid. Subsequently, synthesis of nascent DNA, using the invaded strand as a template, occurs, and it is annealed to the other side of the DSB. (Fig. 1.4)

Importantly, the 3' ssDNA overhang is highly vulnerable to the formation of DNA-RNA hybrids. The activities of RNA helicases, such as DDX1, help resolve hybrids that are generated at this stage [72]. If hybrids are left unresolved, it can result in failure in the HR pathway, as well as replication fork collapse and ensuing genomic instability. (Fig. 1.4).

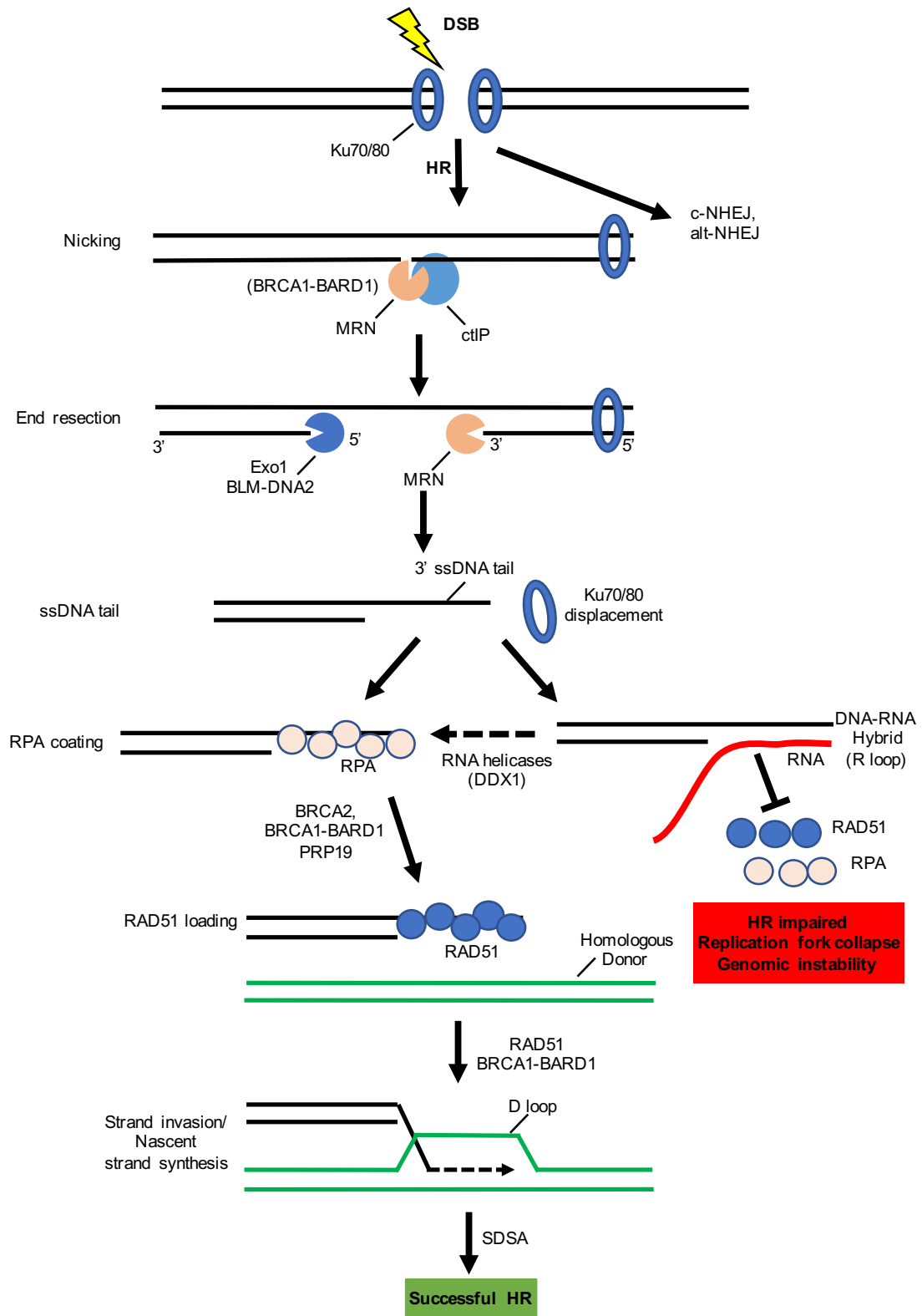


Figure 1.4: The Homologous Recombination Repair Pathway. Adapted from Scully et al. *Nature Reviews Molecular Cell Biology* (2019) [73].

1.6 Genomic Instability

One hallmark of cancer that has come to light in the era of next generation sequencing is the occurrence of genomic instability. It describes variations in the genome, from increased base pair mutations all the way to chromosomal aberrations, including gross changes in their number and structure. Microsatellite instability and chromosomal instability are observed in most sporadic cancers. Chromosomal translocations that result from genomic instability can lead to fusions of proto-oncogenes that result in their activation. Specific fusions, such as BCR-ABL and EWS-FLI1 characterize specific cancers [74, 75].

The drivers of genomic instability are difficult to pinpoint due to the incidence of passenger mutations that concordantly occur. However, mutations in DNA repair genes such as BRCA have been identified as one cause of genomic instability in hereditary cancers [76]. Indeed, failure to respond and repair DNA damage can result in propagation of point mutations or in chromosomal breakages and rearrangements. One key source of genomic instability is when high levels of DNA damage are coupled with the rapid cell division that is required in proliferating cancer, (known as DNA replication stress) [77]. When proliferation progresses in an unchecked fashion, often through deficiencies in cell cycle checkpoints, genomic instability ensues. Genomic instability occurs in sporadic cancers as well, but is seemingly not caused by DNA repair mutations [78]. An emerging source of genomic instability is when there is a failure to resolve DNA-RNA hybrids or triple stranded DNA-RNA-DNA structures (R loops), which occur naturally during transcription.

Indeed, hybrid or R loop persistence causes chromosomal rearrangements and replication fork stalling [79].

Genomic instability can be identified on a small scale, including the spontaneous induction of γ H2AX phosphorylation without a DNA damaging agent, and/or the presence of spontaneous micronuclei; or, more globally, such as the presentation of an irregular karyotype profile.

Genomic instability is problematic because it can generate tumors that are molecularly heterogeneous, which may not respond to a single therapy. Further, tumors with unstable genomes can rapidly evolve, and resistant subpopulations of tumor cells can be selected for when treatment is applied (Fig. 1.1).

1.7 EZH2

Enhancer of zeste homolog 2 (EZH2) is a nuclear enzyme defined as the catalytic subunit of the polycomb repressive complex PRC2. Polycomb group proteins are a group of conserved epigenetic modifiers that help maintain gene silencing through the placement of posttranslational modifications on histones, thereby affecting processes such as development, cellular plasticity, and cancer progression [80]. Polycomb proteins encompass members of two repressive complexes, PRC1 and PRC2. PRC2 is composed of four core subunits, namely EZH2, SUZ12, EED, and RbAp46/48, as well as accessory subunits that help regulate the activity of PRC2 depending on the molecular context. EZH2, the catalytic core of PRC2, catalyzes the placement of methylation marks on histone H3 at

lysine 27, which promotes chromatin compaction and transcriptional silencing (Fig. 1.6). However, EZH2 is not able to place methylation marks on H3K27 alone, as its interaction with SUZ12 and EED are required for its role in transcriptional silencing [81, 82]. EED interacts directly with EZH2 and functions as a scaffold, SUZ12 is required for nucleosome recognition, and RbAp46/48 helps mediate histone binding of the complex. Auxiliary subunits can further enhance activity of PRC2 (AEBP2, JARID2) [83].

Structurally, EZH2 contains a conserved SET domain in its c-terminus, which is responsible for its methyltransferase function [84]. Within the SET domain exists a conserved catalytic triad known as the NHS motif, which helps govern both the recognition of the H3 peptide tail and the binding of the methyl group donor, S-adenosyl-methionine (SAM) to EZH2. The histidine residue of the NHS motif is essential for histone methyltransferase function, where mutation of histidine to alanine abolishes EZH2 catalytic activity [85]. EZH2 also contains an n-terminal WD40 binding domain which mediates its interaction with other PRC2 members EED, a cysteine rich domain (CXC), and two SANT domains, which are responsible for EZH2's interactions with histones [80, 86]. EZH2 interacts with SUZ12 within a domain referred to as "domain 1" in a dephosphorylated state. Phosphorylation at threonine 311 impairs EZH2-SUZ12 interaction [87]. (Fig. 1.5)

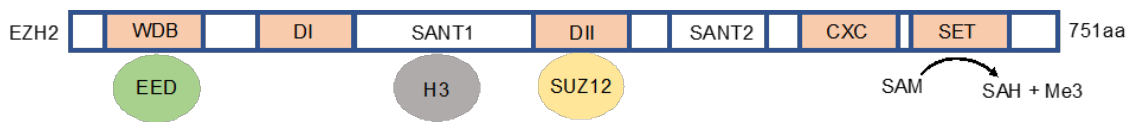


Fig. 1.5 Domain Map of EZH2

EZH2 contains an N-terminal WDB domain, two SANT domains, Domain I and II, a CXC domain and a C-terminal SET domain. The WDB domain binds PRC2 member EED; the SANT1 domain binds H3; Domain II binds PRC2 member SUZ12; and the SET domain, which is responsible for the catalytic function of EZH2, catalyzing the transfer of methyl groups from an S-adenosylmethionine (SAM) donor, yielding S-adenosylhomocysteine (SAH).

PRC2 is responsible for gene silencing, including in areas of active transcription. Methylation on H3K27 serves as a docking site for DNA methyltransferases, and histone deacetylases that can further enhance PRC2 initiated transcriptional silencing, and promote heterochromatin formation, a form of gene silencing that is more stable and long lasting. For example, EZH2 serves as one of the key mediators of X chromosome inactivation that exists in females [88]. Beyond its canonical role in PRC2, EZH2 can also methylate non-histone proteins, thereby regulating their function. EZH2 also has an emerging role as a transcriptional activator, which may occur independently of its methyltransferase function (Fig. 1.6).

Functionally, gene silencing via EZH2 is a key contributor to several biological processes, some of which directly contradict others. For example, EZH2 promotes stem cell maintenance by silencing genes that are required for differentiation [89]. Conversely, EZH2 can also promote cellular differentiation by suppressing genes that promote stemness [90]. The specific cell type may dictate the function of EZH2. Similarly, EZH2 has been reported to play a dual role in cancer, where it is capable of both tumor promotion and suppression. However, EZH2's oncogenic functions are far more established.

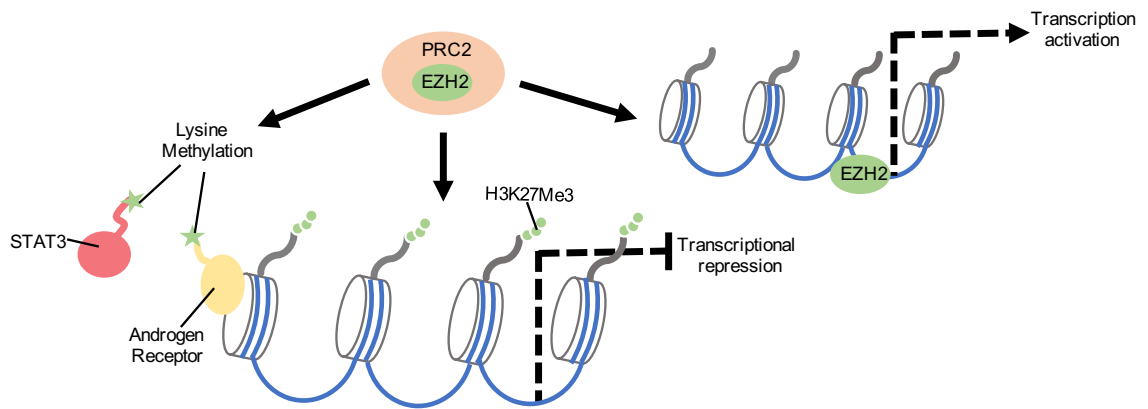


Fig. 1.6: Overview of EZH2 functions: Adapted from Kim et al. “Targeting EZH2 in Cancer” *Nature Medicine* (2016) [91].

The canonical function of EZH2 is to serve as the catalytic subunit of PRC2, where EZH2 catalyzes the placement of methylation marks on H3K27 on chromatin. EZH2 has been reported to methylate targets other than histones, including lysine residues on proteins such as STAT3 and Androgen Receptor, thereby regulating their function [92, 93]. Recently, EZH2 has been implicated in transcriptional activation, where it may act independently of its methyltransferase activity [94].

1.8 EZH2 in Cancer

Epigenetic modifications are well documented to drive cancers. Across all histone methyltransferases, EZH2 has emerged as one of the key epigenetic modifiers implicated in cancer, where it is frequently overexpressed or otherwise dysregulated. EZH2 overexpression is thought to occur in SCLC through the loss of RB and resulting increase in E2F [95]. Beyond its overexpression, gain of function mutations within the SET domain of EZH2 are oncogenic, and result in increased methyltransferase activity. They have been frequently observed in cancers such as follicular lymphoma, diffuse B cell lymphoma, and melanoma [96].

On a cellular level, EZH2 promotes proliferation and its overexpression can promote cellular transformation [97]. In patients, high EZH2 expression is associated with poor outcome across epithelial based cancers, including lung, ovarian, breast, gastric, bladder, endometrial, hepatocellular and melanoma, in hematological malignancies, and in pediatric soft tissue sarcomas. Furthermore, EZH2 overexpression is associated with advanced and metastatic disease in lung, breast, prostate, bladder, and endometrial cancers and melanoma [98]. Indeed, EZH2 expression level is used as a biomarker to independently predict patient outcome in breast cancer [99]. In epithelial cancers, EZH2 may promote cancer stem cell properties, thereby facilitating epithelial to mesenchymal transition, which facilitates invasion and metastasis [100]. Furthermore, upregulation of EZH2 can lead to aberrant silencing of tumor suppressors, promoting tumorigenesis. For example, EZH2 silences

tumor suppressive microRNA mir31, a negative regulator NF- κ B, which aids in the evasion of apoptosis [101].

1.9 EZH2 in the DNA Damage Response

There is increasing evidence that EZH2 plays a role in the DNA damage response. Perhaps the most compelling evidence supporting this role is the direct localization of EZH2 to sites of double strand breaks [102]. While the underlying mechanism for this is poorly understood, DSBs are notably coupled with increased H3K27Me3. This may serve as a protective function in the cell, silencing areas of active transcription occurring near a DSB such that proper gene expression is maintained. EZH2 is also indirectly involved in the DDR through transcriptional silencing of its mediators, such as RAD51, consequently impairing homologous recombination [103, 104]. EZH2 and the HR protein BRCA1 have been functionally linked as well, where EZH2 acts upstream to regulate or transcriptionally silence BRCA1 [105]. EZH2 also plays dual roles in replication fork maintenance, where it promotes replication fork progression, but it also mediates degradation of stalled replication forks [106]. Moreover, EZH2 regulates cell cycle G1/S and G2/M checkpoints [107]. Although its specific role in the DDR may be multifaceted, EZH2 has been described to mediate resistance to DNA damaging agents across several cancers [108-111].

1.10 RNA Helicases

RNA helicases are the enzymes responsible for mediating the unwinding of RNA duplexes and promoting structural rearrangements of RNP complexes. They are ATP dependent molecules that are critically involved in nearly every aspect of RNA metabolism, including transcription, splicing, nuclear export, translation, ribosome biogenesis and decay, and can also function to separate RNA-protein duplexes [112].

From a structural perspective, RNA helicases are classified by their evolutionarily conserved motifs. There are 6 RNA helicase superfamilies (SF1-6) categorized by structure and function. The underlying mechanisms of RNA helicases are being actively investigated, including how they are recruited to specific targets and what cofactors are needed to aid in their biological functions.

1.11 RNA Helicases in the DNA Damage Response

There is increasing evidence that the DNA damage response and RNA processing activities functionally intersect. The list of proteins found capable of binding both DNA and RNA is ever increasing. Moreover, RNA processing molecules are mediators of genomic stability, where they prevent interactions between nascent RNA and template DNA. These DNA-RNA hybrids threaten genomic integrity, as they can result in the formation of strand breaks and genomic instability. There is direct evidence of the involvement of DNA-RNA hybrids in the DNA damage response, where they are found to form spontaneously at DSBs, or at stalled replication forks, particularly in areas of active transcription [72, 113]. Indeed, RNaseH1, an exonuclease that specifically degrades DNA-RNA hybrids during

transcription, rapidly localizes to sites of DNA damage in response to laser microirradiation [114].

RNA helicases have been implicated in the resolution of DNA-RNA hybrids that maintain the DDR. SETX, a well characterized RNA helicase involved in hybrid resolution during transcription, was recently found to be recruited to DSBs in areas of active transcription in response to damage, where it removes DNA-RNA hybrids, promotes RAD51 loading in HR, and prevents chromosomal translocations [115]. Similarly, the RNA helicase DDX1 was recently found to facilitate HR by removing DNA-RNA hybrids, and promoting RAD51 loading [72]. The functional interplay between RNA helicases involved in HR and DNA-RNA hybrid resolution in HR has yet to be elucidated. Moreover, the involvement of RNA helicases in HR is a fairly recent finding, and there may be other RNA helicases involved in HR or in other DNA repair pathways.

1.12 HELZ

Helicase with Zinc finger (HELZ) is a poorly characterized protein, described as a putative RNA helicase. Functionally, HELZ has been reported to be involved in RNA processes including translation initiation and mRNA decay. [116-118]. HELZ has also been implicated in impairing cancer growth, where mRNA levels of HELZ were found to be reduced across a panel of cancer cell lines [118]. However, little else is known about HELZ, including if it is indeed a functional RNA helicase.

To better understand its biological function, we look to its structure. It is a member of superfamily 1 (SF1) of eukaryotic helicases. HELZ is 1942 nucleotides in length and contains most of the classical SF1 motifs, including a Walker A motif, which generally facilitates NTP binding, a DEAA box motif, a PAM2 motif, and a C3H1-type zinc finger motif at its amino terminus. HELZ shares domain homology with the well characterized RNA helicase eIF4A. The Walker A motif in eIF4A is important for its ATP binding and helicase activity. The consensus sequence of the Walker A motif is (G/A)xxxxGK(T/S), where mutation of the conserved lysine to asparagine impairs eIF4A ATPase and unwinding activity. The DEAA and PAM2 motifs are known to be required for HELZ's interaction with poly(A) binding protein (PABP) [116]. The c-terminal tail is largely unstructured and plays a role in mRNA decay [117]. (Fig. 1.7)



Fig. 1.7 Domains and Motifs of HELZ

HELZ contains an N-terminal Zinc Finger domain, a Walker A motif, a DEAA box, a PAM2 motif, two LxxLAP motifs, including one that resides within the PAM2 motif, and a largely unstructured c terminal tail. Walker A motifs are critical for ATP binding and unwinding activity in other helicases.

1.12 Scope of this Dissertation

In this dissertation, we performed high throughput siRNA screens to identify genes that, when depleted, re-sensitize EP resistant SCLC to cisplatin and etoposide. In chapter two, we identify EZH2 as a mediator of cisplatin resistance in SCLC and characterize its role in crosslink resolution through a novel catalytic and PRC2 independent function in nucleotide excision repair. In chapter three, we identify HELZ, a poorly characterized helicase, as a mediator of etoposide resistance in SCLC, and characterize its role in governing homologous recombination, DNA-RNA hybrid resolution, and in maintaining genomic stability. Collectively, this work provides mechanistic insight into EP resistance in SCLC, proposes EZH2 and HELZ as two molecules of high interest for the design of targeted therapies, and details the molecular roles of EZH2 and HELZ in responding to chemotherapy through the DNA damage response. Together, this work provides substantial rationale for the future development and design of inhibitors to EZH2 and HELZ in SCLC.

Chapter 2: EZH2 has a Non-Catalytic and PRC2-Independent Role in Stabilizing DDB2 to Promote Nucleotide Excision Repair

Allyson E. Koyen¹, Matthew Z. Madden¹, Dongkyoo Park¹, Elizabeth V. Minten¹, Priya Kapoor- Vazirani¹, Erica Werner¹, Neil T. Pfister¹, Ramona Haji-Seyed-Javadi¹, Hui Zhang¹, Jie Xu¹, Nikita Deng¹, Duc M. Duong², Turner J. Pecan⁴, Zoë Frazier³, Zachary D. Nagel⁴, Jean-Bernard Lazaro³, Kent W. Mouw³, Nicholas T. Seyfried², Carlos S. Moreno⁵, Taofeek K. Owonikoko⁶, Xingming Deng¹, and David S. Yu^{1,*}

¹ Department of Radiation Oncology, Emory University School of Medicine, Atlanta, GA 30322, USA, ² Department of Biochemistry, Emory University School of Medicine, Atlanta, GA 30322, USA, ³ Department of Radiation Oncology, Dana-Farber Cancer Institute, Brigham and Women's Hospital, Boston, MA 02215, USA, ⁴ Department of Environmental Health, Harvard School of Public Health, Boston, MA 02115, ⁵ Department of Pathology and Laboratory Medicine, Emory University School of Medicine, Atlanta, GA 30322, USA, ⁶ Department of Hematology and Medical Oncology, Emory University School of Medicine, Atlanta, GA 30322, USA.

2.1 Author's Contribution and Acknowledgement of Reproduction

This work was adapted with minor edits from Koyen et al. *EZH2 has a Non-Catalytic and PRC2-Independent Role in Stabilizing DDB2 to Promote Nucleotide Excision Repair*. **Oncogene**, 2020, in press.

AUTHOR CONTRIBUTIONS

Conceptualization, A.E.K., M.Z.M, and D.S.Y.; Investigation, A.E.K., M.Z.M., D.P., E.V.M., P.K., E.W., N.T.P., R.H.J., H.Z., J.X., N.D., T.J.P., Z.F., D.M.D., J.L, and C.S.M.; Writing – Original Draft, A.E.K. and D.S.Y.; Writing – Review and Editing, A.E.K., M.Z.M., D.P., E.V.M., P.K., E.W., N.T.P., R.H.J., H.Z., J.X., N.D., D.M.D., T.J.P., Z.F., Z.D.N, J.L., K.W.M., N.T.S., C.S.M., T.K.O., X.D., and D.S.Y.; Supervision – J.L., Z.D.N., K.W.M., N.T.S., C.S.M., T.K.O., X.D., and D.S.Y.; Funding Acquisition, A.E.K., N.T.P., Z.D.N, X.D., and D.S.Y.

2.2 Abstract

Small cell lung cancer (SCLC) is a highly aggressive malignancy with poor outcomes associated with resistance to cisplatin-based chemotherapy. Enhancer of Zeste Homolog 2 (EZH2) is the catalytic subunit of Polycomb Repressive Complex 2 (PRC2), which silences transcription through trimethylation of histone H3 lysine 27 (H3K27me3) and has emerged as an important therapeutic target with inhibitors targeting its methyltransferase activity under clinical investigation. Here, we show that EZH2 has a non-catalytic and PRC2 independent role in stabilizing DDB2 to promote nucleotide excision repair (NER) and govern cisplatin resistance in SCLC. Using a synthetic lethality screen, we identified important regulators of cisplatin resistance in SCLC cells, including EZH2. EZH2 depletion causes cellular cisplatin and UV hypersensitivity in an epistatic manner with DDB1-DDB2. EZH2 complexes with DDB1-DDB2 and promotes DDB2 stability by impairing its ubiquitination independent of methyltransferase activity or PRC2, thereby facilitating DDB2 localization to cyclobutane pyrimidine dimer (CPD) crosslinks to govern their repair. Furthermore, targeting EZH2 for depletion with DZNep strongly sensitizes SCLC cells and tumors to cisplatin. Our findings reveal a non-catalytic and PRC2-independent function for EZH2 in promoting NER through DDB2 stabilization, suggesting a rationale for targeting EZH2 beyond its catalytic activity for overcoming cisplatin resistance in SCLC.

2.3 Introduction

SCLC is a highly aggressive malignancy with a 5-year survival rate of only 7 percent [119]. The first-line treatment regimen for SCLC consists of platinum-based EP chemotherapy: cisplatin or carboplatin, DNA crosslinking agents, in combination with etoposide, a topoisomerase II inhibitor. While most SCLC patients will initially respond to EP treatment, the majority will ultimately develop treatment resistance [120]. Response rates for second-line topoisomerase I inhibitors for SCLC are much lower [121], and SCLC currently lacks any FDA-approved targeted therapies. Therefore, novel therapeutic approaches for SCLC treatment are urgently needed.

The DNA damage response (DDR) is critical for responding to DNA damage induced by chemotherapy. Cisplatin primarily induces cytotoxicity by creating 1,2-intrastrand d(GpG) adducts. The major mechanism for repair of these DNA intrastrand crosslinks is nucleotide excision repair (NER), which is also involved in the repair of other helix-distorting DNA lesions, including UV-induced CPD and 6–4 pyrimidine-pyrimidone photoproducts (6–4PP) [40]. The Damage Specific DNA Binding Protein 1 and 2 (DDB1-DDB2) heterodimer is a component of the CUL4-RING E3 ubiquitin ligase complex (CRL4), which promotes the repair of NER lesions through the global genome branch of the NER pathway. DDB2 recognizes DNA lesions [122] and recruits downstream NER factors to repair the lesion [56]. Upon lesion detection, DDB2 is ubiquitinated and targeted for degradation by CRL4 [56, 123, 124], although the mechanism by which DDB2 ubiquitination is regulated is not fully understood.

EZH2 is the catalytic subunit of the PRC2, which functions together with Embryonic Ectoderm Development (EED) and Suppressor of Zeste 12 (SUZ12) as a histone methyltransferase to silence areas of active transcription through H3K27me3. EZH2 is an oncogene that is overexpressed in many cancer types, including SCLC [125-127], and high EZH2 expression is correlated with tumorigenesis, cancer progression, metastasis, and poor prognoses [126, 128-135]. As such, EZH2 has emerged as an important therapeutic target. Several EZH2 inhibitors targeting its methyltransferase activity have been developed [136-141] and are currently undergoing clinical trial testing. However, it is unclear if inhibiting EZH2's catalytic activity is sufficient to impair its activities governing cancer cell survival, as non-catalytic and PRC2-independent roles for EZH2, largely involving transcriptional regulation independent of H3K27me3, have also been reported [92, 93, 142-146]. EZH2 has also been shown to directly methylate non-histone proteins to promote their degradation [144, 147].

A role for EZH2 in genome maintenance has previously been described. EZH2 has been reported to mediate resistance to DNA damaging agents, including etoposide in SCLC [108-111] and cisplatin in several other cancer cell types [125, 148-151], localize to DNA damage sites [152, 153], and promote DNA double-strand break (DSB) repair [104, 152], degradation of stalled replication forks [106], and checkpoint signaling [107]; however, these functions have largely been attributed to H3K27Me3, either through transcriptional repression or a recently-described function for H3K27Me3 in the recruitment of MUS81

[106]. Significantly, a role for EZH2 in promoting NER, as well as in promoting genome maintenance independent of its catalytic activity or PRC2, has previously not been shown. Here, we define a novel role for EZH2 in governing cisplatin resistance in SCLC by promoting NER. We show that EZH2 has a non-catalytic and PRC2-independent role in stabilizing DDB2 by impairing its ubiquitination, thereby facilitating DDB2 localization to CPD crosslinks to govern their repair. Furthermore, targeting EZH2 for depletion with DZNep strongly sensitizes SCLC cells and tumors to cisplatin, revealing a potential rationale-driven approach for overcoming cisplatin resistance in SCLC.

2.4 Materials and Methods

Cell lines

All cell lines were originally purchased from the American Type Culture Collection (ATCC, Manassas, VA). Human SCLC cell lines (H128, H146, H187, H69, DMS114 and DMS153) were provided by the laboratory of Dr. Taofeek Owonikoko [154]. H128, H187, H69, and H146 cells were grown in RPMI 1640 (Gibco) with 7.5% fetal bovine serum (FBS). DMS114 and DMS153 cells were grown in Waymouth's medium (Gibco) with 5% FBS. HeLa, U2OS, HEK293T, and HCT116 cells were grown in DMEM (Gibco) with 7.5% FBS. BEAS-2B were cultured in DMEM/F-12 medium with 10% FBS. Primary small airway epithelial cells (HSAEC) were grown in Airway Basal Medium (ATCC PCS-300-030) with one Bronchial Epithelial Growth Kit (ATCC PCS-300-040) according to manufacturer's instructions. All cell lines were grown at 37°C under humidified conditions with 5% CO₂ and 95% air.

Drug Treatments

For drug treatments, cells were pre-treated with 1-50 μ M cycloheximide (CHX) (Sigma) for 2 hours to measure DDB2 stability. To inhibit proteasomal degradation, cells were treated for 4-6 hours with 5 μ M MG132 (Sigma). To achieve EZH2 depletion, cells were pre-treated with 2.5-5 μ M DZNep (Sigma) for 4-6 days. To target the catalytic activity of EZH2, cells were pre-treated with 1 μ M EPZ-6438 (APExBIO) for 4 days. Cells were treated with cisplatin (Sigma) between 1-72 hours and at a concentration of 1-50 μ M, as indicated, depending on the assay.

Transfections

siRNA was purchased from Dharmacon and transfected with Lipofectamine RNAiMAX (Invitrogen) according to the manufacturer's instructions. siRNA sequences are as follows:

NT: AUGAACGUGAAUUGCUCUCAAUU

EZH2-1: CAAAGAAUCUAGCAUCAUA

EZH2-2: GAAUGGAAACAGCGAAGGA

EZH2-3: CGGUGGGACUCAGAAGGCA

siERCC1: GAGAAGAUCUGGCCUUAUG

siDDB1: ACCUAUCACAAUGGUGACAAA

siDDB2: AGGGAUCAAGCAGUUAUUUGA

siSUZ12: GUCGCAACGGACCAGUUA

siATR: CCUCCGUGAUGUUGCUUGA

siXPA: GCAA AUGGCUUCUAUCGAA

For overexpression studies, plasmids were transfected with Lipofectamine 2000 (Invitrogen) according to the manufacturer's instructions. EmGFP-EZH2-wild-type

plasmid was generously provided by Dr. Damian Yap [155] (British Columbia Cancer Agency) and was used to generate EmGFP-EZH2-H689A by site-directed mutagenesis. The FLAG-DDB2 plasmid was a gift of Dr. Qi-En Wang (The Ohio State University). Plasmids for EZH2 PRC2 mutants were a gift of Dr. Lixin Wan (Moffit Cancer Center). pcDNA3-2xHA-DDB1 was purchased from Addgene (Plasmid #19909).

Primary cisplatin siRNA screen

A custom siRNA library targeted 1,006 nuclear enzymes in a 96-well plate SMARTpool format, with each well containing 4 siRNAs targeting unique sequences within the same gene (Dharmacon). Each plate had 9 negative control siNT wells, three positive sensitivity control siATR wells, three control siERCC1 wells, and one blank well. We included siCHK1, siATRIP, mock transfected (no siRNA), and non-transfected (no transfection reagent) control wells on the final plate.

Each well in the 96-well plates received 12,000 H128 cells and 0.3 μ L of Lipofectamine RNAiMAX (Invitrogen), as well as a final siRNA concentration of 25 nM and a final volume of 100 μ L. After 24 hours, each transfection plate was split into 4 clear-bottomed plates with final well volumes of 100 μ L. After another 24 hr, 50 μ L of media was added to the two non-treated plates while 50 μ L of cisplatin-containing media was added to one plate each with a final concentration of 10 μ M. After a further 72 hr, 10 μ L of Resazurin reagent (R&D Systems) was added to each well for a final concentration of 1X in media. Fluorescence, corresponding to the number of live cells per well, was measured 8 hr later. Average cell viability was calculated from the treated-to-untreated viability ratio for each

gene, normalized to each plate's NT control and averaged over a number of replicates. Cisplatin sensitization hits were considered based on the following criteria: a log₂ average viability of < -0.75, an average SSMD of < -2 and a 2-tailed t-test p value of <0.05.

Of the 118 hits, we selected 23 genes for further analysis. 13/23 were validated to reproduce the cisplatin sensitization phenotype across at least two individual siRNAs.

To assess screen quality, Z-factor was calculated using the means and standard deviations of both positive (siATR) and negative (siNT) controls. The cisplatin siRNA screen fell in the excellent range (between 0.5 and 1.0) with a calculated Z-factor of 0.556.

Site-Directed Mutagenesis

The EmGFP-EZH2 H689A mutant was generated by site-directed mutagenesis, as previously described [156]. Briefly, PCR primers were designed to generate the H689A mutation:

EmGFP-EZH2 H689A Forward:

CAAAATTCGTTTTGCAAATGCTTCGGTAAATCCAAACTG

EmGFP-EZH2 H689A Reverse:

CAGTTTGGATTTACCGAAGCATTGCAAAACGAATTTTG

EmGFP-EZH2 wild type was used as a template and PCR reaction was performed. The template was then digested with DpnI for 2 hours at 37°C. The H689A mutation was confirmed by sequencing.

Generation of DDB2 Deletion Constructs

FLAG-DDB2 deletion constructs were generated by PCR based cloning off of full length FLAG-DDB2 (FL) into the pcDNA3.1 multiple cloning site. FLAG-DDB2 deletion mutants included FLAG-DDB2 1-115, 1-196, 1-290, 1-390, and Δ 40.

Gene Ontology (GO) and Network analysis

The Gene Ontology (GO) and network analysis were performed in Cytoscape [157] using ClueGO [158] and CluePedia [159] plugins. GO analysis using fused GO terms is represented. Significant processes (p -value ≤ 0.01) are shown. Categories were identified and sorted by the percent associated genes found. Only cisplatin sensitization hits were used to build the network.

Cell Viability Assay

Cell viability assays were performed as previously described [160]. Cells were seeded in 96-well plates at the appropriate density (H128: 10,000 cells/well H146: 20,000 cells/well) and were treated with varying doses of cisplatin (0-50 μ M). For UV treatment, cells were irradiated with the indicated dose of UV prior to seeding. After treatment, cells were grown in 96-well plates for 72 hours and then treated with Resazurin reagent at a final concentration of 1X in media. Cells were then incubated at 37°C for 3 hours. The Resazurin signal was then read as fluorescence (excitation wavelength: 544 nm, emission wavelength: 590 nm) on a Synergy H1 microplate reader (BioTek) in conjunction with Gen5 Microplate Reader Software (BioTek). Percent cell viability was quantified relative to the Resazurin

signal in the untreated group, including subtracting the background the Resazurin signal for wells with no cells and media with Resazurin only.

Colony formation Assay

U2OS cells were seeded sparsely in 6 well plates, at 100 cells/well for low doses or 200 cells/well for high doses of damage. Cells were given 8-24 hours to adhere and then irradiated with UV. Cells were grown until the untreated group formed colonies of approximately 50 cells in density, which, depending on the doubling time of the cell line, took between 10 and 14 days. To visualize colonies, cells were washed once with ice-cold PBS and then fixed in 3% crystal violet in methanol for 15 minutes. Crystal violet was removed by gently submerging plates in water. Visible colonies were then quantified with Bantex colony counter 920A.

Immunoblotting

Cells were lysed in Laemmli sample buffer and sonicated briefly followed by denaturation by boiling at 100°C for 7 minutes. Whole-cell lysate was run on SDS-PAGE at 80V for 2-3 hours followed by transfer to PVDF membrane at 40V overnight. Membranes were blocked in 5% BSA in TBST for 30 minutes followed by probing with the indicated antibodies in TBST supplemented with 1% BSA and 0.05% sodium azide at the indicated dilutions. To quantify band intensity, densitometry was performed using ImageJ software. Signals of interest are represented as normalized to tubulin.

Antibodies

EZH2 (cell signaling #5246, 1:500 for immunoblotting, 1-4 µg per 1mg whole cell lysate for IP), DDB2 (Abcam # ab181136, 1:500 for immunoblotting), DDB1 (Bethyl, #A300-462A, 1:500 for immunoblotting), HA (Sigma, #H3663, 1:500 for immunoblotting, 1 µg per 1mg whole cell lysate for IP), GFP (Abcam, #ab6556, 1:500 for immunoblotting, 1 µg per 1mg whole cell lysate for IP),), GFP (Abcam, #ab290, 2 µg per 1.5 mg whole cell lysate for IP), H3K27Me3 (Cell Signaling, #C36B11, 1:500 for immunoblotting), SUZ12 (Cell Signaling, #3737, 1:500 for immunoblotting), Normal Rabbit IgG (Millipore, #NI01, 1-4 µg per 1mg whole cell lysate for IP), p21 (Abcam #ab109520, 1:200 for immunoblotting), total Histone 3 (Millipore, #06-755, 1:500 for immunoblotting), alpha-tubulin (Sigma, T6074, 1:500 for immunoblotting), GAPDH (Santa Cruz, #sc-47724, 1:500 for immunoblotting), CPD (Kamiya Biomedical Company, #MC-062, 1:200 for immunofluorescence, 1:2000 for slot blot analysis), anti-FLAG (Cell Signaling, #2368, 1:500 for immunofluorescence) and anti-γH2AX (Cell Signaling, #2577, 1:200).

Co-Immunoprecipitation and protein digestion for MS

HeLa cells were transiently transfected with GFP-EZH2. 72 hours post-transfection, cells were treated with 25 µM cisplatin and harvested and lysed 4 hours later, and GFP-EZH2 was immunoprecipitated (IP'd) with GFP antibody or IgG conjugated to protein A agarose beads (Sigma). Beads were washed in PBS and processed for mass spectrometry (MS) analysis for protein-protein interactions. The supernatant was removed from the bead solution and 200 µl of 50 mM NH₄HCO₃ was added. The samples were then treated with 1 mM (final concentration) dithiothreitol (DTT) at 25°C for 30 minutes. This was followed by 5 mM (final concentration) iodoacetamide (IAA) at 25°C for 30 minutes in the dark.

Protein was digested with 1:100 (w/w) lysyl endopeptidase (Wako) at 25°C for 2 hours and trypsin (Promega) was added at 1:50 (w/w). The digestion was allowed to proceed overnight. Resulting peptides were desalted with a Sep-Pak C18 column (Waters) and dried under vacuum.

LC-MS/MS analysis

Dried peptides were reconstituted in 10 μ L of loading buffer (0.1% formic acid, 0.03% TFA, 1% acetonitrile). The sample (2 μ L) was loaded onto and eluted from a self-packed C18 fused silica column (25 cm x 75 μ M internal diameter (ID); New Objective, Woburn, MA) driven by a Dionex Ultimate 3000 RSLCNano UPLC system. Elution was performed over a 120 minute gradient at a rate of 300 nl/min with buffer B ranging from 3% to 65% (buffer A: 0.1% formic acid in water, buffer B: 0.1 % formic in acetonitrile). The spectra were monitored on a Fusion Mass Spectrometer (ThermoFisher Scientific, San Jose, CA). The mass spectrometer cycle was programmed to collect at top speed for 3-second cycles with higher-energy collision dissociation (HCD) fragmentation. The Mass Spectrometry (MS) scans (400-1600 m/z range, 200,000 AGC, 50 ms maximum ion time) were collected at a resolution of 120,000 at m/z 200 in profile mode while the HCD MS/MS spectra (0.7 m/z isolation width, 30% collision energy, 10,000 AGC target, 35 ms maximum ion time) were detected in the ion trap. Dynamic exclusion was set to exclude previous sequenced precursor ions for 20 seconds within a 10 ppm window. Precursor ions with +1, and +7 or higher charge states were excluded from sequencing.

Immunoprecipitation (IP)

IP analysis was performed as previously described [161]. Briefly, cells were lysed in 0.75% CHAPS lysis buffer, sonicated, and then lysis buffer was diluted to 0.375% CHAPS. Lysate was added to beads as indicated: HA conjugated beads (Sigma) for HA-DDB1 IP; Protein A agarose beads (Sigma) for GFP and EZH2 IP. Lysate and beads were incubated with antibodies as indicated on a rotor overnight at 4°C. Beads were subsequently washed four times as follows: each IP mixture was centrifuged at 1.0xg for 1 minute, supernatant was removed, and beads were washed in fresh lysis buffer. After the final wash, all liquid was removed from beads with a gage needle, and beads were denatured with 1X SDS sample buffer. Bead-sample buffer mixture was then loaded directly into wells of an SDS-PAGE gel.

UV irradiation

Cells were irradiated with a Spectro-Linker XL-1500 at 254 nm (UVC) at the indicated doses.

Laser microirradiation

The laser microirradiation assay was performed as described previously [162]. Briefly, cells were transfected with the indicated constructs and grown on glass bottom plates (MatTek Corporation) to 70% confluency. Live GFP-positive cells were located on a Zeiss Observer Z1 microscope while irradiation was performed using a Micropoint Laser Illumination and Ablation System (Photonic Instruments). Cells were irradiated at a wavelength of 365 nm and a laser output of 80%, tracing the pattern of the line. Real time images were captured by the Zeiss Observer Z1 microscope.

UV Micropore Assay

Cells were transfected with the indicated constructs and grown in glass bottom plates (MatTek Corporation) to 70% confluency. Cells were then washed in PBS and an isopore membrane with a 5 μm pore size (Millipore) was placed on the layer of cells. Cells were then UV irradiated at 100 J/m^2 followed by incubation at 37°C for 1 hour. Cells were then fixed in 4% PFA, permeabilized in 0.5% Triton X-100, blocked in 5% BSA in PBS, and stained with the indicated antibodies: anti-FLAG (1:500) anti- γH2AX (1:200), and anti-CPD (1:200). After washing off primary antibody in PBS, cells were stained secondarily with Alexa Fluor 488 or 555 antibodies. Cells were mounted in media with DAPI. For CPD staining, cells were denatured in 2N HCl for 30 minutes at room temperature prior to blocking and staining. Images were captured by the Zeiss Observer Z1 microscope.

Cell fractionation

Cellular fractionation was adapted from the literature as described [163]. Briefly, cells were harvested and pellets were lysed in hypotonic buffer (10 mM tris-HCl pH 7.3, 10 mM KCl, 1.5mM MgCl₂, 10 mM Beta-mercaptoethanol, 0.2 M PMSF), homogenized by 40 strokes in a Dounce homogenizer, and centrifuged at $2000 \times g$ for 15 minutes. Pellets were lysed in nuclear lysis buffer (15mM tris-HCl pH 7.3, 1 mM EDTA, 0.4 M NaCl, 1 mM MgCl₂, 10% glycerol, 10 mM Beta- mercaptoethanol, 0.2 M PMSF) for 30 minutes on ice, and centrifuged at maximum speed for 10 minutes. The supernatant was discarded and pellet was briefly washed in nuclear lysis buffer. Pellet was re-suspended in CS buffer (20 mM Tris-HCl pH 7.5, 100 mM KCl, 2 mM MgCl₂, 1 mM CaCl₂, 0.3 M sucrose, 0.1% Triton

X-100 and complete protease inhibitors) and digested with 2 Units MNase (Thermo Fisher) for 10 minutes at room temperature, to solubilize chromatin bound proteins. Digestion was stopped with 5 mM EGTA and 5 mM EDTA and samples were centrifuged at 2000xg for 5 minutes. The supernatant was collected as the solubilized chromatin fraction, denatured with sample buffer, and subjected to western blotting.

Slot blot assay

Cells were harvested under the conditions indicated and genomic DNA was isolated with a QIAamp kit (Qiagen). DNA was measured by nanodrop. For CPD detection, 25 ng of DNA were added in an excess of 0.4 M NaOH and 10mM EDTA buffer and was denatured by boiling at 100°C for 10 minutes. Samples were neutralized in 2 M ammonium acetate (pH 7.0). A nitrocellulose membrane was presoaked in 6 x SSC buffer and placed in a slot blot apparatus (Whatman Schleicher & Schuell Minifold I). Slots were first washed in 1 x TE buffer. DNA samples were then loaded in slots and washed in 2 x SSC buffer. The membrane was baked at 80°C for 2 hours, blocked in 5% BSA, and probed for CPDs at a dilution of 1:2,000. Total DNA was measured by SYBR Gold (Invitrogen) staining of the membrane at a concentration of 1:10,000.

FM-HCR Assay for NER Repair Capacity

NER reporter plasmid cocktails were transfected into HCT116 cells using lipofectamine 2000 (Invitrogen). For each experimental group, plasmids transfected included tagBFP and either an untreated mCherry plasmid or a mCherry plasmid that was UV irradiated with UVC light at a dose of 800J/m². After 24 hours, cells were analyzed for fluorescent

reporters by flow cytometry. NER repair capacity was calculated in terms of % reporter expression as previously described [164].

RNA extraction and RT-PCR

To extract RNA, cells were lysed in Trizol (Ambion) for 3 minutes followed by chloroform phase separation and isopropanol precipitation of RNA. cDNA synthesis was performed using FirstStrand SuperScript III CellsDirect cDNA Synthesis System (Invitrogen) using SuperScript III reverse transcriptase and Oligo(dT) primers. PCR was performed using TaqMan Fast Universal PCR Master Mix (ThermoFisher) and Taqman probes (ThermoFisher) to DDB2 and GAPDH transcripts. The 7500 Fast Real-Time PCR system was used in conjunction with 7500 software (LifeTechnologies) to perform the PCR reaction. Preliminary experiments were performed to determine the cycle numbers that were in the linear range of amplification for each transcript. RNA content was calculated by normalizing the amplification cycle number relative to a standard curve generated for each transcript of interest.

DDB2 ubiquitination

HEK-293T cells expressing Histidine-tagged ubiquitin (Addgene) maintained in 100 μ g/ml hygromycin were transfected, treated with cycloheximide and MG132, and/or damaged with UV as indicated. Cells were harvested at the indicated time points and lysed in a buffer containing 0.1M NaH₂PO₄ pH8, 600 mM NaCl, 8 M Urea, and 0.1% NP40, supplemented with anti-proteases and 10 mM *N*-Ethylmaleimide. For each IP, 3 mg of whole cell lysate was applied to 30 μ L of His-Tag Dynabeads (Thermo Fisher) for 2 hours.

Beads were then washed extensively in lysis buffer supplemented with 20 μ M Imidazole and subsequently denatured. The supernatant was then run on an SDS-PAGE.

Tumor Xenograft

Lung cancer tumor xenografts and treatments. Six-week-old female Nu/Nu nude mice were purchased from Envigo (Indianapolis, IN) and housed under pathogen-free conditions in microisolator cages. All animal treatments were undertaken in accordance with protocols approved by the Institutional Animal Care and Use Committee at Emory University. 1×10^7 H128 cells in 100 μ L PBS (Corning Inc., Corning, NY) were injected into subcutaneous tissue at the flank region of nude mice. Tumor-bearing mice were randomly grouped, and the tumors were allowed to grow about 150mm³ before treatment. Mice were treated with DZNep, cisplatin, or the combination intraperitoneally (i.p). Each group included 5 mice. During treatment, tumor volumes (V) were measured by caliper measurements once every two days and calculated with the formula: $V=(L \times W^2)/2$ (L: length; W: width). Mice were euthanized by inhaled CO₂ at the end of treatment. No blinding was performed. Power and sample size: For pairwise comparisons of interest with respect to mean tumor volume at the end of four weeks, we will be able to detect a minimum effect size of 2.0 with 80% power with 5 mice per group and a Type I error of 0.05 using a two-sample t-test for each comparison.

Statistical Analysis

Unless indicated, all experiments were performed in triplicate and data are represented as mean \pm standard deviation. P values were calculated with GraphPad Prism software using

a two-tailed Student's T-test. For correlation studies, the Pearson correlation coefficient and two-tailed P value were calculated. P values are represented as indicated: * $P \leq 0.05$
** $P \leq 0.01$ and *** $P \leq 0.001$.

Data Availability

The mass spectrometry proteomics data have been deposited to the ProteomeXchange Consortium via the PRIDE [165] partner repository (<http://www.ebi.ac.uk/pride>) with the dataset identifier PXD015683. Data can be accessed by reviewers during the peer-review process by using the following login credentials on the PRIDE partner repository website:

Username: reviewer52521@ebi.ac.uk

Password: SgIUmGm0

2.5 Results

A siRNA screen targeting nuclear enzymes identifies genes that mediate cisplatin resistance in SCLC

To identify genes critical for governing platinum resistance in SCLC, we performed a cisplatin sensitivity screen with siRNAs targeting 1,006 genes, biased towards nuclear enzymes for future translational application, in SCLC cells. We have previously used our nuclear enzyme siRNA library to perform drug sensitivity screens in other cancer cell types to identify novel regulators of the DDR [166, 167]. We chose the SCLC cell line H128, a cell line with intact DNA repair pathways from a treatment-refractory tumor. H128 cells are strongly resistant to cisplatin, with over 80 percent viability 72 hours following continuous cisplatin treatment at 5 μ M, the upper threshold of cisplatin dose achievable in patients. The screen was conducted in triplicate in 96-well plates using siRNA targeting ERCC1 and ATR as positive controls and a non-targeting (NT) siRNA as a negative control. Cells were transfected with the siRNA library, treated after 48 hours with or without cisplatin for 72 hours, and assayed for cell viability with resazurin reagent (**Fig. 2.1 A**). Sensitivity results from the screen are shown as a volcano plot of log₂-transformed average viability against strictly standardized mean difference (SSMD) (**Fig. 2.1 B**). We identified 118 cisplatin sensitization hits based on the following criteria: an average cell viability of <0.6, an average SSMD of <-2, and a two-tailed t-test p-value of <0.05. The Z-factor of the screen, an indicator of screen quality, was 0.556, which is in the excellent range, indicating that our screen is robust.

To characterize common pathways and potential interactions of our cisplatin sensitization hits, we performed gene ontology (GO) analysis (**Fig. 2.1 C**, **Fig. 2.2 A**) and network analysis (**Fig. 2.2 B**). As anticipated, DNA repair pathways, including NER, DNA replication, interstrand cross-link repair, and UV protection, emerged as key processes among the cisplatin sensitization hits, demonstrating that our screen can yield DDR proteins previously defined for mediating cisplatin resistance. We also identified histone modification, ubiquitination, chromosome separation, DNA geometric change, and peptidyl-arginine N-methylation, among other processes associated with the cisplatin sensitization hits.

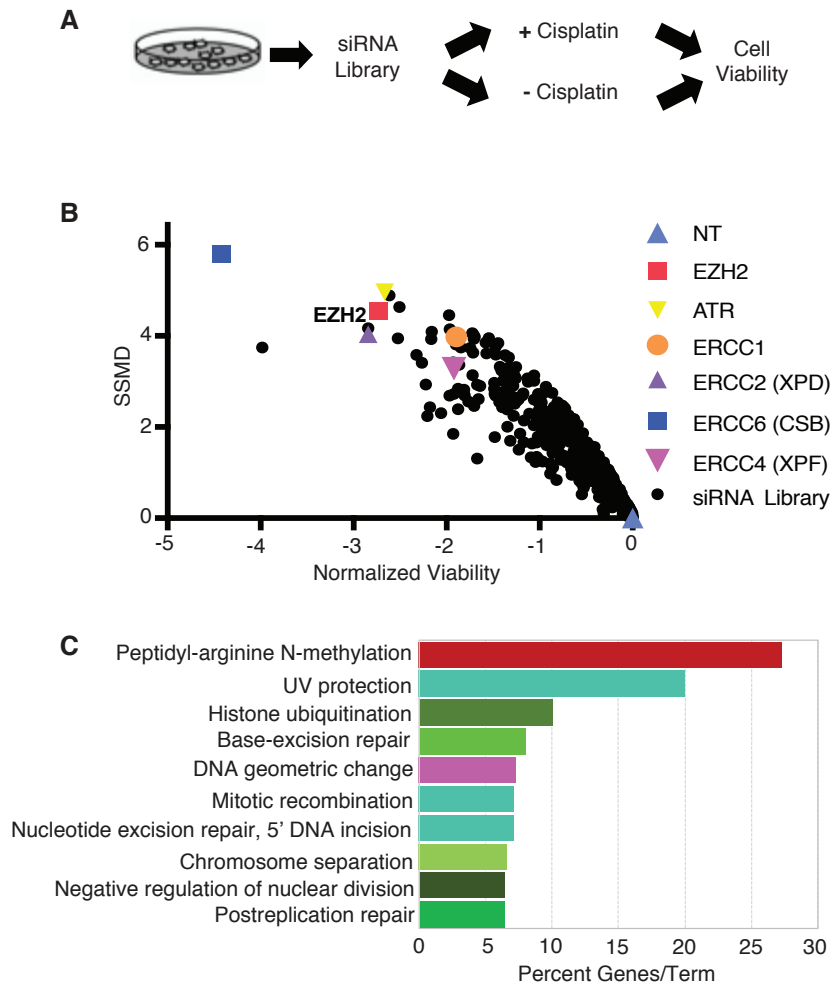


Fig. 2.1. A siRNA screen targeting nuclear enzymes identifies genes that mediate cisplatin resistance in SCLC.

(A) Primary screen format: H128 cells were transfected with a siRNA library biased towards targeting nuclear enzymes. 48 hours post-transfection, cells were treated with or without 10 μ M cisplatin for 72 hours prior to measuring cell viability. **(B)** Primary screen results: the normalized cell viability was plotted against the strictly standardized mean difference (SSMD) for each gene targeted by the library. Normalized viability was

calculated as the \log_2 ratio of treated versus untreated cell viability relative to the non-targeting (NT) siRNA control. **(C)** Summary of most enriched categories from Gene Ontology (GO) analysis of cisplatin sensitization hits ($n = 118$). The top 10 significant processes ($p \leq 0.01$) are shown, sorted by the percent associated genes found.

(A) Results of complete Gene Ontology (GO) analysis of cisplatin sensitization hits (n = 118). Hits met three requirements: log₂ average viability of <-0.75, an average SSMD of <-2, and a 2-tailed t-test p value of <0.05. ClueGO plugin was used with Cytoscape to perform the GO analysis. Red asterisks indicate statistical significance (p-value ≤0.01).

(B) Enriched GO network of cisplatin sensitization hits (n = 118). Only cisplatin sensitization hits were used to build the network. The GO terms enriched among the significant hits are represented by nodes, shown with color filled circles, where each color represents a GO category. The label of the most significant GO term within the category is used as leading group term. The size of the node indicates the term significance (all nodes p-value ≤0.05) and the color of the node represent the grouping by GO categories. For example, the DNA repair term shown in the maroon filled circle associated with 23 genes (small maroon-filled dots) from the input list. The GO term nodes are connected (edges) based on their kappa score (>=0.4) and shows the relationships between the terms and genes.

Indeed, a number of NER factors emerged as cisplatin sensitization hits in our primary screen: ERCC1, ERCC2, ERCC4 and ERCC6. EZH2 was among the most efficient sensitizing hits identified, which when silenced, sensitized H128 cells to cisplatin to a similar magnitude as the NER hits. EZH2 is intriguing because it was the only cisplatin sensitization hit that showed significant overexpression in SCLC tissue compared to normal lung epithelial tissue [168, 169], and EZH2 overexpression has been shown to mediate cisplatin resistance in several other cancer cell types [148-151]. One microarray expression dataset reported that EZH2 mRNA was expressed 21 ($p=6.01E-9$)* fold greater in SCLC versus normal lung tissue [168], while another reported that EZH2 mRNA was expressed 3.9 ($p=3.01E-4$)* fold greater in SCLC versus normal lung tissue [169]. We also found that EZH2 protein level was overexpressed in SCLC cell lines compared to nontumorigenic BEAS-2B and HSAEC lung epithelial cells (**Fig. 2.4 A**). Thus, EZH2 may be a promising therapeutic target for overcoming cisplatin resistance in SCLC.

EZH2 mediates cisplatin resistance in SCLC

From the primary screen, 23 hits were selected for further validation based on previous identification in other high-throughput DNA damage sensitivity screens, putative interactions with known DNA repair proteins by mass spectrometry (MS), or potential disease relevance, including in SCLC. To validate each target, we tested if the cisplatin sensitization phenotype could be achieved across more than one individual siRNA to rule out off-target effects of the pooled siRNA used in the primary screen. Of the 23 hits tested, 13 were validated, including EZH2. Two unique siRNAs targeting EZH2 sensitized H128 cells to cisplatin (**Fig. 2.3 A, Fig. 2.4 B**) and western blot confirmed successful EZH2

knockdown (**Fig. 2.3 B**). We validated this phenotype in H146 SCLC cells (**Fig. 2.3 C-D**), though the results were not as strong as H128 cells, perhaps due to the lower EZH2 levels in H146 cells (**Fig. 2.3 E**). Of note, a correlation between the degree of EZH2 knockdown with cisplatin sensitization was observed between the two siRNAs (**Fig. 2.3 A-D and Fig. 2.4 B**), and furthermore, a third unique siRNA targeting EZH2 sensitized H128 cells to cisplatin, which could be rescued with GFP-EZH2 expression (**Fig. 2.10 E**), providing additional support that the cisplatin sensitization phenotype following EZH2 depletion in SCLC cells is not due to an off-target effect.

EZH2 expression level positively correlates with cisplatin resistance across SCLC

Because EZH2 is highly expressed in SCLC and EZH2 depletion in SCLC cells causes cisplatin hypersensitivity, we hypothesized that EZH2 levels could be an important determinant of cisplatin resistance in SCLC. To this end, we examined a panel of six SCLC cell lines for EZH2 protein expression compared to cisplatin IC50 [154] (**Fig. 2.3 E-F**). We found a positive correlation between EZH2 expression and cisplatin IC50 trending towards significance, suggesting that as EZH2 expression increases, SCLC cells become more resistant to cisplatin.

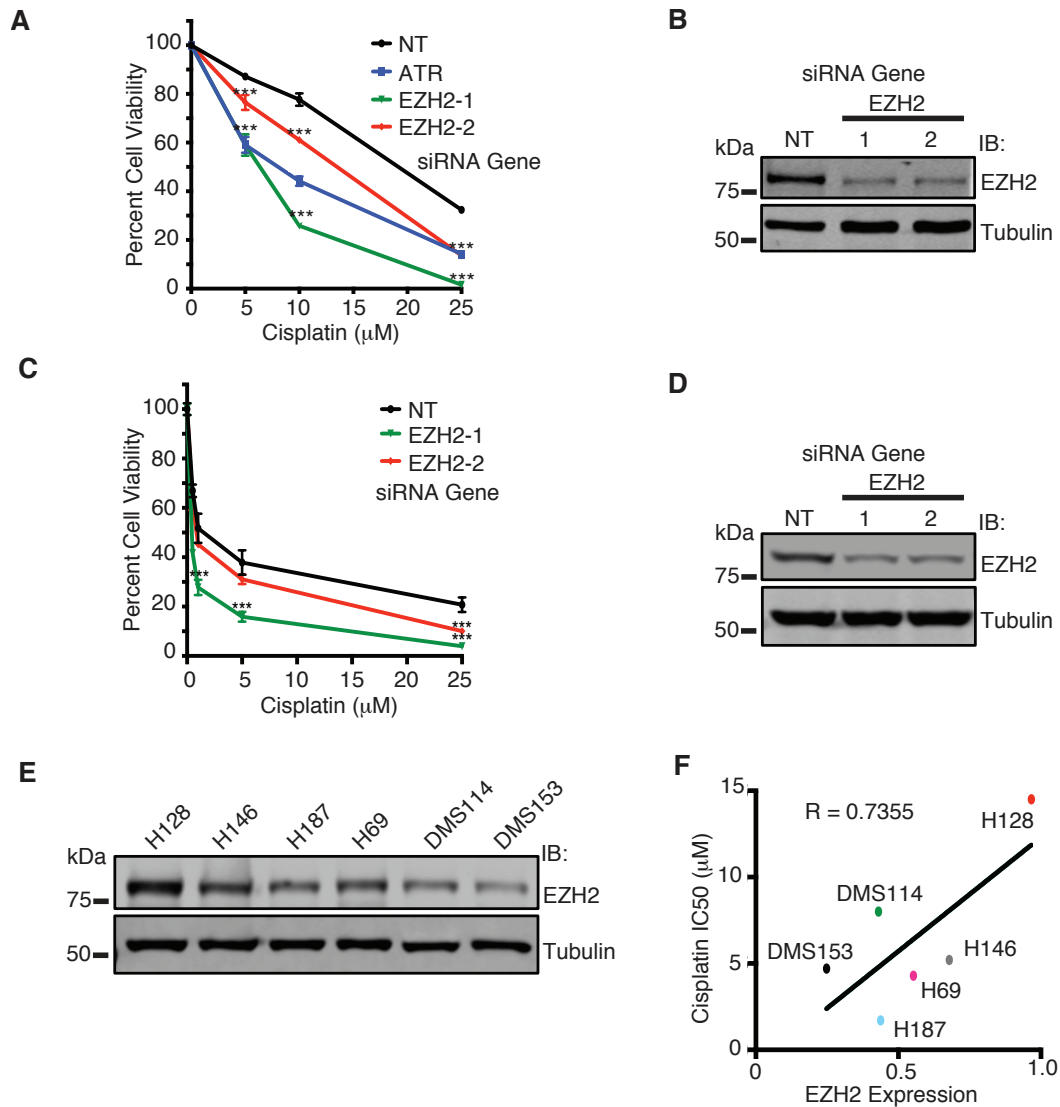


Fig. 2.3. EZH2 mediates cisplatin resistance in SCLC.

(A) H128 and (C) H146 cells were transfected with siRNA targeting EZH2, ATR, or a NT control. 72 hours after transfection, cells were treated with cisplatin for 72 hours prior to measuring cell viability. (B and D) Western blot analysis of EZH2 expression in (B) H128 and (D) H146 cells, respectively, demonstrating EZH2 knockdown. (E) Western blot analysis of EZH2 expression across a panel of SCLC cell lines. (F) Densitometry quantification of EZH2 expression corresponding to e was plotted against cisplatin IC50

[154] across a panel of SCLC cell lines, with a correlation of 0.7355. (For **A** and **C**, mean and standard deviation of three replicas is shown.) *** indicates $p < 0.001$.

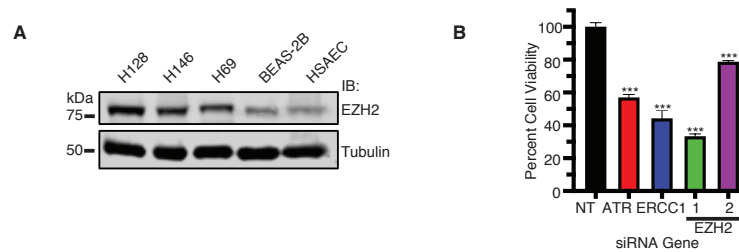


Fig. 2.4. EZH2 mediates cisplatin resistance and is overexpressed in SCLC cells.

(A) Western blot analysis showing that expression of EZH2 is increased in SCLC cells (H128, H146 and H69) compared with nontumorigenic lung epithelial cells (BEAS-2B and HSAEC). **(B)** Cell viability analysis of H128 cells transfected with siRNAs targeting ATR, ERCC1, or EZH2. Knockdown of ATR, ERCC1 and EZH2 all sensitized H128 cells to 10 μ M cisplatin treatment for 72 hours.

EZH2 localizes to UV damage sites and promotes repair of UV-induced CPD lesions

Cisplatin and UV-induced damage can be repaired by multiple DNA repair pathways, including NER. To determine if EZH2 plays a role in NER, we examined if EZH2 knockdown sensitizes SCLC cell lines to UV damage, which is primarily repaired by NER. We found that EZH2 depletion sensitized H128, H146 and U2OS cells to UV (**Fig. 2.5 A-D, Fig. 2.6 A-E**). EZH2 has been reported to localize to DSBs and DNA damage sites induced by laser microirradiation [152, 153]. We similarly found that GFP-EZH2 expressed in cells localizes to DNA damage sites induced by laser microirradiation at 365 nm (**Fig. 2.5 E**), which causes multiple forms of DNA damage, including CPDs, DSBs, single-strand breaks, crosslinks, and ROS-DNA damage. To determine if EZH2 responds more specifically to lesions repaired by NER, we examined if EZH2 could comparably localize to damage sites induced by a UVC lamp filtered through a micropore membrane overlaying the cells. Indeed, GFP-EZH2 localized to UV damage sites marked by the NER lesion CPD as well as γ H2AX (**Fig. 2.5 F, Fig. 2.6 F**), suggesting that EZH2 may have a role in the repair of UV damage requiring its direct localization. A number of factors involved in the NER pathway are established to localize to the chromatin soluble fraction of internucleosomal DNA in response to UV, including DDB1, DDB2, and XPC [170]. As expected, EZH2 was associated with a chromatin insoluble fraction both before and after UV damage, likely due to its canonical role in PRC2 (data not shown). Interestingly, we found that a population of EZH2 was recruited to the chromatin soluble internucleosomal fraction in response to UV damage (**Fig. 2.5 G**). Given that EZH2 co-localizes with CPD at UV damage sites, we then examined if EZH2 could promote the resolution of CPD lesions. Using slot blot analysis, we found that EZH2 knockdown impaired the resolution

of CPD lesions in response to UV (**Fig. 2.5 H, 2.5 I**). More directly, we observed that EZH2 knockdown caused a reduction in NER repair capacity using a fluorescence based multiplex host cell reactivation (FM-HCR) assay [164] (**Fig. 2.5 J**). Collectively, these data indicate that EZH2 mobilizes to and governs the repair of CPD crosslinks induced by UV irradiation.

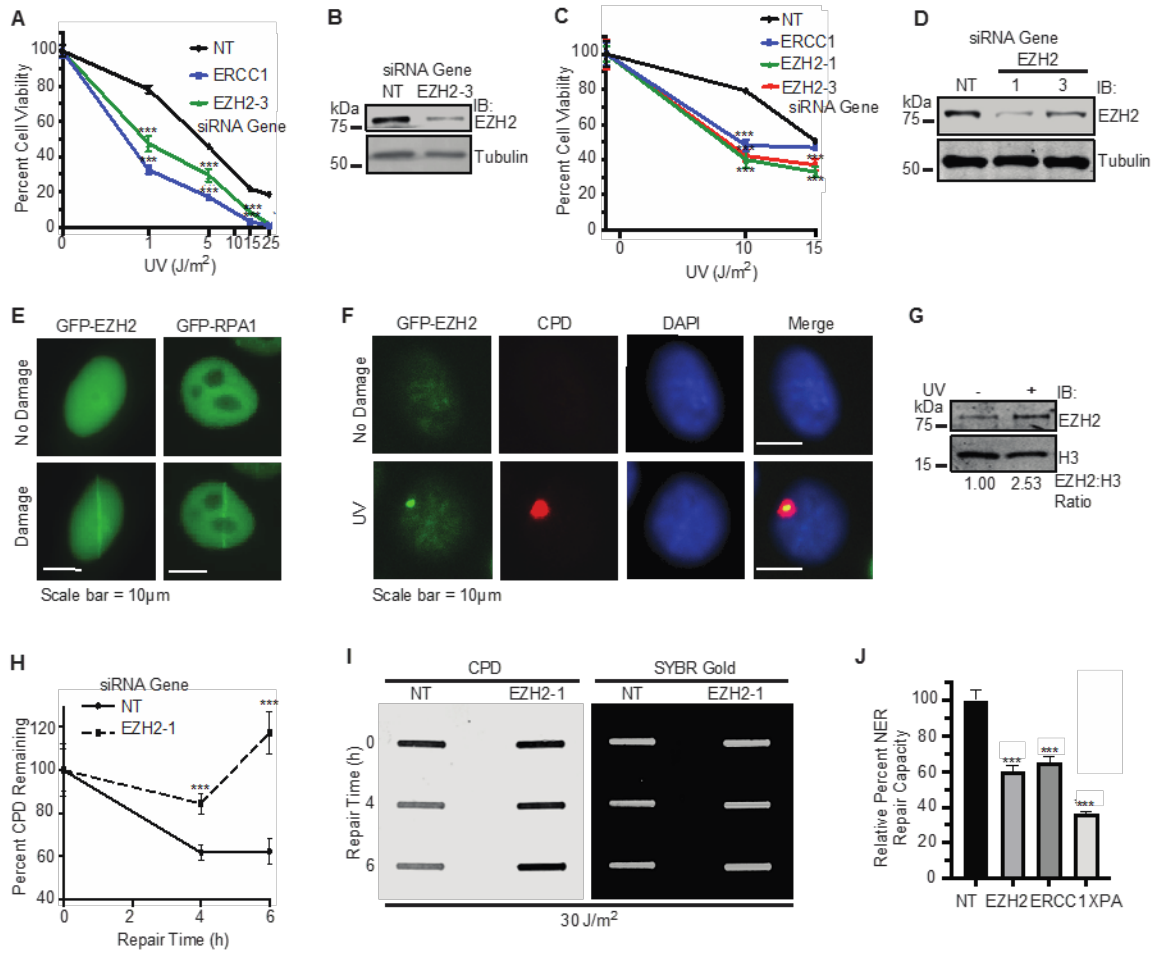


Fig. 2.5. EZH2 localizes to and promotes repair of UV-induced CPD lesions.

(A) H128 and (C) H146 cells were transfected with siRNAs targeting EZH2, ERCC1, or a NT control. 72 hours after transfection, cells were treated with UV. Cell viability was measured 72 hours after UV irradiation. (B) and (D) Western blot analysis of EZH2 expression (for (B) H128; and (D) H146 cells) demonstrating knockdown. (E) HeLa cells were transiently transfected with GFP-EZH2 or GFP-RPA1. 72 hours post-transfection, cells were subjected to laser microirradiation at 365 nm wavelength. Representative images of GFP localization as seen before and seconds after laser microirradiation are shown. Scale bars represent 10 μ m. (F) HeLa cells were transfected with GFP-EZH2 and 24 hours

post transfection, cells were UV irradiated at 100 J/m^2 through a $5 \text{ }\mu\text{m}$ micropore membrane. Cells were fixed and stained with the indicated markers after one hour recovery. Representative images are shown. **(G)** HeLa cells were left untreated or UV irradiated at 30 J/m^2 . Cells were lysed and fractionated to obtain the chromatin soluble fraction by salt extraction followed by 10 minutes of MNase digestion at room temperature. This fraction was run on SDS-PAGE and probed for EZH2 and H3 for loading. **(H and I)** Slot blot analysis of the repair of CPD lesions over time in H128 cells in response to 30 J/m^2 of UV. **(H)** Quantitation of percent of CPD lesions remaining over time. **(I)** Representative slot blot. SYBR Gold signal indicates total DNA loaded. (For **A**, **C**, and **H**, mean and standard deviation of three replicas is shown. **(J)** NER repair capacity as measured by FM-HCR was quantified in cells transfected with siRNAs targeting EZH2, ERCC1, XPA or NT control. Relative NER repair capacity was normalized to a NT control. *** indicates $p < 0.001$. For **G** and **I-J**, representative blots from 3 independent experiments ($n=3$) is shown).

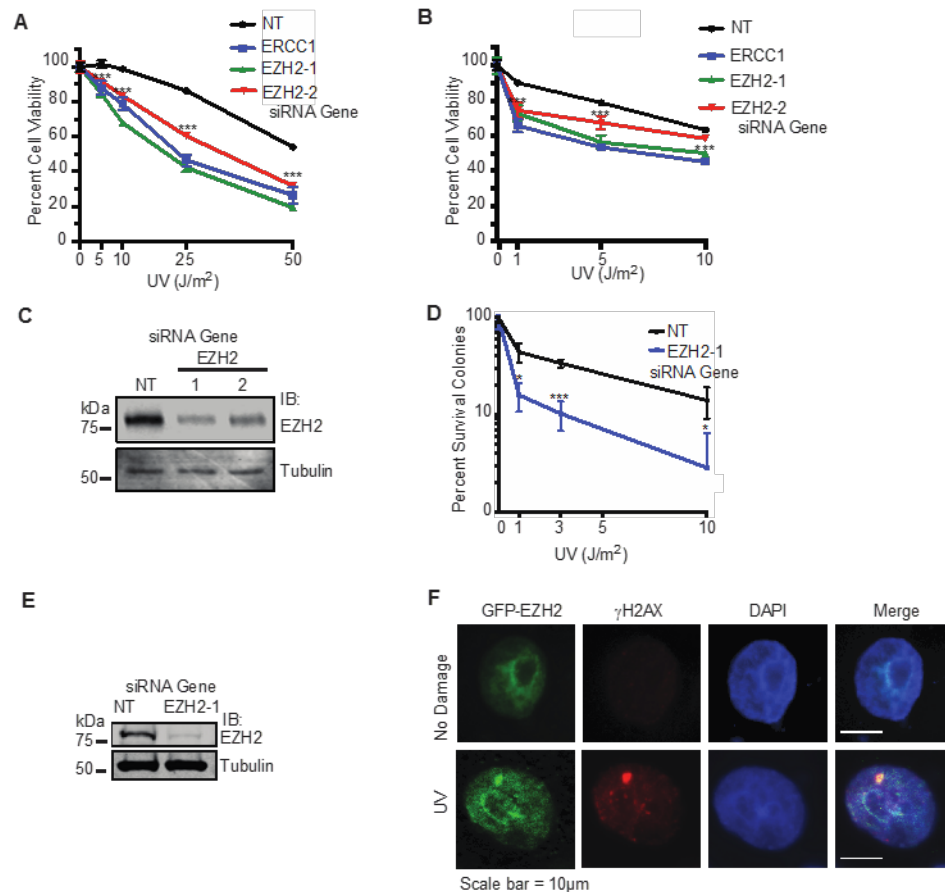


Fig. 2.6. EZH2 localizes to and promotes repair of UV-induced CPD lesions.

(A) H128 and (B) H146 cells were transfected with siRNAs targeting EZH2, ERCC1, or a NT control. 72 hours after transfection, cells were treated with UV. Cell viability was measured 72 hours after UV irradiation. (C) Western blot analysis of H146 (corresponding to b) showing knockdown of EZH2 across indicated siRNAs was achieved. (D) Clonogenic assay of U2OS cells sensitized to UV in response to EZH2 knockdown. Cells were transfected with siRNAs targeting EZH2 (siEZH2-1) as well as a non-targeting siRNA. 48 hours after transfection, cells were plated sparsely and treated the following day with UV. Colonies were grown until untreated colonies reached 50 cells or greater in number and

were non-overlapping. Colonies were stained with crystal violet and quantified. Mean and standard deviation of three replicas is shown. * indicates $p < 0.05$, *** indicates $p < 0.001$.

(E) Western blot analysis (corresponding to **D**) to show knockdown of EZH2 was achieved in U2OS. **(F)** EZH2 co-localizes with γ H2AX at sites of UV damage generated by UV irradiation filtered through a 5 μ m micropore membrane. HeLa cells were transfected with GFP-EZH2 and 24 hours post transfection, cells were UV irradiated at 100 J/m² through a micropore membrane and given one hour to recover. Cells were fixed and stained with the indicated markers. Representative images of sites of UV damage through the micropore are shown.

EZH2 interacts with and is epistatic with DDB1-DDB2 in sensitizing SCLC cells to cisplatin and UV

To provide insight into how EZH2 governs cisplatin and UV resistance, we performed MS analysis of GFP-EZH2 purified from cells treated with cisplatin (**Fig. 2.7 A**). As expected, we found enrichment of EZH2 as well as key members of the PRC2 complex, SUZ12 and EED (**Fig. 2.7 B**). Interestingly, we also found enrichment of DDB1, a member of the NER pathway. Co-IP of GFP-EZH2 pulled down HA-DDB1 (**Fig. 2.7 C**), and similarly, reciprocal co-IP of HA-DDB1 pulled down GFP-EZH2 in cells (**Fig. 2.7 D**). This interaction was preserved following benzonuclease treatment (**Fig. 2.8 A**), suggesting that the interaction is not mediated through DNA. No change in interaction was observed following cisplatin treatment (**Fig. 2.8 B**), implying that the interaction is not regulated by DNA damage in this context. Co-IP of GFP-EZH2 also pulled down both endogenous DDB1 and DDB2, its interacting partner (**Fig. 2.7 E**). We also validated the endogenous interaction of EZH2 with DDB1-DDB2 in H128 cells by co-IP (**Fig. 2.7 F**), confirming that EZH2 complexes with DDB1-DDB2 in SCLC cells. To identify the region of DDB2 that interacts with EZH2, we generated FLAG-DDB2 deletion mutants and performed co-IP of FLAG-DDB2 WT and mutants with GFP-EZH2 in HEK293T cells. FLAG-DDB2 1-196 but not DDB2 Δ 40 co-IP'd with GFP-EZH2 (**Fig. 2.8 C**), indicating that DDB2 1-196 is sufficient and DDB2 1-40 is necessary for interaction with EZH2 and suggesting that EZH2 interacts with the N-terminus of DDB2. Because EZH2 and DDB1-DDB2 mediate resistance to UV [40] we performed epistasis experiments to determine if they function together in a common pathway. Indeed, combined knockdown of EZH2 and DDB1/DDB2 caused no further sensitization of SCLC cells to UV and cisplatin compared with

knockdown of EZH2 or DDB1/DDB2 alone (**Fig. 2.7 G-K**), implying that EZH2 and DDB1-DDB2 function together in governing UV and cisplatin resistance in SCLC cells.

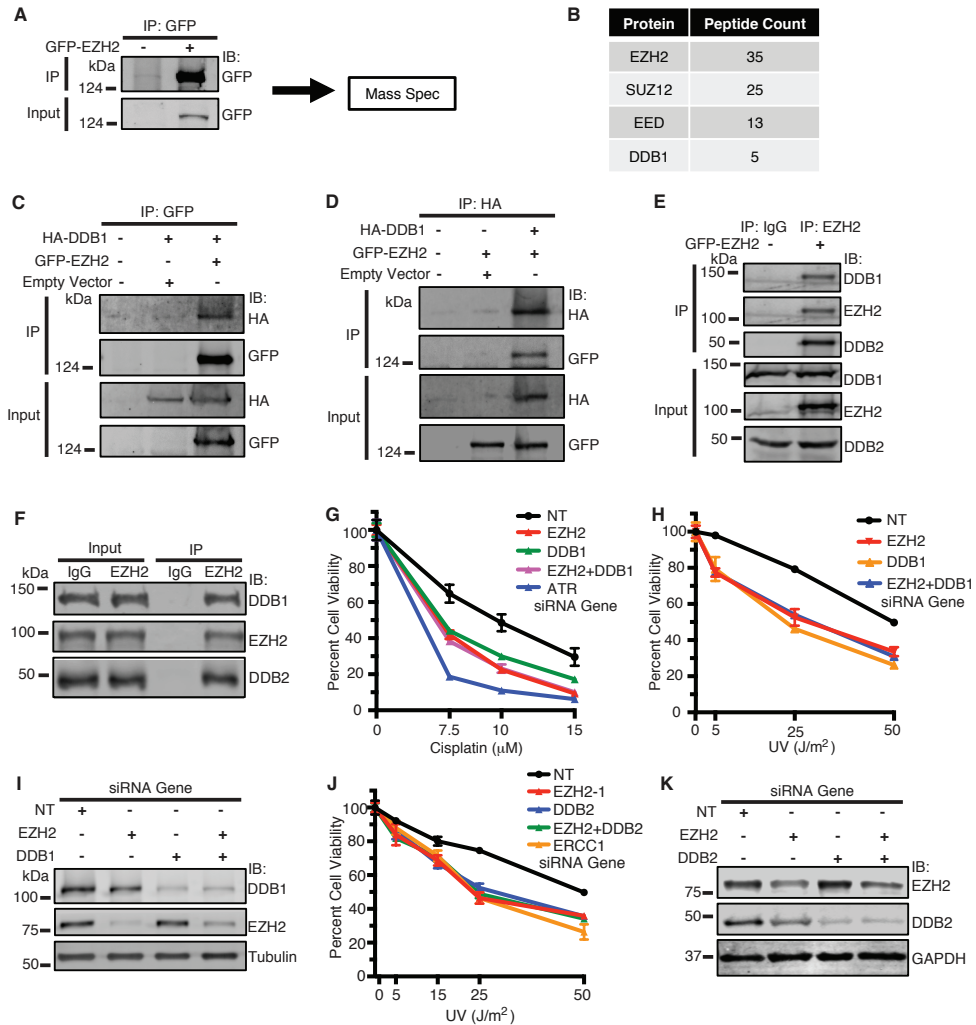


Fig. 2.7. EZH2 interacts with and is epistatic with DDB1-DDB2 in sensitizing SCLC cells to cisplatin and UV.

(A) HeLa cells were transiently transfected with GFP-EZH2. 72 hours post-transfection, cells were treated with 25 μ M cisplatin and harvested 4 hours later, and GFP-EZH2 was immunoprecipitated (IP'd) with protein A agarose beads. Beads were washed and processed for mass spectrometry (MS) analysis for protein-protein interactions. (B) Summary of IP-MS results for GFP-EZH2. (C) and (D) HeLa cells were transfected with

HA-DDB1 and GFP-EZH2 or empty vector and IP'd with an anti-GFP antibody **(C)** or anti-HA antibody **(D)** respectively, run on SDS-PAGE, and immunoblotted with indicated antibodies. **(E)** HeLa cells were transfected with GFP-EZH2. Cells were harvested, lysed, and IP'd with an anti-EZH2 antibody or IgG as indicated. Samples were run on SDS-PAGE and immunoblotted with indicated antibodies. **(F)** H128 cells were lysed and IP'd with an anti-EZH2 antibody or IgG as indicated. Samples were run on SDS-PAGE and immunoblotted with indicated antibodies. **(G)**, **(H)** and **(J)** H128 cells were transfected with siRNAs targeting EZH2, DDB1, DDB2, ATR, ERCC1, or a NT control. 72 hours after transfection, cells were treated with cisplatin or UV. Cell viability was measured 72 hours after treatment. **(I)** Western blot analysis of samples corresponding to **(G)** and **(H)**. **(K)** Western blot analysis of samples corresponding to **(J)**. (For **G**, **H** and **J**, mean and standard deviation of three replicas is shown. For **C-F**, representative blots from 3 independent experiments (n=3) is shown).

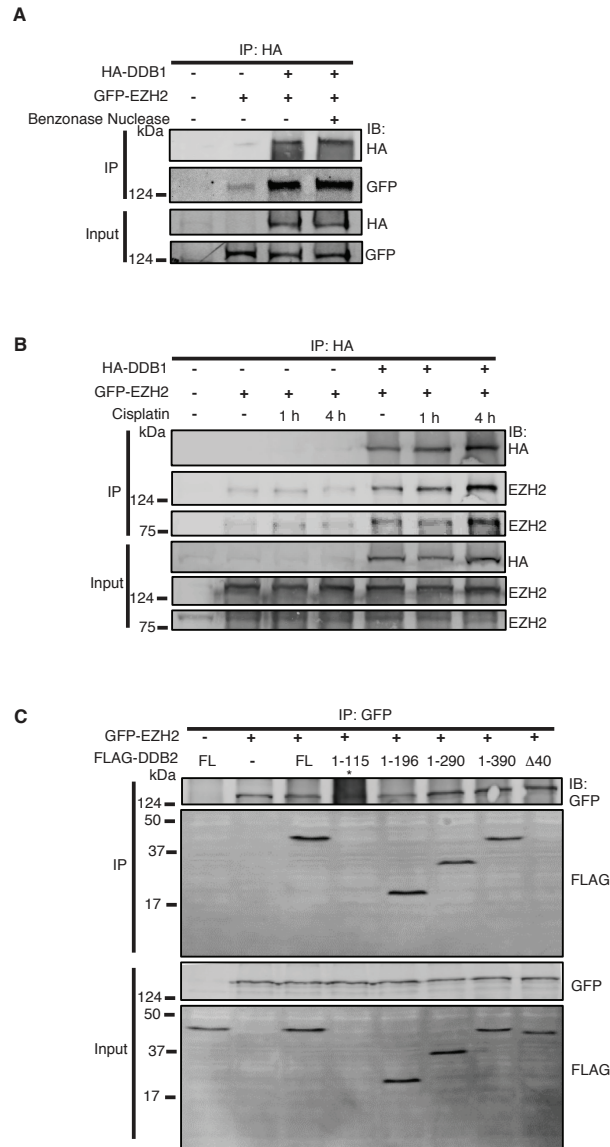


Fig. 2.8. EZH2 interacts with and is epistatic with DDB1/DDB2 in sensitizing SCLC cells to cisplatin and UV. **(A)** HeLa cells were transfected with GFP-EZH2 and HA-DDB1 as indicated. Cells were treated with no drug or 25 μ M cisplatin and harvested after 1 hour or 4 hours of continuous drug treatment. Cells were lysed and IP'd with an anti-HA antibody, run on SDS-PAGE, and immunoblotted with indicated antibodies. **(B)** HeLa cells were transfected with GFP-EZH2 and HA-DDB1 as indicated. Cells were harvested, and lysis buffer was left untreated or treated with 20 U/mL benzonase nuclease (Sigma) per sample.

Samples were IP'd with an anti-HA antibody, run on SDS-PAGE, and immunoblotted with indicated antibodies. (C) HEK-293T cells were transfected with GFP-EZH2 and FLAG-DDB2 deletion constructs as indicated. Cells were lysed and IP'd with an anti-GFP antibody, run on SDS-PAGE, and immunoblotted with indicated antibodies. Asterisk * indicates that FLAG-DDB2 1-115 failed to express. Whole cell lysate of each sample IP'd is represented by input. (For A-C, representative blots from 3 independent experiments (n=3) is shown).

EZH2 promotes DDB2 stability independent of its catalytic activity and PRC2

Given that EZH2 complexes with and is epistatic with DDB1-DDB2 in mediating cisplatin and UV resistance in SCLC and promotes CPD crosslink repair, we sought to determine if EZH2 plays a specific role in the NER pathway. Interestingly, EZH2 knockdown decreased DDB2 but not DDB1 protein levels both at baseline and more prominently in response to UV and cisplatin treatment in H128 and HCT116 cells (**Fig. 2.9 A-B, Fig. 2.10 A**). Quantitative RT-PCR revealed no corresponding significant decrease in DDB2 mRNA levels following EZH2 knockdown (**Fig. 2.9 C, Fig. 2.10 B**), suggesting that the EZH2-mediated decrease in DDB2 protein levels is likely not through EZH2's canonical role in transcription. Consistently, the DDB2 degradation phenotype was alleviated by proteasomal inhibition with MG132 (**Fig. 2.9 D**), implying that the decrease in DDB2 levels are a result of proteasomal degradation and that EZH2 promotes DDB2 stability. Overexpression of GFP-EZH2 in HCT116 cells also increased DDB2 protein levels at baseline and in response to UV (**Fig. 2.9 E**).

To determine if EZH2 methyltransferase activity promotes DDB2 stability, we overexpressed catalytically inactive GFP-EZH2 H689A and found a similar increase in DDB2 levels (**Fig. 2.9 E, Fig. 2.10 C**). Furthermore, the decrease in DDB2 levels resulting from EZH2 depletion in H128 cells was rescued by expression of GFP-EZH2 WT and H689A (**Fig. 2.9 F**), suggesting that EZH2 has a non-catalytic role in promoting DDB2 stability. Consistently, treatment of H128 and HCT116 cells with EPZ-6438, a S-Adenosyl-l-methionine (SAM) competitive EZH2 inhibitor, which targets its catalytic activity but does not deplete EZH2 levels, did not decrease DDB2 levels at baseline or in

response to UV (**Fig. 2.9 G, Fig. 2.10 D**). We also found that the cisplatin hypersensitivity of H128 cells depleted of EZH2 is alleviated by expression of GFP-EZH2 WT and to a lesser extent H689A (**Fig. 2.10 E**), suggesting that EZH2 also has a catalytically inactive role in mediating cisplatin resistance; however, because GFP-EZH2 H689A only partially rescued the cisplatin hypersensitivity of EZH2 depletion, EZH2's noncatalytic role in promoting DDB2 stability may not fully account for its effects on mediating cisplatin resistance.

To determine if EZH2 promotes DDB2 stability in association with PRC2, we overexpressed phospho-mimetic FLAG-EZH2 T311E, which impairs its interaction with SUZ12 and its methyltransferase activity [87]. Overexpression of FLAG-EZH2 T311E but not non-phosphorylatable FLAG-EZH2 T311A strongly increased DDB2 levels, indicating that when EZH2 is decoupled from PRC2, it is able to participate in stabilizing DDB2 and promoting NER. (**Fig. 2.9 H**). Moreover, SUZ12 knockdown in H128 cells failed to decrease DDB2 levels at baseline or in response to UV (**Fig. 2.9 I**). Given that DDB2 is targeted for degradation by ubiquitination, we tested the effect of EZH2 depletion on DDB2 ubiquitination and found that it was enhanced in response to UV damage (**Fig. 2.9 J**). DDB2 has been reported to negatively regulate p21 levels in NER [171, 172] so, we examined if EZH2 depletion results in p21 upregulation. Indeed, EZH2 knockdown also caused a corresponding increase in p21 levels with a decrease in DDB2 levels at baseline and in response to cisplatin treatment (**Fig. 2.10 F**), providing further support that EZH2 promotes DDB2 stability and that EZH2 may promote NER through DDB2. Collectively,

our findings suggest that EZH2 promotes DDB2 stability by impairing its ubiquitination independent of its catalytic activity and PRC2.

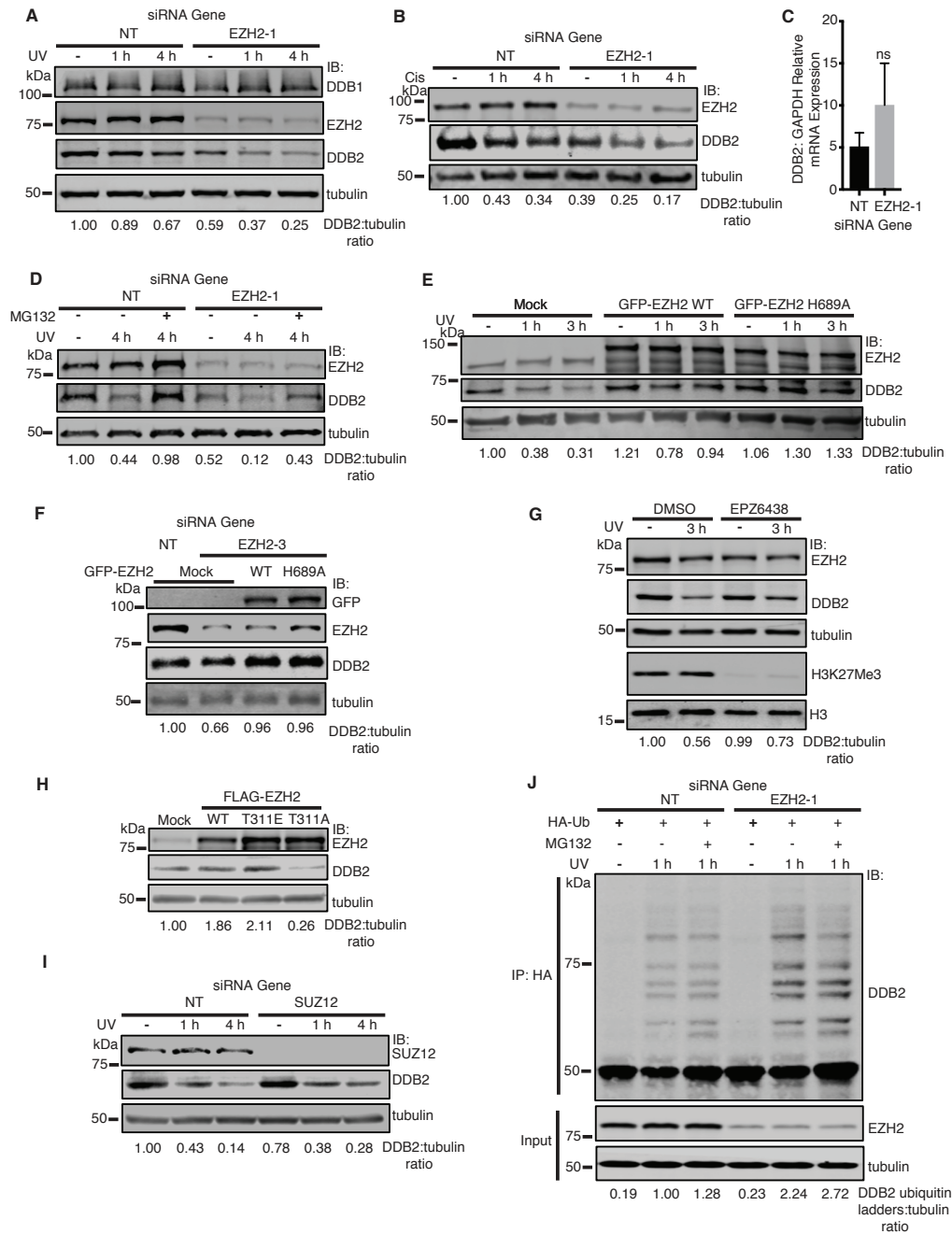


Fig. 2.9. EZH2 promotes the stability of DDB2 independent of its catalytic activity and PRC2.

(A-D) EZH2 promotes the stability of DDB2. H128 cells were transfected with siRNAs targeting EZH2 or a NT control. 72 hours after transfection, cells were pre-treated with cycloheximide (CHX) for 2 hours, and UV irradiated at 30 J/m^2 (A), treated with $15 \mu\text{M}$

cisplatin **(B)**, or left untreated (-). Cells were harvested after treatment as indicated. Whole cell lysates were run on SDS-PAGE and immunoblotted with the indicated antibodies. **(C)** EZH2 knockdown does not alter mRNA levels of DDB2. H128 cells were transfected with siRNAs targeting EZH2 or a NT control and RT-PCR analysis was performed to measure DDB2 and GAPDH mRNA levels. The relative ratio of DDB2 to GAPDH mRNA level is represented. Mean and standard deviation of three replicas is shown. **(D)** H128 cells were transfected with siRNAs targeting EZH2 or a NT control. 72 hours post transfection, cells were pre-treated with 5 μ M MG132 for 4 hours, and CHX for 2 hours for all groups. Cells were then UV irradiated at 30 J/m² and harvested at the indicated timepoints prior to SDS-PAGE and western blot analysis with indicated antibodies. **(E-I)** EZH2 stabilization of DDB2 is independent of its PRC2 function. **(E)** HCT116 cells were transfected with GFP-EZH2 WT or GFP-EZH2 catalytic inactive mutant (H689A) plasmids. 24 hours post transfection, cells were pre-treated with CHX for 2 hours, and left untreated (-) or UV irradiated at 30 J/m², harvested after UV treatment as indicated, run on SDS PAGE, and probed with indicated antibodies. **(F)** H128 cells were knocked down with siRNAs targeting the EZH2 5'UTR (EZH2-3) or a NT control, and the following day, transfected with GFP-EZH2 WT or GFP-EZH2 catalytic inactive mutant (H689A) or mock transfected. 48 hours post-transfection, groups were pre-treated with CHX for 2 hours, harvested, run on SDS PAGE, and probed with the indicated antibodies. **(G)** HCT116 cells were pre-treated with 1 μ M SAM-competitive EZH2 inhibitor EPZ-6438 or DMSO for 4 days. Cells were then pre-treated with CHX for 2 hours. Cells were left untreated (-) or UV irradiated at 30 J/m² and harvested after 3 hours recovery. Whole cell lysates were run on SDS-PAGE and immunoblotted with the indicated antibodies. **(H)** HeLa cells were

transfected with FLAG-EZH2 WT or PRC2 mutants (FLAG-EZH2 T311E/A). 48 hours post transfection, cells were pre-treated with CHX for 2 hours, and harvested. Whole cell lysates were run on SDS-PAGE and immunoblotted with the indicated antibodies. **(I)** HCT116 Cells were transfected with siRNAs targeting SUZ12 or a NT control. 72 hours after transfection, cells were pre-treated with CHX for 2 hours, and left untreated (-) or UV irradiated at 30 J/m², and harvested after UV treatment as indicated. Whole cell lysates were run on SDS-PAGE and immunoblotted with the indicated antibodies. **(J)** His-Ubi HEK-293T cells were transfected with indicated siRNA and 72 hours post transfection, cells were pre-treated with CHX and MG132 where indicated. Ubiquitinated DDB2 was measured. (For **A-B** and **D-J**, representative blots from 3 independent experiments (n=3) is shown).

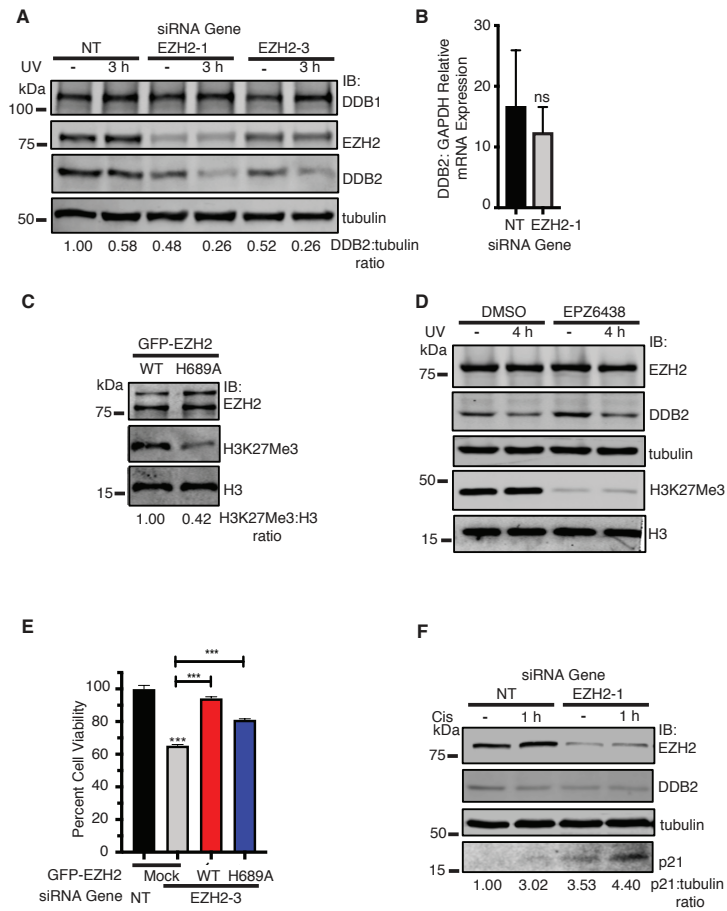


Fig. 2.10. EZH2 promotes the stability of DDB2 independent of its catalytic activity and PRC2.

(A) HCT116 cells were transfected with siRNAs targeting EZH2 or a NT control. 72 hours after transfection, cells were pre-treated with cycloheximide (CHX) for 2 hours, and left untreated (-) or UV irradiated at 30 J/m^2 , and harvested after UV treatment as indicated. Whole cell lysates were run on SDS-PAGE and immunoblotted with the indicated antibodies. (B) HCT116 cells were transfected with indicated siRNA and RT-PCR analysis was performed to measure DDB2 and GAPDH mRNA levels. Relative DDB2 to GAPDH mRNA ratio is represented. Mean and standard deviation of three replicas is shown.

(C) HCT116 cells were transfected with the indicated plasmids. Proteins were acid extracted and run on SDS-PAGE gel prior to western blot analysis with indicated antibodies. (D) HCT116 cells were pre-treated with EPZ6438 or DMSO for 4 days. Cells were then pre-treated with CHX for two hours. Cells were left untreated (no damage) or UV irradiated at 30 J/m^2 and harvested after three hours recovery. Whole cell lysates were run on SDS-PAGE and immunoblotted with the indicated antibodies. (For A, C and D, representative blots from 3 independent experiments (n=3) is shown). (E) H128 cells were transfected with siRNAs targeting the EZH2 5'UTR (EZH2-3) or a NT control. The following day, cells were transfected with plasmids GFP-EZH2 WT, H689A mutant or mock transfected. 48 hours after transfection, cells were treated with $6.25 \mu\text{M}$ cisplatin. Cell viability was measured 72 hours after cisplatin treatment. (F) H128 cells were transfected with siRNAs targeting EZH2 or a NT control. 72 hours after transfection, cells were pre-treated with CHX for 2 hours, and left untreated (-) or $15 \mu\text{M}$ cisplatin, and harvested after 1 hour of treatment. Whole cell lysates were run on SDS-PAGE and immunoblotted with the indicated antibodies.

DDB2 functions downstream of EZH2 in promoting NER

To determine if EZH2 facilitates DDB2 function in NER, we examined DDB2 localization to UV micropore-generated CPD foci. EZH2 knockdown significantly impaired DDB2 localization to CPD foci (**Fig. 2.11 A-B**), suggesting that EZH2 promotes DDB2 localization to CPD lesions. Furthermore, the expression of FLAG-DDB2 rescued the impairment in resolution of CPD lesions following EZH2 knockdown (**Fig. 2.11 C-D**), showing unequivocally that EZH2 promotes the repair of CPD lesions through DDB2. The expression of FLAG-DDB2 also alleviated the cisplatin hypersensitivity of EZH2 depletion (**Fig. 2.11 E-F**), suggesting that EZH2 mediates cisplatin resistance at least in part through DDB2.

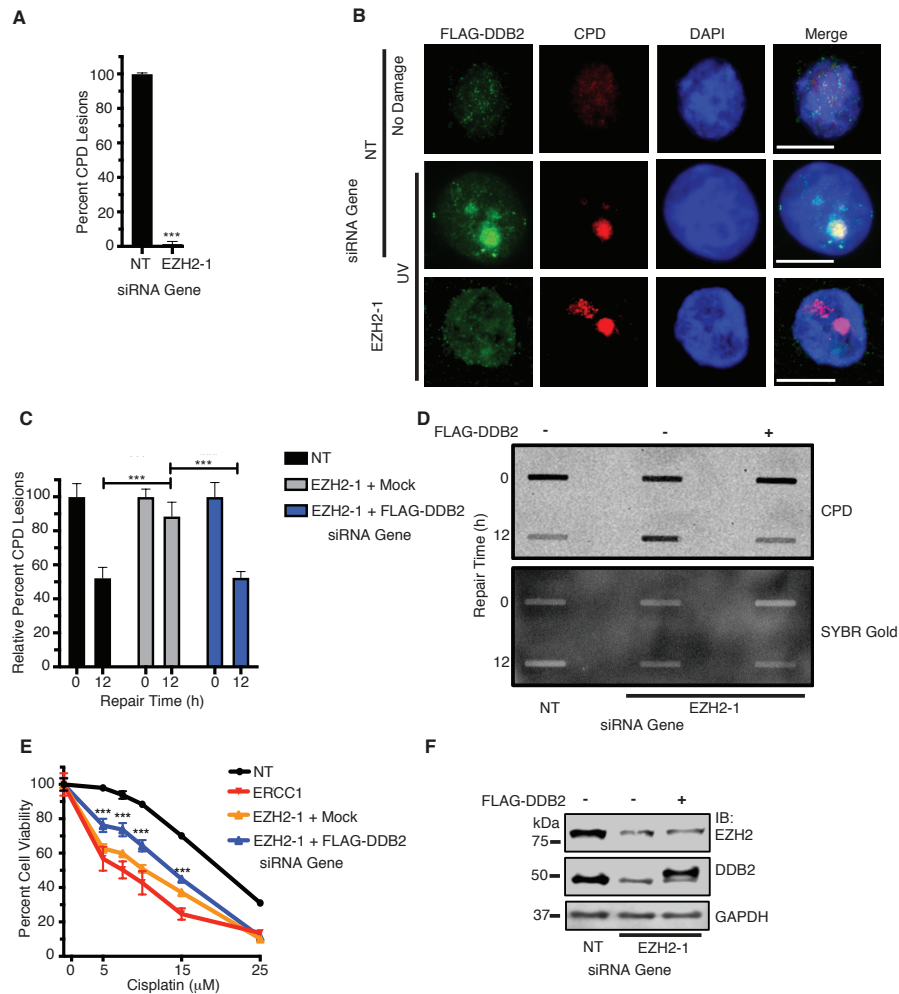


Fig. 2.11. DDB2 functions downstream of EZH2 in NER and in mediating cisplatin resistance in SCLC.

(A and B) EZH2 knockdown impairs DDB2 recruitment to CPD lesions. HeLa cells were transfected with siRNAs targeting EZH2 or a NT control. The following day, both groups were transfected with FLAG-DDB2. Cells were UV-irradiated at $100\text{J}/\text{m}^2$ through a micropore membrane, fixed, and stained for CPD lesions and FLAG-DDB2. Relative percent of CPD stained lesions that were positive for DDB2 staining, normalized to NT,

was quantified **(A)**. Representative images are shown **(B)**. **(C and D)** FLAG-DDB2 rescues impaired resolution of CPD lesions that occur through EZH2 knockdown. H128 cells were transfected with siRNAs targeting EZH2 or a NT control. The following day, both groups were transfected with FLAG-DDB2. Cells were UV irradiated, and harvested immediately (0h) or after 12h of repair time. Slot blot analysis was performed. **(C)** Quantitation of percent of CPD lesions remaining over time as normalized to 0 hrs of repair time. **(D)** Representative slot blot. SYBR Gold signal indicates total DNA loaded. **(E)** FLAG-DDB2 alleviates the sensitization of SCLC to cisplatin upon EZH2 knockdown. H128 cells were transfected with siRNAs corresponding to EZH2, ERCC1 or a NT control. The following day, groups were transfected with FLAG-DDB2 or mock control. 48 hours post overexpression, cell viability analysis was performed. **(F)** Western blot of FLAG-DDB2 expression achieved in H128 corresponding to panels **(C-E)**. (For **A-B**, quantification was achieved through 3 independent experiments counting at least 50 independent CPD lesion events per group (n=50) and representative images are shown. **C-D**, representative blots from 3 independent experiments (n=3) is shown). *** indicates $p < 0.001$.

EZH2 depletion with DZNep sensitizes SCLC cells and tumors to cisplatin

Given that siRNA mediated depletion but not catalytic inhibition of EZH2 decreases DDB2 levels, we tested the effect of DZNep, an EZH2 inhibitor that depletes EZH2 [137], on cisplatin sensitization and found that DZNep strongly sensitized H128 cells to cisplatin (**Fig. 2.12 A**). In contrast, we observed no significant effect on cisplatin sensitization when cells were treated with EPZ-6438. In addition, we tested the impact of DZNep on DDB2 levels in SCLC cells. DZNep treatment depleted EZH2 levels in H128 cells, leading to decreased DDB2 levels, phenocopying EZH2 depletion by knockdown (**Fig. 2.12 B**). Furthermore, the expression of GFP-EZH2 WT and H689A partially rescued the DZNep mediated decrease in DDB2 (**Fig. 2.13 A**), suggesting that DZNep targets a noncatalytic function of EZH2 in depleting DDB2 levels. DZNep treatment was also epistatic with DDB2 knockdown in sensitizing SCLC cells to cisplatin and UV damage (**Fig. 2.13 B-C**). Together, these data indicate that targeting DDB2 stability can be achieved by depleting EZH2 through DZNep to sensitize SCLC cells to cisplatin.

To determine if DZNep sensitizes SCLC tumors to cisplatin *in vivo*, we generated tumor xenografts using H128 cells in Nu/Nu mice. Treatment of the mice with the combination of DZNep and cisplatin strongly suppressed the growth of tumors compared with treatment with DZNep or cisplatin alone (**Fig. 2.12 C-D**), providing *in vivo* validation that DZNep sensitizes SCLC tumors to cisplatin. Consistent with findings in other tumor types [173, 174] treatment of the mice with DZNep alone also significantly delayed tumor growth but to a lesser extent than combined treatment with DZNep and cisplatin. No significant

difference in body weight was observed in treatment groups compared to controls, indicating treatments were well tolerated. **(Fig. 2.12 E)**.

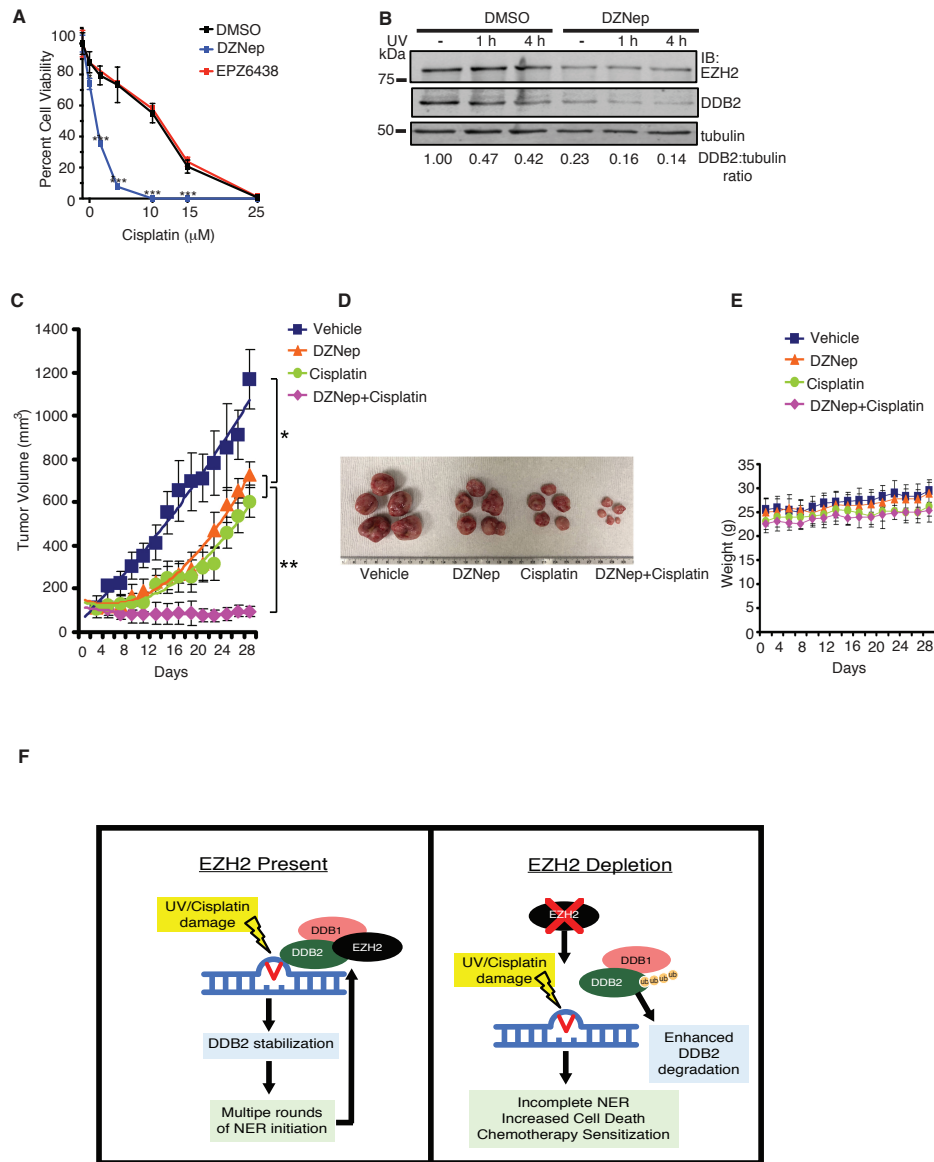


Fig. 2.12. EZH2 depletion with DZNep sensitizes SCLC to cisplatin *in vitro* and *in vivo* and model for EZH2 in NER.

(A) H128 cells are sensitized to cisplatin through EZH2 depletion but not through S-Adenosyl-l-methionine (SAM) competitive inhibition. H128 cells were treated with DZNep, EPZ-6438, or DMSO for 72 hours followed by cisplatin treatment for 72 hours prior to assaying for cell viability. (B) DZNep-mediated EZH2 depletion destabilizes

DDB2. H128 cells were treated with DZNep or DMSO for 6 days followed by 2 hours of CHX pretreatment and 30 J/m² UV damage, and allowed to recover at the times indicated. Cells were then harvested, lysed, and run on SDS-PAGE. **(C-E)** The combination of DZNep and cisplatin synergistically suppresses SCLC tumor growth *in vivo*. **(C and D)** Nu/Nu mice with H128 lung cancer xenografts were treated with DZNep (2.5mg/kg; 2 times per week), cisplatin (2.5mg/kg; 2 times per week), or the combination i.p. for 28 days. Each group included 5 mice. Tumor volumes were measured once every 2 days. The error bars indicate \pm SD. **(E)** Weights corresponding to figure c were measured once every 2 days. The error bars indicate \pm SD. * indicates $p < 0.05$, by 2-tailed *t* test. ** indicates $p < 0.01$, by 2-tailed *t* test. **(F)** Model for EZH2 function in NER. Following cisplatin or UV damage, EZH2 mobilizes to DNA damage sites where it complexes with DDB1-DDB2 and promotes DDB2 stability by preventing its ubiquitination independent of its methyltransferase activity or PRC2. EZH2 stabilization of DDB2 may facilitate DDB2 binding and assembly of CRL4 at the site of the NER lesion, which in turn promotes the ubiquitination of critical downstream NER targets to facilitate NER. In the absence of EZH2 or with EZH2 depletion by DZNep, there is increased ubiquitination of DDB2 leading to its degradation and impaired NER and thereby causing sensitization to cisplatin and UV damage. (For **B**, a representative blot from 3 independent experiments (n=3) is shown).

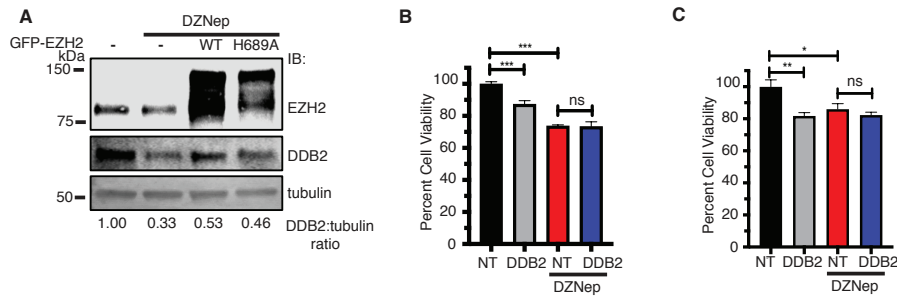


Fig. 2.13. EZH2 depletion with DZNep sensitizes SCLC to cisplatin *in vitro*.

(A) H128 cells were pretreated for 4 days with DZNep or DMSO, and then transfected with GFP-EZH2 WT or GFP-EZH2 catalytic inactive mutant (H689A) plasmids or mock transfected. 24 hours post-transfection, groups were pre-treated with CHX, harvested, run on SDS PAGE, and probed with the indicated antibodies. **(B and C)** H128 cells were pretreated for 3 days with DZNep or DMSO, and then transfected with siRNAs targeting DDB2 or NT control. 72 hours after knockdown (in the presence of DZNep or DMSO), cells were treated with **(B)** 5 μ M cisplatin or **(C)** 5J/m² UV. Cell viability was measured 72 hours after UV or cisplatin treatment.

2.6 Discussion

Our findings reveal a non-catalytic and PRC2 independent function for EZH2 in promoting NER through DDB2 stabilization to govern cisplatin resistance in SCLC. Using a synthetic lethality screen of a siRNA library biased towards nuclear enzymes, we identified a number of important regulators of cisplatin resistance in SCLC cells, including EZH2. We found that EZH2 depletion in SCLC cells causes cellular cisplatin and UV hypersensitivity in an epistatic manner with DDB1-DDB2, and moreover that EZH2 mobilizes to damage sites to govern the repair of CPD crosslinks, supporting a novel role for EZH2 in promoting NER. Mechanistically, we showed that EZH2 complexes with DDB1-DDB2 and promotes DDB2 stability by impairing its ubiquitination independent of its methyltransferase activity or PRC2, thereby facilitating DDB2 localization to CPD lesions, defining a novel paradigm for EZH2 in promoting the stability of proteins independent of its canonical role in H3K27Me3. Furthermore, we found that targeting EZH2 for depletion with DZNep but not inhibiting its catalytic activity with EPZ-6438 strongly sensitizes SCLC cells and tumors to cisplatin. Thus, our findings reveal a non-catalytic and PRC2 independent function for EZH2 in promoting NER through DDB2 stabilization, suggesting a rationale for targeting EZH2 beyond its catalytic activity to overcome cisplatin resistance in SCLC.

Based on our findings, we propose a model whereupon following genotoxic insults by cisplatin or UV, EZH2 complexes with DDB1-DDB2 and promotes DDB2 stability by preventing its ubiquitination independent of its methyltransferase activity or PRC2, thereby facilitating DDB2 localization to CPD crosslinks to govern their repair (**Fig. 7F**). Since EZH2 interacts with the N-terminus of DDB2 where the majority of its autoubiquitination

sites are located [175], EZH2 interaction in this region may prevent DDB2 autoubiquitination. EZH2 stabilization of DDB2 may facilitate its binding and assembly of CRL4 at the site of the NER lesion. There, the E3 ligase complex promotes ubiquitination of critical downstream NER targets, including XPC, H3, H4, and DDB2 itself before DDB2 is degraded and the E3 ligase complex disassembles. Our data support a PRC2 independent function for EZH2 in stabilizing DDB2 as SUZ12 knockdown failed to decrease DDB2 levels similarly to EZH2, and overexpression of FLAG-EZH2 T311E, which has impaired interaction with SUZ12 [87], but not FLAG-EZH2 T311A, stabilizes DDB2 levels. Our data suggest that when EZH2 is constitutively phosphorylated, it is able to more efficiently participate in stabilizing DDB2 and promote NER, potentially by becoming decoupled from SUZ12/PRC2. In contrast, overexpression of FLAG-EZH2 T311A, which is functional in its role with PRC2, destabilized DDB2, potentially acting as a dominant negative when EZH2 is not uncoupled from PRC2.

Our data suggest a non-catalytic role for EZH2 in promoting NER by stabilizing DDB2 that is distinct from its canonical role in H3K27Me3-mediated transcriptional silencing. Indeed, EZH2 depletion did not decrease DDB2 mRNA levels and inhibiting the catalytic activity but not total levels of EZH2 with EPZ-6438 decreased H3K27Me3 but failed to decrease DDB2 protein levels or sensitize SCLC cells to cisplatin. Furthermore, the decrease in DDB2 levels following EZH2 knockdown was rescued by expression of GFP-EZH2 H689A. However, because GFP-EZH2 H689A and FLAG-DDB2 only partially rescued the cisplatin hypersensitivity of EZH2 depletion, our results suggest that the noncatalytic role of EZH2 in promoting DDB2 stability may not fully account for its effects

on mediating cisplatin resistance. Interestingly, it has been reported that EZH2 is capable of silencing XPA at its promoter through H3K27Me3, thereby impairing NER in nasopharyngeal carcinoma cells [176]. It is possible that EZH2 could have roles in both activating and inactivating NER that are cancer subtype dependent, which will be critical in assessing whether EZH2 should be targeted to overcome cisplatin resistance.

Consistent with our findings, increased DDB2 levels were associated with cisplatin resistance in melanoma cells [177]. On the other hand, DDB2 overexpression has been reported to lead to cisplatin sensitivity in ovarian cancer, and DDB2 has been reported not to be required for the repair of cisplatin-induced DNA damage [178]. Thus, it is possible that the role of DDB2 in responding to cisplatin may also be cancer cell type specific, perhaps depending on dysregulation of other DDR genes. In addition, these contrasting findings may, in part be attributed to the idea that to facilitate NER, DDB2 levels must be tightly and dynamically regulated, as DDB2 must first be stabilized and then degraded in order to promote NER lesion resolution [179]. Thus, while EZH2 knockdown causes cisplatin hypersensitivity in SCLC cells at least in part through DDB2 degradation, it is also possible that too much DDB2 could also impair NER and thus paradoxically lead to cisplatin hypersensitivity. In addition, while our data show that EZH2 promotes DDB2 stability, DDB2 has been reported to recruit EZH2 to the promoters of *NEDD4L* and *RNF43* [180, 181] suggesting a possible feed-forward mechanism of EZH2 in regulating DDB2 stability, which in turn regulates EZH2's function in transcriptional repression.

EZH2 has been reported to have a non-canonical role in directly methylating non-histone proteins to promote their degradation [144, 147]. Our data suggest a new role for EZH2 in promoting protein stability independent of its methyltransferase activity or PRC2. DDB2 ubiquitination has previously been shown to be regulated by the COP9 signalosome (CSN), XPC, Ku, PARP1, and USP24 [175, 182-185]. Our data indicate that EZH2 also impairs DDB2 ubiquitination, highlighting the importance of tight regulation of DDB2 levels in controlling its functions in NER. Of note, EZH2 was recently reported to recruit USP7 to mediate neuronal gene expression [186]; however, whether this is mediated through its methyltransferase activity, PRC2, or H3K27Me3 such as it is for MUS81 [106] was not explored. It is possible that the non-catalytic and PRC2 independent function of EZH2 in stabilizing DDB2 may be a more generalized mechanism in control of the stability of other proteins in addition to DDB2.

Beyond our main findings with EZH2, many hits from the primary screen were largely consistent with the existing literature, however, there were also some surprising results. Arginine methylation, for example, was the most enriched pathway among the cisplatin sensitization hits. Arginine methylation is emerging as a key pathway involved in cell cycle regulation [187], and dysregulation of the cell cycle can render cancers vulnerable to cisplatin treatment. In addition, many reports have demonstrated that BRCA1 and POLQ are promising therapeutic targets that, when depleted, sensitize cancer to cisplatin or other DNA damaging agents. This has been predominantly explored in pancreatic, breast and ovarian cancers [188-191]. Data from our H128 screen, however, indicates that BRCA1 and POLQ depletion promotes cisplatin resistance in H128 cells. Taken together, our data

suggest that targeting BRCA1 and POLQ may be advantageous but only in specific cancer subtypes or molecular contexts.

When viewed through a therapeutic lens, our finding that EZH2 has a non-catalytic and PRC2 independent role in promoting NER has important implications in the rationale design and application of EZH2 inhibitors that are currently being investigated for cancer therapy. While EZH2 does govern the repair of some types of DNA damage through H3K27Me3 [108, 109, 111] our data suggest that catalytic inhibition of EZH2 may not fully suppress its role in governing cisplatin resistance. Our assembled data provide rationale for the therapeutic potential of novel anti-cancer strategies including targeting EZH2 with depleting agents such as with DZNep, or disrupting the EZH2-DDB2 interaction with small molecule inhibitors, to overcome cisplatin resistance.

2.7 Acknowledgements

EmGFP-EZH2 WT plasmid was a gift of Damian Yap (British Columbia Cancer Research Center) [155]. EZH2 PRC2 mutant plasmids were a gift of Lixin Wan (Moffit Cancer Center) [87]. FLAG-DDB2 plasmid was a gift of Qi-En Wang (The Ohio State University) [192].

2.8 Funding

This work was supported by NIH/NCI [R01CA178999 to D.S.Y., F31CA225119 to A.E.K, R01CA193828 to X.D., P01CA092584 to Z.D.N.]; NIH/NIEHS [U01ES029520 to

Z.D.N.]; Lung Cancer Research Foundation [51347 and 60208 to D.S.Y]; Conquer Cancer Foundation of ASCO Young Investigator Award, supported by GO2 Foundation for Lung Cancer [15212 to N.T.P.]. Any opinions, findings, and conclusions expressed in this material are those of the author(s) and do not necessarily reflect those of the ASCO®, Conquer Cancer®, or GO2 Foundation for Lung Cancer.

2.9 Conflict of Interest

The authors declare no competing interests.

Chapter 3: RNA Helicase HELZ Promotes Homologous Recombination Repair to Maintain Genomic Stability

Allyson E. Koyen¹, Matthew Z. Madden¹, Ramona Haji-Seyed-Javadi,¹ Dongkyoo Park¹, Nicholas T. Seyfried², Taofeek K. Owonikoko³, and David S. Yu^{1,*}

¹ Department of Radiation Oncology, Emory University School of Medicine, Atlanta, GA 30322, USA, ² Department of Biochemistry, Emory University School of Medicine, Atlanta, GA 30322, USA, ³ Department of Hematology and Medical Oncology, Emory University School of Medicine, Atlanta, GA 30322, USA.

[This manuscript is in preparation for publication.]

3.1 Author Contributions

Conceptualization, A.E.K., M.Z.M., and D.S.Y.; Investigation, A.E.K., M.Z.M., R.H.J., and D.M.D.; Writing – Original Draft, A.E.K. and D.S.Y.; Writing – Review and Editing, A.E.K., M.Z.M., R.H.J., D.M.D., N.T.S., T.K.O., and D.S.Y.; Supervision – N.T.S., T.K.O., and D.S.Y.; Funding Acquisition, A.E.K., and D.S.Y.

3.2 Abstract

Small cell lung cancer (SCLC) is a highly aggressive malignancy with poor outcomes associated with resistance to etoposide-based chemotherapy. Using a synthetic lethality screen, we identified important regulators of etoposide resistance in SCLC cells. One of the strongest mediators of etoposide resistance was a novel protein, Helicase with Zinc finger (HELZ), which has not been well characterized. Here, we show that HELZ promotes homologous recombination and helps to maintain genomic stability. HELZ governs etoposide resistance in SCLC, as well as resistance to other DSB inducing agents. HELZ localizes to DSBs in a PARP1 dependent manner, and HELZ depletion mitigates RAD51 localization to DSB sites. Furthermore, HELZ depletion causes DNA-RNA hybrid accumulation, decreased HR, and genomic instability. HELZ complexes with PRP19 and DDX1 which are involved in DNA-RNA hybrid resolution and promote HR. Moreover, increased HELZ expression is associated with poor outcome in cancers. We suggest HELZ functions together with PRP19 and DDX1 to promote DNA-RNA hybrid resolution to promote HR and help maintain genomic stability, contributing to DSB resistance and poor outcome in cancer.

3.3 Introduction

SCLC is a highly aggressive malignancy with a 5-year survival rate of only 7 percent [119]. The first-line treatment regimen for SCLC consists of a combination of two chemotherapeutic agents: a platinum agent (cisplatin or carboplatin), with etoposide, a topoisomerase inhibitor (EP). Though SCLC patients initially respond to EP treatment, resistance quickly develops, particularly in advanced SCLC [120]. Response rates for second-line treatment of topotecan are poor, and come with substantial side effects [121]. PD1/PDL1 checkpoint inhibitors were recently approved for first line use, but are only marginally effective, as they have shifted the median survival in patients by an order of months [15]. Therefore, novel therapeutic approaches for SCLC treatment are urgently needed, particularly those that may work to enhance the efficacy of EP.

The DNA damage response (DDR) is critical for responding to DNA damage induced by chemotherapy. Etoposide, a highly potent anticancer treatment routinely used across cancers, specifically targets type II DNA topoisomerases promoting DSBs. Functionally, etoposide targets topoisomerases in their active state, during G2/S phase of the cell cycle, where it stabilizes topoisomerase-DNA interactions after the induction of a topoisomerase mediated double strand break (DSB) to facilitate DNA unwinding. This complex, when stabilized by etoposide, is unable to re-ligate the topoisomerase mediated DNA double-strand break back together resulting in DSB accumulation [33].

The most conservative mechanism of repair of DSBs is the homologous recombination repair pathway (HR). HR is restricted to S/G2 phases of the cell cycle where it uses the homologous sister chromatid as a template for repair of the DSB [65]. There is an emerging role for RNA and RNA processing molecules in homologous recombination, and their roles in this pathway are actively being investigated. The HR pathway is characterized by DNA end resection, a process where one strand of the DNA around the DSB is removed, a single stranded DNA overhang is exposed, which under normal HR conditions, is later adapted to invade the sister chromatid as a template for repair [67, 162]. The ssDNA filament is highly vulnerable to the binding of RNA, particularly in areas of active transcription, and can result in the formation of DNA-RNA hybrids. RNA-DNA hybrids are highly stable structures that, when unresolved, cause aberrations, such as the accumulation of DSBs and genomic instability [193]. Failure to properly resolve DNA-RNA hybrids results in incomplete homologous recombination.

RNA helicases are ATP dependent molecules that bind RNA and unwind RNA duplexes [112]. RNA helicases can function to unwind DNA-RNA hybrids and maintain the integrity of the HR pathway. However, the specific role of hybrid resolution in promoting homologous recombination efficiency is only recently defined and incompletely understood [72, 115].

Helicase with Zinc Finger (HELZ) is an understudied protein, defined as a putative RNA helicase. It is an evolutionarily conserved member of RNA helicase superfamily 1. Functionally, HELZ has been implicated in cell proliferation via a role in translation initiation and translational repression through mRNA decay [116, 117]. There is also

evidence that HELZ is downregulated in some cancers and can serve a tumor suppressive function when overexpressed [118]. Beyond this, the biological function of HELZ remains largely undefined.

Here, we define a novel role for HELZ in governing etoposide resistance in SCLC by promoting HR, DNA-RNA hybrid resolution, and the maintenance of genomic stability. HELZ was identified in our siRNA screen as a novel and significant mediator of etoposide resistance in SCLC. Importantly, we demonstrate that depletion of HELZ impairs HR and RAD51 foci formation in response to DSBs, induces markers of genomic instability and results in the accumulation of spontaneous and etoposide derived DNA-RNA hybrids, where it is further implicated through its interaction with DDX1. Moreover, loss of HELZ sensitizes cancers to DSB agents, including SCLC to etoposide, suggesting HELZ as a promising therapeutic target in cancer.

3.4 Materials and Methods

Cell lines

All cell lines were originally purchased from the American Type Culture Collection (ATCC, Manassas, VA). H128 cells were provided by the laboratory of Dr. Taofeek Owonikoko [47] and were grown in RPMI 1640 (Gibco) with 7.5% fetal bovine serum (FBS). HeLa, U2OS, HEK293T, and HCT116 cells were grown in DMEM (Gibco) with 7.5% FBS. Calu-3 cells were grown in EMEM (Gibco) with 10% FBS. RPE1 cells were

cultured in DMEM/F-12 medium with 10% FBS. All cell lines were grown at 37°C under humidified conditions with 5% CO₂ and 95% air.

Drug Treatments

Cells were treated with etoposide (Teva Pharmaceuticals) between 1-72 hours and at a concentration of 5-25 µM; Camptothecin (CPT) between 4-72 hours and at a concentration of 25nM-2µM; Hydroxyurea for 72 hours and at a concentration of 0.1-1.6 mM; and ABT888 for 1-72 hours and at a concentration of 1-25 µM. Treatments were administered as indicated, and varied between assays.

Transfections

siRNA was purchased from Dharmacon and transfected with Lipofectamine RNAiMAX (Invitrogen) according to the manufacturer's instructions. siRNA sequences are as follows:

NT: AUGAACGUGAAUUGCUCUCAAU

HELZ-1 GGAAAUAGAACGCAUCAAA

HELZ-2: CAGCACACCUUGUUAAAUC

HELZ-3: GAUAUCACGUGGAAGACUU

HELZ-4: CUACAGAAGAUCUCGAAUA

HELZ-5: GGAAAUAGAACGCAUCAAA

siATR: CCUCCGUGAUGUUGCUUGA

siBRCA2: GAGACACAAUACAACUAAA

siCTIP: GCUAAAACAGGAACGAAUC

siCHD5: GGAAAGACCUGCCCUACGA

For overexpression studies, plasmids were transfected with Lipofectamine 2000 (Invitrogen) according to the manufacturer's instructions.

Primary etoposide siRNA screen

A custom siRNA library targeted 1,006 nuclear enzymes in a 96-well plate SMARTpool format, with each well containing 4 siRNAs targeting unique sequences within the same gene (Dharmacon). Each plate had 9 negative control siNT wells, three positive sensitivity control siATR wells, and one blank well. We included siCHK1, siATRIP, mock transfected (no siRNA), and non-transfected (no transfection reagent) control wells on the final plate.

Each well in the 96-well plates received 12,000 H128 cells and 0.3 μ L of Lipofectamine RNAiMAX (Invitrogen), as well as a final siRNA concentration of 25 nM and a final volume of 100 μ L. After 24 hours, each transfection plate was split into 4 clear-bottomed plates with final well volumes of 100 μ L. After another 24 hr, 50 μ L of media was added to the two non-treated plates while 50 μ L of etoposide-containing media was added to one plate each with a final concentration of 10 μ M. After a further 72 hr, 10 μ L of Resazurin reagent (R&D Systems) was added to each well for a final concentration of 1X in media. Fluorescence, corresponding to the number of live cells per well, was measured 8 hr later. Etoposide sensitization hits were considered based on the following criteria: a log₂ average viability of < -0.5, an average SSMD of < -2 and a 2-tailed t-test p value of <0.05.

Of the 56 hits, we selected 21 genes for further analysis. 14/21 were validated to reproduce the etoposide sensitization phenotype across at least two individual siRNAs.

To assess screen quality, Z-factor was calculated using the means and standard deviations of both positive (siATR) and negative (siNT) controls. The etoposide siRNA screen fell in the excellent range (between 0.5 and 1.0) with a calculated Z-factor of 0.534.

Gene Ontology (GO) and Network analysis

The Gene Ontology (GO) and network analysis were performed in Cytoscape [3] using ClueGO [4] and CluePedia [5] plugins. GO analysis using fused GO terms is represented. Significant processes (p-value ≤ 0.01) are shown. Categories were identified and sorted by the percent associated genes found. Only etoposide sensitization hits were used to build the network.

Site-Directed Mutagenesis

The HA-HELZ K674N mutant was generated by site-directed mutagenesis, as previously described [2]. Briefly, HELZ cDNA was purchased from Dharmacon (Accession: BC144083; Clone ID: 9052603) and was used to generate the HA-HELZ K674N mutant by site-directed mutagenesis. PCR primers were designed to generate the K674N mutation:

EmGFP-EZH2 K674N Forward:

CCCTATGGGACAGGCAACACGTTCACTCTAGCT

EmGFP-EZH2 K674N Reverse:

AGCTAGAGTGAACGTGTTGCCTGTCCCATAGGG

HELZ cDNA was used as a template and PCR reaction was performed. The template was then digested with DpnI for 2 hours at 37°C. The K674N mutation was confirmed by sequencing.

Cell Viability Assay

Cell viability assays were performed as previously described [6]. Cells were seeded in 96-well plates at the appropriate density (H128: 10,000 cells/well H146: 20,000 cells/well) and were treated with varying doses of etoposide (10-25 μ M). For UV treatment, cells were irradiated with the indicated dose of UV prior to seeding. After treatment, cells were grown in 96-well plates for 72 hours and then treated with Resazurin reagent at a final concentration of 1X in media. Cells were then incubated at 37°C for 3 hours. The Resazurin signal was then read as fluorescence (excitation wavelength: 544 nm, emission wavelength: 590 nm) on a Synergy H1 microplate reader (BioTek) in conjunction with Gen5 Microplate Reader Software (BioTek). Percent cell viability was quantified relative to the Resazurin signal in the untreated group, including subtracting the background the Resazurin signal for wells with no cells and media with Resazurin only.

Colony formation Assay

Cells were seeded sparsely in 6 well plates, at 100 cells/well for low doses or 200 cells/well for high doses of damage. Cells were given 8-24 hours to adhere and then irradiated with UV. Cells were grown until the untreated group formed colonies of approximately 50 cells in density, which, depending on the doubling time of the cell line, took between 10 and 14 days. To visualize colonies, cells were washed once with ice-cold PBS and then fixed in

3% crystal violet in methanol for 15 minutes. Crystal violet was removed by gently submerging plates in water. Visible colonies were then quantified with Bantex colony counter 920A.

Immunoblotting

Cells were lysed in 1% NP40 lysis buffer (150mM NaCl, 50mM Tris-Cl pH 8.0) and sonicated briefly followed by denaturation by boiling at 100°C for 7 minutes. Whole-cell lysate was run on SDS-PAGE at 80V for 2-3 hours followed by transfer to PVDF membrane at 40V overnight. Membranes were blocked in 5% BSA in TBST for 30 minutes followed by probing with the indicated antibodies in TBST supplemented with 1% BSA and 0.05% sodium azide at the indicated dilutions. To quantify band intensity, densitometry was performed using ImageJ software. Signals of interest are represented as normalized to tubulin.

Antibodies

HELZ (custom generated through ThermoFisher, 6 µg per 1mg whole cell lysate for IP, 1:50 for immunoblotting and immunofluorescence), anti-HA (Sigma, #H3663, 1:500 for immunoblotting), Normal Rabbit IgG (Millipore, #NI01, 6 µg per 1mg whole cell lysate for IP), alpha-tubulin (Sigma, T6074, 1:500 for immunoblotting), GAPDH (Santa Cruz, #sc-47724, 1:500 for immunoblotting), anti-myc tag (Abcam #ab9106, 1:100 for immunofluorescence) anti-RAD51 (Calbiochem #PC130, 1:500 for immunofluorescence), anti-γH2AX (Cell Signaling, #2577, 1:200 for immunofluorescence), anti-γH2AX (Millipore #05-636, 1:4000 for immunofluorescence), anti-total-RPA32 (sc-14692, 1:250

for immunoblotting), anti-phospho-RPA32-Ser4/8 (Bethyl #A300-245A, 1:500 for immunoblotting), anti-phospho-RPA32-Ser33 (Bethyl #A300-246A2, 1:500 for immunoblotting), anti-pATR-T1989 (KeraFAST #EVU001, 1:200 for immunoblotting), anti-total-CHK1 (Santa Cruz #8408, 1:200 for immunoblotting), anti-total-DNAPKCs (Thermo #MA5-13244, 1:500 for immunoblotting), anti-pDNAPKCs S2056 (Abcam #ab124918, 1:1000 for immunoblotting), anti-FLAG (Cell Signaling, #2368, 1:500 for immunofluorescence), anti-DDX1 (Bethyl #A300-521A, 1:500 for immunoblotting), anti-DNA-RNA Hybrid (Millipore #MABE1095, 1:600 for immunoblotting) and anti-ssDNA (Millipore #MAB3031, 1:4000 for immunoblotting).

Immunofluorescence

Cells were seeded on coverslips and treated with drugs or irradiated where indicated. After the indicated recovery time, cells were fixed with 4% (wt/vol) paraformaldehyde (EMD Chemicals) for 10 minutes at room temperature, permeabilized with 0.5% Triton X-100 (Fisher Scientific) for 10 minutes, and then blocked with 5% BSA in PBS. Cells were stained with primary antibodies in 1% BSA in PBS, followed by Alexa Fluor 488, or 555 anti-rabbit/mouse secondary antibodies (Life technologies) diluted in 1% BSA in PBS. Coverslips were mounted with DAPI Fluoromount-G (Southern Biotech) on slides and images were captured using a Zeiss Observer Z1 microscope equipped with Axiovision Rel 4.8 software. For quantification, the percentage of cells with greater than 5 foci was counted as positive, from three replicate experiments with at least 100 cells counted per replicate. The presence of γ H2AX foci after treatment with a DNA damaging agent was used as a positive control for damaged cells.

Analysis of DNA Double-Strand Break Repair in Mammalian Cells

U2OS cells stably expressing the DR-GFP, EJ5 or EJ2 reporters were transfected with siRNA as indicated. 48 hours post transfection, groups were transiently transfected with an ISCE-1 plasmid or mock transfected. 72 hours post knockdown, cells were harvested, fixed in 1% PFA (wt/vol) in PBS and FACS analysis was performed. GFP positive cells were gated in FITC plotted against PE as a compensation standard, and analyzed for % GFP positive cells induced as a readout for HR, NHEJ or alternative NHEJ repair efficiency.

Micronucleus Assay

Cells were transfected with siRNA as indicated. 24 hours post knockdown, cells were seeded on coverslips and allowed to adhere overnight. The following day, cells were treated with 3 μ g/ml cytochalasin B or left untreated for 12 hours, prior to fixation at 72 hours post knockdown. Cells were fixed in 4% paraformaldehyde (wt/vol), stained with DAPI, mounted on coverslips and imaged using a 63x oil objective on a Zeiss Observer Z1 microscope equipped with Axiovision Rel 4.8 software. Percent of binucleated cells with one or more DAPI positive micronucleus were quantified. 300 binucleated cells were counted per group.

Slot blot assay measuring DNA-RNA Hybrids

Cells were transfected with siRNA as indicated. 72 hours post knockdown, cells were harvested and DNA was extracted with the DNeasy Blood and Tissue kit (QIAGEN) following the manufacturer's instructions. A nitrocellulose membrane was presoaked in

SSC buffer. For DNA-RNA hybrid detection, one microgram of undenatured DNA was spotted directly on a nitrocellulose membrane using a slot blot apparatus (Whatman Schleicher & Schuell Minifold I). For single stranded DNA loading control, one microgram of DNA was first denatured for 10 min in 0.5 N NaOH, 1.5 M NaCl, and neutralized for another 10 min in 1 M NaCl, 0.5 M Tris-HCl pH7.0, and then spotted directly on a nitrocellulose membrane using a slot blot apparatus. Membranes were UV-crosslinked at 0.12 J/m² and blocked with 5% milk in TBST. The undenatured replicate was probed with the mouse S9.6 antibody (1:600) in 1% milk/TBST and the denatured replicate was probed with a single-strand DNA antibody (1:4000, Millipore) at 4 degrees C overnight. Detection was performed with the LI-COR Odyssey system.

Co-Immunoprecipitation and protein digestion for MS

HEK-293T cells were treated with 10GY IR, 25 µM etoposide or left untreated and harvested and lysed after the indicated recovery period. HELZ was immunoprecipitated (IP'd) with HELZ antibody or normal rabbit IgG antibody as a negative control, conjugated to protein A agarose beads (Sigma). Beads were washed in PBS and processed for mass spectrometry (MS) analysis for protein-protein interactions. The supernatant was removed from the bead solution and 200 ml of 50 mM NH₄HCO₃ was added. The samples were then treated with 1 mM (final concentration) dithiothreitol (DTT) at 25°C for 30 minutes. This was followed by 5 mM (final concentration) iodoacetimide (IAA) at 25°C for 30 minutes in the dark. Protein was digested with 1:100 (w/w) lysyl endopeptidase (Wako) at 25°C for 2 hours and trypsin (Promega) was added at 1:50 (w/w). The digestion was allowed to

proceed overnight. Resulting peptides were desalted with a Sep-Pak C18 column (Waters) and dried under vacuum.

LC-MS/MS analysis

Dried peptides were reconstituted in 10 mL of loading buffer (0.1% formic acid, 0.03% TFA, 1% acetonitrile). The sample (2 mL) was loaded onto and eluted from a self-packed C18 fused silica column (25 cm x 75 mM internal diameter (ID); New Objective, Woburn, MA) driven by a Dionex Ultimate 3000 RSLCNano UPLC system. Elution was performed over a 120 minute gradient at a rate of 300 nl/min with buffer B ranging from 3% to 65% (buffer A: 0.1% formic acid in water, buffer B: 0.1 % formic in acetonitrile). The spectra were monitored on a Fusion Mass Spectrometer (ThermoFisher Scientific, San Jose, CA). The mass spectrometer cycle was programmed to collect at top speed for 3-second cycles with higher-energy collision dissociation (HCD) fragmentation. The Mass Spectrometry (MS) scans (400-1600 m/z range, 200,000 AGC, 50 ms maximum ion time) were collected at a resolution of 120,000 at m/z 200 in profile mode while the HCD MS/MS spectra (0.7 m/z isolation width, 30% collision energy, 10,000 AGC target, 35 ms maximum ion time) were detected in the ion trap. Dynamic exclusion was set to exclude previous sequenced precursor ions for 20 seconds within a 10 ppm window. Precursor ions with +1, and +7 or higher charge states were excluded from sequencing.

Immunoprecipitation (IP)

IP analysis was performed as previously described [7]. Briefly, cells were lysed in 0.75% CHAPS lysis buffer, and then lysis buffer was diluted to 0.375% CHAPS. Lysate was

added to beads as indicated: HA conjugated beads (Sigma) for HA-HELZ IP; Streptavidin beads (ThermoFisher) for SFB-PRP19 IP. Lysate and beads were incubated with antibodies as indicated on a rotor overnight at 4°C. Beads were subsequently washed four times as follows: each IP mixture was centrifuged at 1.0xg for 1 minute, supernatant was removed, and beads were washed in fresh lysis buffer. After the final wash, all liquid was removed from beads with a gage needle, and beads were denatured with 1X SDS sample buffer. Bead-sample buffer mixture was then loaded directly into wells of an SDS-PAGE gel.

Human Pathology Atlas

Kaplan Meier curves were generated using the human pathology atlas within the Human Protein Atlas [194]. Briefly, the pathology atlas contains correlation analysis comparing mRNA expression level in human cancer tissue to clinical outcome data. Using this database, we mined HELZ in cancers for correlations between expression and clinical outcome. Importantly, only genes that have a highly significant p value ($p < 0.001$) are listed as significant in the database.

3.5 Results

A siRNA screen targeting nuclear enzymes identifies genes that mediate etoposide resistance in SCLC

To identify genes critical for governing etoposide resistance in SCLC, we performed an etoposide sensitivity screen with siRNAs targeting 1,006 genes, biased towards nuclear

enzymes for future translational application, in SCLC cells. We have previously used our nuclear enzyme siRNA library to perform drug sensitivity screens in other cancer cell types to identify novel regulators of the DDR [48, 49]. We chose the SCLC cell line H128, a cell line with intact DNA repair pathways from a treatment-refractory tumor. H128 cells are strongly resistant to etoposide, with an IC₅₀ of 10 μ M after 72 hours of continuous treatment. A typical intravenous dose of 100 mg/m² etoposide over 2 h in vivo, results in a peak plasma etoposide concentration of 15 μ g/ml (approximately 25 μ M); however, this rapidly falls to 1 μ g/ml (approximately 2 μ M) after 24 h [195]. Thus, 10 μ M etoposide is a challenging dose to continuously reach in patients. The screen was conducted in triplicate in 96-well plates using siRNA targeting ATR and ATRIP as positive controls and a non-targeting (NT) siRNA as a negative control. Cells were transfected with the siRNA library, treated after 48 hours with or without etoposide for 72 hours, and assayed for cell viability with resazurin reagent (**Fig. 3.1 A**). Sensitivity results from the screen are shown as a volcano plot of log₂-transformed average viability against strictly standardized mean difference (SSMD) (**Fig. 3.1 B**). We identified 56 etoposide sensitization hits based on the following criteria: an average cell viability of <0.6, an average SSMD of <-2, and a two-tailed t-test p-value of <0.05. The Z-factor of the screen, an indicator of screen quality, was 0.534, which is in the excellent range, indicating that our screen is robust.

To characterize common pathways and potential interactions of our etoposide sensitization hits, we performed gene ontology (GO) analysis (**Fig. 3.1 C**) and network analysis (**Fig. 3.2 A**). As anticipated, pathways involved in the DNA damage response and cell cycle regulation, including cyclin-dependent protein serine/threonine kinase activity and DNA metabolism emerged as a key process among the etoposide sensitization hits. We also

identified enrichment in genes related to chromatin condensation, cell migration in angiogenesis, synthesis of pyridine rings, and threonine phosphorylation among the sensitization hits.

Indeed, a number of DDR factors emerged as etoposide sensitization hits in our primary screen: 9-1-1 complex member HUS1, DNA glycosylase SMUG1, checkpoint protein RAD9A, and DNA repair proteins RNF8, and HELLS, among others [196, 197]. These results demonstrate that our screen can yield DDR proteins previously defined for mediating etoposide resistance.

One intriguing hit that emerged was Helicase with zinc finger (HELZ), a poorly characterized protein implicated as an RNA helicase. Interestingly, HELZ was among the most efficient sensitizing hits identified, which when silenced, sensitized H128 cells to etoposide to a similar magnitude as HELLS, another helicase that was similarly poorly characterized until recently, where its role in DNA end resection was defined [197]. Thus, HELZ may be an uncharacterized mediator of the DNA damage response.

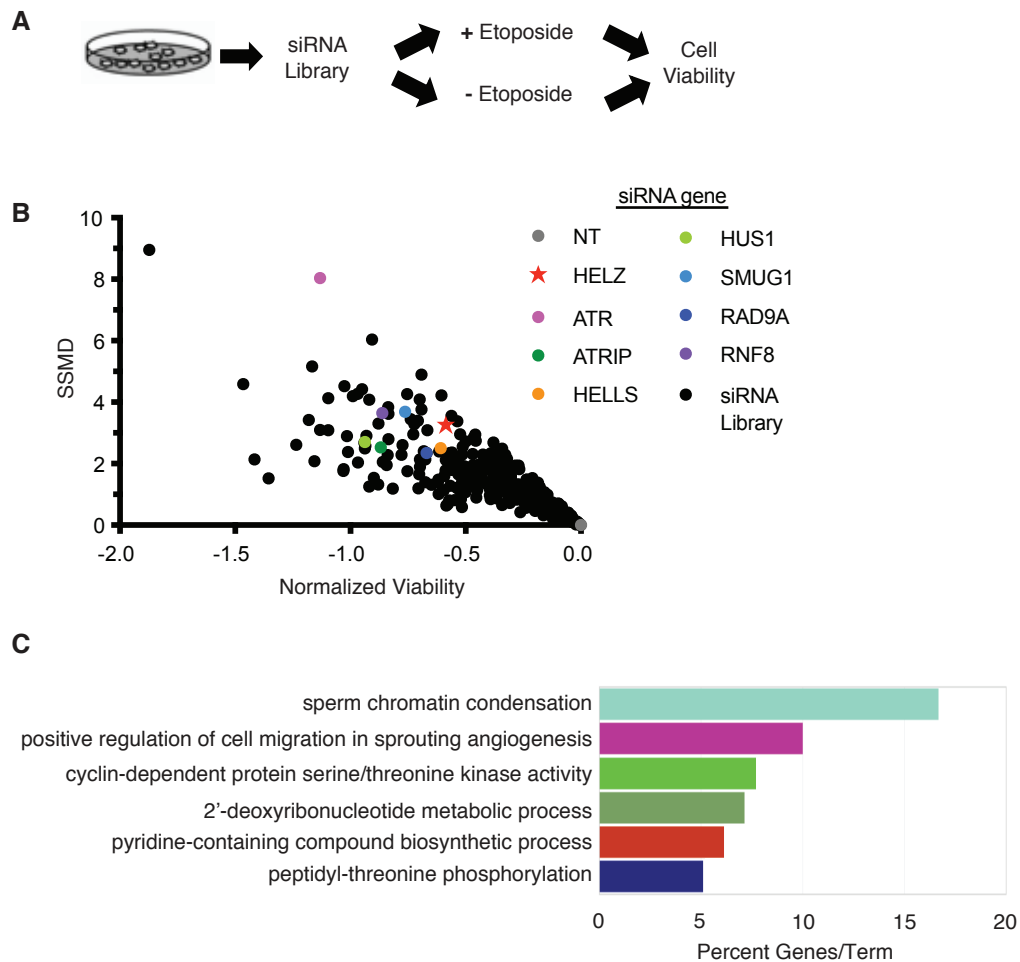


Fig. 3.1. A siRNA screen targeting nuclear enzymes identifies genes that mediate etoposide resistance in SCLC.

(A) Primary screen format: H128 cells were transfected with a siRNA library biased towards targeting nuclear enzymes. 48 hours post-transfection, cells were treated with or without 10 μ M etoposide for 72 hours prior to measuring cell viability. **(B)** Primary screen results: the normalized cell viability was plotted against the strictly standardized mean difference (SSMD) for each gene targeted by the library. Normalized viability was calculated as the \log_2 ratio of treated versus untreated cell viability relative to the non-

targeting (NT) siRNA control. **(C)** Summary of most enriched categories from Gene Ontology (GO) analysis of etoposide sensitization hits (n = 56). The top 6 significant processes ($p \leq 0.01$) are shown, sorted by the percent associated genes found.

A

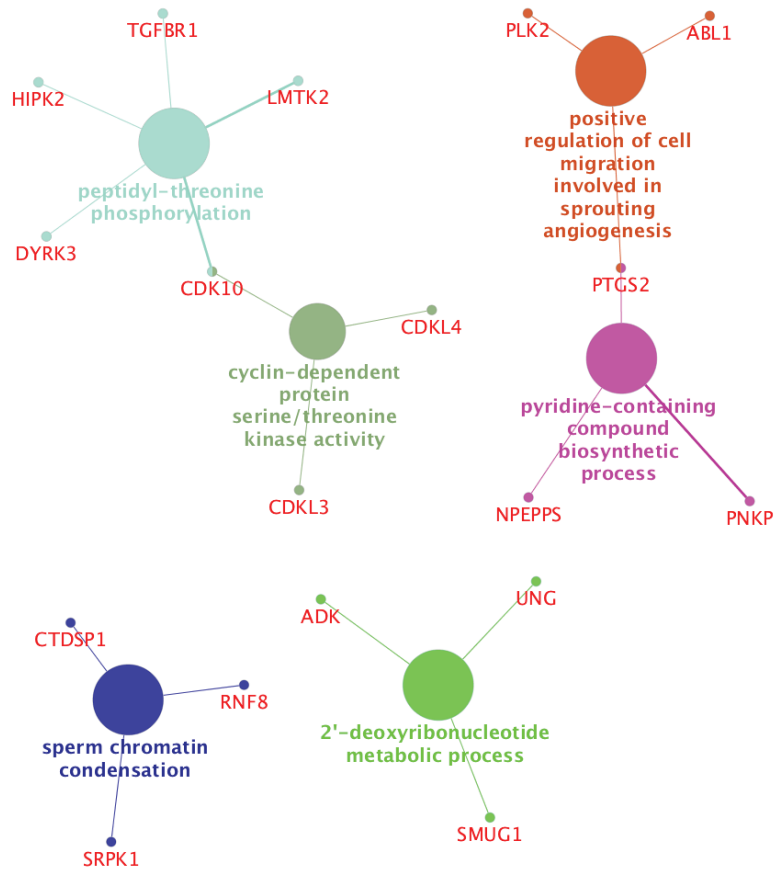


Fig. 3.2. A siRNA screen targeting nuclear enzymes identifies genes that mediate etoposide resistance in SCLC.

(A) Enriched GO network of etoposide sensitization hits (n = 56). Only etoposide sensitization hits were used to build the network. The GO terms enriched among the significant hits are represented by nodes, shown with color filled circles, where each color represents a GO category. The label of the most significant GO term within the category is used as leading group term. The size of the node indicates the term significance (all nodes p-value ≤ 0.05) and the color of the node represent the grouping by GO categories. The GO term nodes are connected (edges) based on their kappa score (≥ 0.4) and shows the relationships between the terms and genes.

HELZ Mediates DSB resistance in Cancer

From the primary screen, 21 hits were selected for further validation based on previous identification in other high-throughput DNA damage sensitivity screens, putative interactions with known DNA repair proteins by mass spectrometry (MS), or potential disease relevance, including in SCLC. To validate each target, we tested if the etoposide sensitization phenotype could be achieved across more than one individual siRNA to rule out off-target effects of the pooled siRNA used in the primary screen. Of the 21 hits tested, 14 were validated, including HELZ. Two unique siRNAs targeting HELZ sensitized H128 cells to etoposide (**Fig. 3.3 A**) and western blot confirmed successful HELZ knockdown (**Fig. 3.3 D**). Given that etoposide results in the generation of both DNA double strand breaks and induces DNA replication stress, we also tested if HELZ knockdown sensitized H128 cells to agents that cause similar effects. We confirmed that HELZ mediated resistance to DSB inducer CPT and replication stress inducer HU in H128 cells (**Fig. 3.3 B-C**). We validated HELZ mediates resistance to IR and PARP inhibitor ABT888 in U2OS cells using clonogenic assays (**Fig. 3.3 E-F**), confirming HELZ was successfully knocked down in U2OS (**Fig. 3.3 G**). Because all of these agents commonly can directly or indirectly result in the accumulation of DSBs, further exploration of the role of HELZ in DSB repair is warranted.

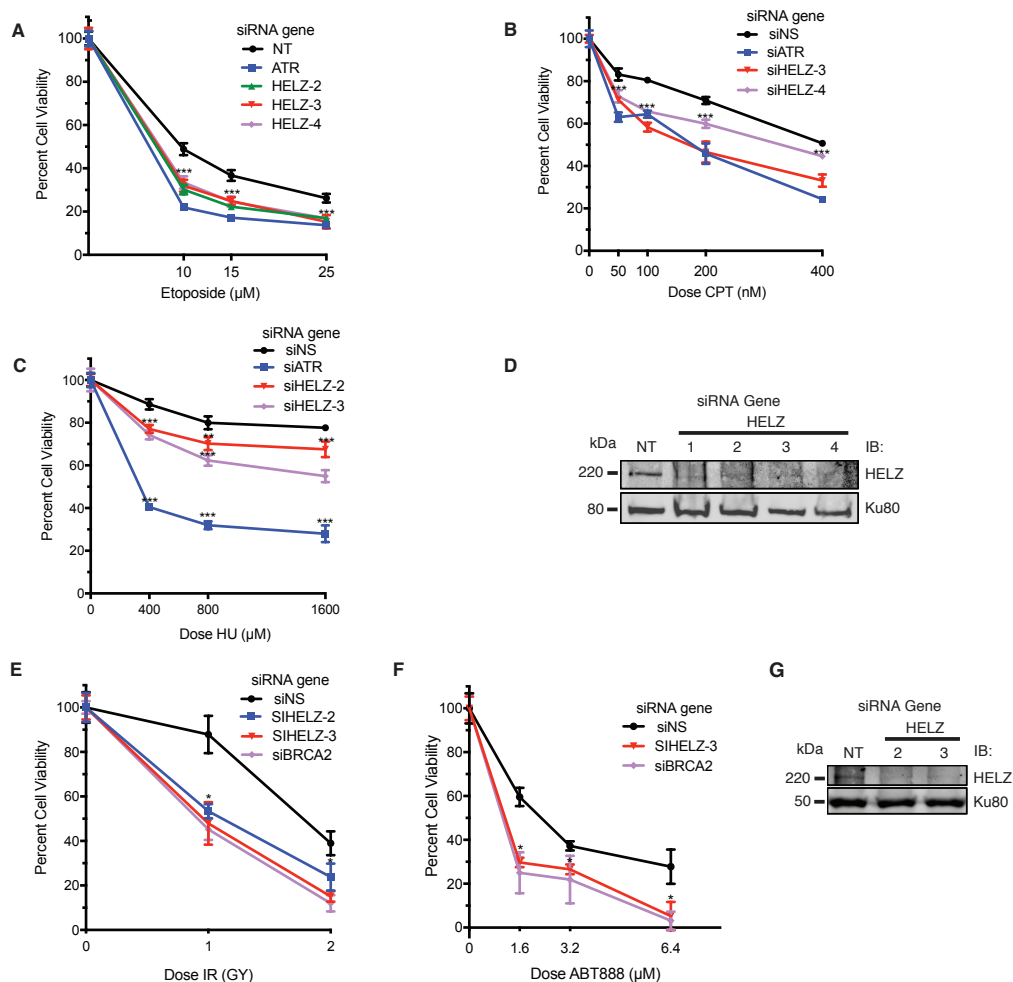


Fig. 3.3. HELZ mediates DSB resistance in cancer.

(A-D) H128 cells were transfected with siRNA targeting EZH2, ATR, or a NT control. 72 hours after transfection, cells were treated with (A) etoposide (B) CPT or (C) HU for 72 hours prior to measuring cell viability. (D) Western blot analysis of HELZ expression in H128 cells, demonstrating HELZ knockdown. (E-F) U2OS cells were transfected with siRNA targeting HELZ, BRCA2, or a NT control. 72 hours after transfection, cells were seeded sparsely and allowed to adhere overnight. After the untreated NT control groups formed colonies of about 50 cells in size, groups were assessed for colony formation. (E)

The day after seeding, adherent groups were irradiated with varying doses of IR. **(F)** Groups were treated with varying doses of fresh ABT888 every 2-3 days. **(G)** Western blot analysis of HELZ expression in U2OS cells, demonstrating HELZ knockdown. (For **A-C** and **E-F**, mean and standard deviation of three replicas is shown.) *** indicates $p < 0.001$.

HELZ Localizes to and Promotes Repair of DNA Double Strand Breaks through the HR Pathway

To further investigate the role of HELZ in DSB repair, we asked if HELZ was recruited to sites of DNA damage. We overexpressed myc-HELZ in U2OS cells and damaged cells with DSB inducing agents including ionizing radiation and etoposide, or left cells undamaged. Interestingly myc-HELZ formed nuclear foci in response to radiation and etoposide (**Fig. 3.4 A**). These foci co-localized with global DNA damage marker γ H2AX, which are described as sites of DNA DSBs. PARP generates PAR chains on chromatin that promote chromatin decondensation around the site of the lesion, making it more accessible to downstream DDR factors. Thus, PARP functionally helps to recruit many DNA damage responders to sites of damage. Furthermore, inhibition of PARP results in the accumulation of DSBs [198]. Given HELZ's role in mediating resistance to PARP inhibition (**Fig. 3.3 F**), our data is suggestive of biological crosstalk between PARP and HELZ. Therefore we asked if myc-HELZ foci localized to DSB sites in a PARP dependent manner. When we treated IR damaged cells with a PARP inhibitor, myc-HELZ foci failed to accumulate at DSB sites, failing to co-localize with DSB marker γ H2AX (**Fig. 3.5 A-B**). Together, our data strongly suggests a role for HELZ in the DSB response.

To more directly pinpoint how HELZ is functioning in the DSB response, including which pathway HELZ may be participating in, we examined HELZ depletion in U2OS cells stably expressing reporters to DSB repair pathways. These reporters function where expression of I-SceI endonuclease generates a DSB that restores GFP expression when repaired. We examined the expression of GFP via the DR-GFP reporter, which measures HR repair, the

EJ5 reporter, which measures classical non-homologous end joining (c-NHEJ), and the EJ2 reporter, which measures alternative NHEJ (alt-NHEJ). We found that HELZ depletion impaired GFP expression within the DR-GFP reporter (**Fig. 3.4 B-C**), suggesting HELZ promotes HR. This is in keeping with our PARP inhibitor sensitivity data, as increased sensitivity to PARP inhibitors is associated with defects in HR. We additionally found that HELZ impaired GFP expression within the EJ5 reporter (**Fig. 3.5 C**) and within the EJ2 reporter (**Fig. 3.5 D**), indicating that HELZ may also be involved in c-NHEJ and alt-NHEJ. Together, these data suggest that HELZ might be functioning far upstream to regulate DNA pathway choice.

One of the earliest events of HR is DNA end resection. Thus, we next asked if HELZ functions upstream of DNA end resection in HR. We proceeded by testing if knockdown of HELZ impaired a marker of HR end resection, pRPA32 S4/8 in response to DSB. Surprisingly, CPT treated cells did not show any deficiency in end resection in response to HELZ knockdown (**Fig. 3.5 E**) suggesting that HELZ may play individual roles further downstream in all three DSB pathways examined.

To this end, we looked further downstream of end resection in the HR pathway to see if HELZ facilitated the later steps of HR. After end resection, RAD51 is loaded onto the ssDNA overhangs generated by end resection, which serve to facilitate strand invasion of the sister chromatid. RAD51 filament formation on ssDNA has been previously demonstrated to be regulated by helicases [72, 199]. So, we asked if HELZ effected RAD51 foci formation in U2OS cells after IR treatment. HELZ depletion resulted in a 75 percent

reduction in RAD51 foci formation (**Fig. 3.4 D-E**). Together, these data place HELZ in the HR pathway after DNA end resection but before RAD51 loading on ssDNA.

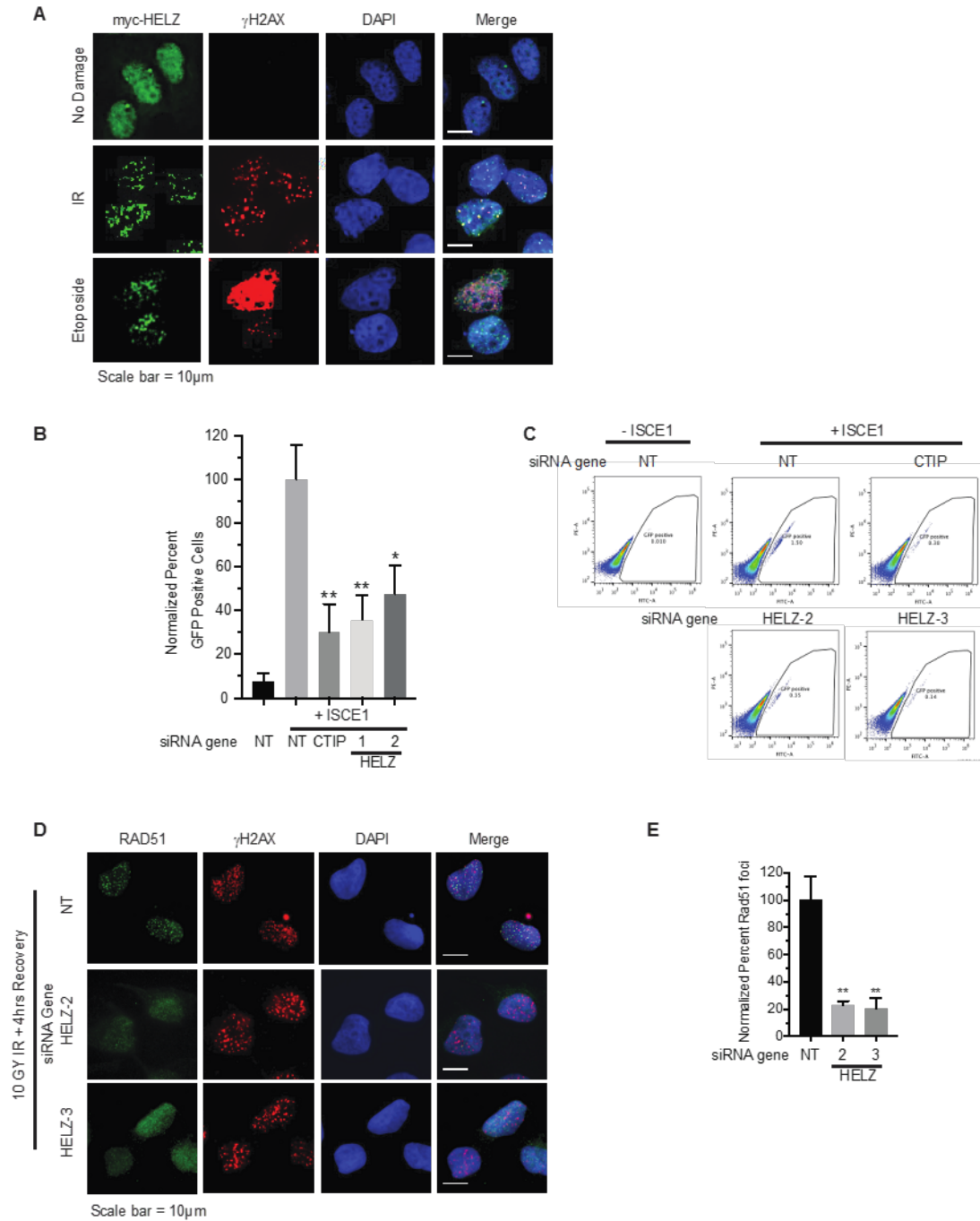


Fig. 3.4. HELZ localizes to and promotes repair of DNA Double Strand Breaks through the HR pathway

(A) HELZ localizes to DSB repair foci. U2OS cells were transiently transfected with myc-HELZ. 72 hours post-transfection, cells were subjected to IR and allowed to recover for

four hours, or treated continuously with etoposide for four hours. Cells were fixed and stained with antibodies for the detection of the indicated markers. Representative images of myc-HELZ nuclear co-localization with γ H2AX as seen before and after treatment with damaging agents are shown. Scale bars represent 10 μ m. **(B-C)** HELZ mediates homologous recombination repair. Analysis was performed in U2OS cells stably expressing the DR-GFP reporter that measures HR. DR-GFP cells were transfected with siRNA targeting HELZ, ctIP, or a NT control. To induce a double strand break, cells were transfected with ISCE1 plasmid. Groups were assessed for the induction of GFP signal, which indicates successful completion of homologous recombination, by flow cytometry. **(B)** Normalized percent of GFP positive cells is represented. **(C)** Cells analyzed by flow cytometry were gated for FITC signal relative to PE-A. **(D-E)** HELZ promotes RAD51 foci formation in response to DSB. U2OS cells were transfected with siRNA targeting HELZ or a NT control. 72 hours after transfection, cells were damaged with IR, given four hours to recover, and then fixed and stained with antibodies for the detection of the indicated markers. **(D)** Representative images of RAD51 foci formation in cells positive for the DSB marker γ H2AX are shown. Scale bars represent 10 μ m. **(E)** Normalized percent of RAD51 foci formed in γ H2AX positive cells is represented. (For **B** and **E** mean and standard deviation of three replicas is shown.) *** indicates $p < 0.001$.

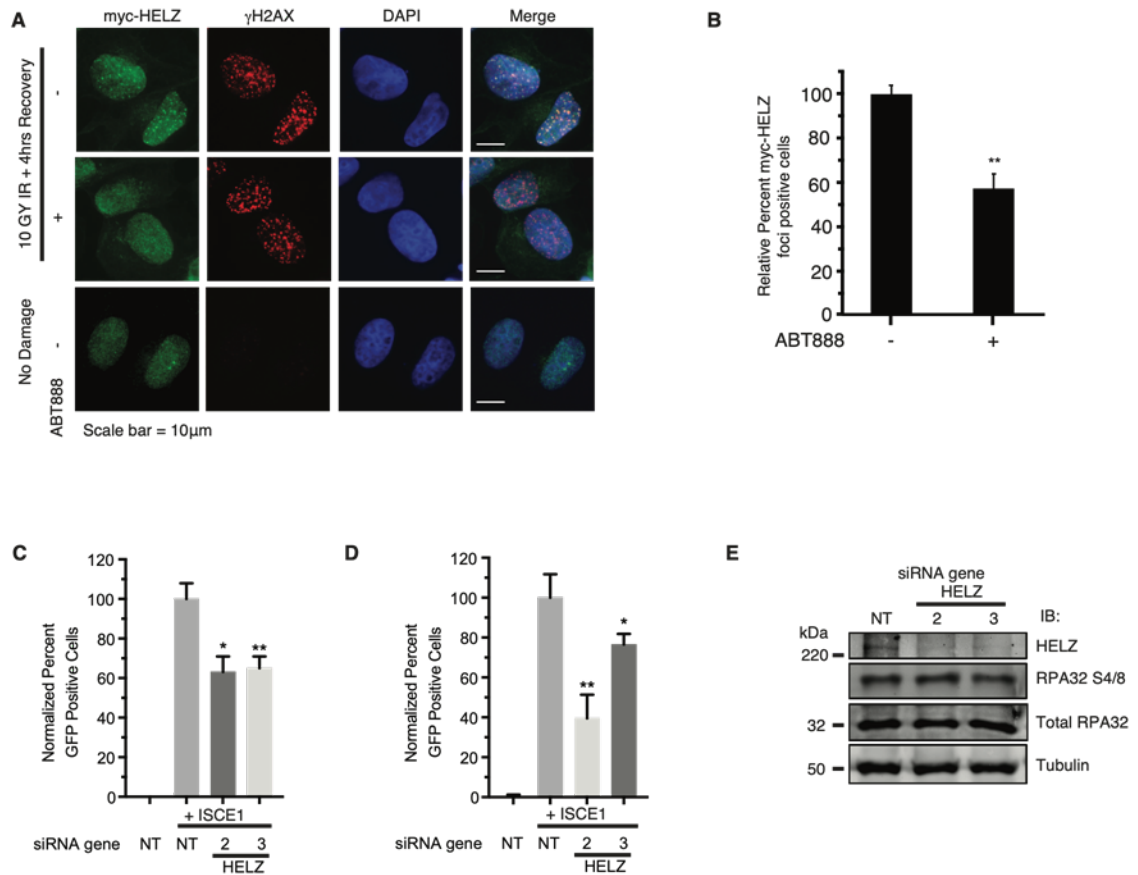


Fig. 3.5. HELZ localizes to and promotes repair of DNA Double Strand Breaks

(A-B) PARP promotes HELZ localization to DSB repair foci. U2OS cells were transiently transfected with myc-HELZ plasmid. 72 hours post-transfection, cells were treated with ABT888 or left untreated, and subjected to IR and allowed to recover for four hours, as indicated. Cells were fixed and stained with antibodies for the detection of the indicated markers. (A) Representative images of myc-HELZ nuclear co-localization with γ H2AX as seen before and after treatment with IR with and without ABT888 are shown. Scale bars represent 10 μ m. (B) Normalized percent of myc-HELZ foci formed in γ H2AX positive cells is represented. (C) HELZ mediates c-NHEJ. Analysis was performed in U2OS cells stably expressing the EJ5 reporter that measures c-NHEJ. EJ5 cells were transfected with

siRNA targeting HELZ or a NT control. To induce a DSB, cells were transfected with ISCE1 plasmid. Groups were assessed for the induction of a GFP signal, which indicates successful completion of alt-NHEJ, by flow cytometry. Normalized percent of GFP positive cells is represented. **(D)** HELZ mediates alt-NHEJ. Analysis was performed in U2OS cells stably expressing the EJ2 reporter that measures alt-NHEJ. EJ2 cells were transfected with siRNA targeting HELZ or a NT control. To induce a DSB, cells were transfected with ISCE1 plasmid. Groups were assessed for the induction of GFP signal, which indicates successful completion of alt-NHEJ, by flow cytometry. Normalized percent of GFP positive cells is represented. **(E)** HELZ does not promote DNA end resection. Cells were transfected with siRNA targeting HELZ or a NT control. 72 hours post knockdown, cells were treated with 2 μ M CPT for four hours to induce DSBs. Cells were harvested, lysed and run on SDS-PAGE. Western blot analysis was performed and cells were analyzed for the induction of pRPA32 S4/8, a key marker of DNA end resection. (For **E**, a representative blot from 3 independent experiments (n=3) is shown. For **B**, **C** and **D**, mean and standard deviation of three replicas is shown.) *** indicates $p < 0.001$.

HELZ Promotes Genomic Stability

Failure to complete homologous recombination or other DSB repair pathways can result in the induction of genomic instability. Given HELZ's role in DSB pathways, and its role in mediating resistance to hydroxyurea (**Fig. 3.3 C**), which functionally induces DNA replication stress, we asked if HELZ helps to maintain genomic stability. We depleted HELZ in immortalized 293T cells and examined markers of genomic instability. RPA32 signaling plays an important role in maintaining genomic stability and cell survival in response to replication stress, marked by the phosphorylation of serine 33 [200]. Depletion of HELZ resulted in spontaneous phosphorylation of RPA32 at S33, suggesting HELZ prevents DNA replication stress (**Fig. 3.6 A**). We then decided to look at more global markers of genomic instability, and found that HELZ depletion resulted in the formation of micronuclei (**Fig. 3.6 B-C**), and the spontaneous induction of γ H2AX (**Fig. 3.6 D-E and Fig. 3.7 A**). Furthermore, we found spontaneous upregulation of other markers of DNA damage, including spontaneous phosphorylation of DNAPKCs at its autophosphorylation site, S2056 (**Fig. 3.6 F**), and phosphorylation of ATR at T1989 (**Fig. 3.7 B**), providing additional evidence that HELZ governs genomic stability.

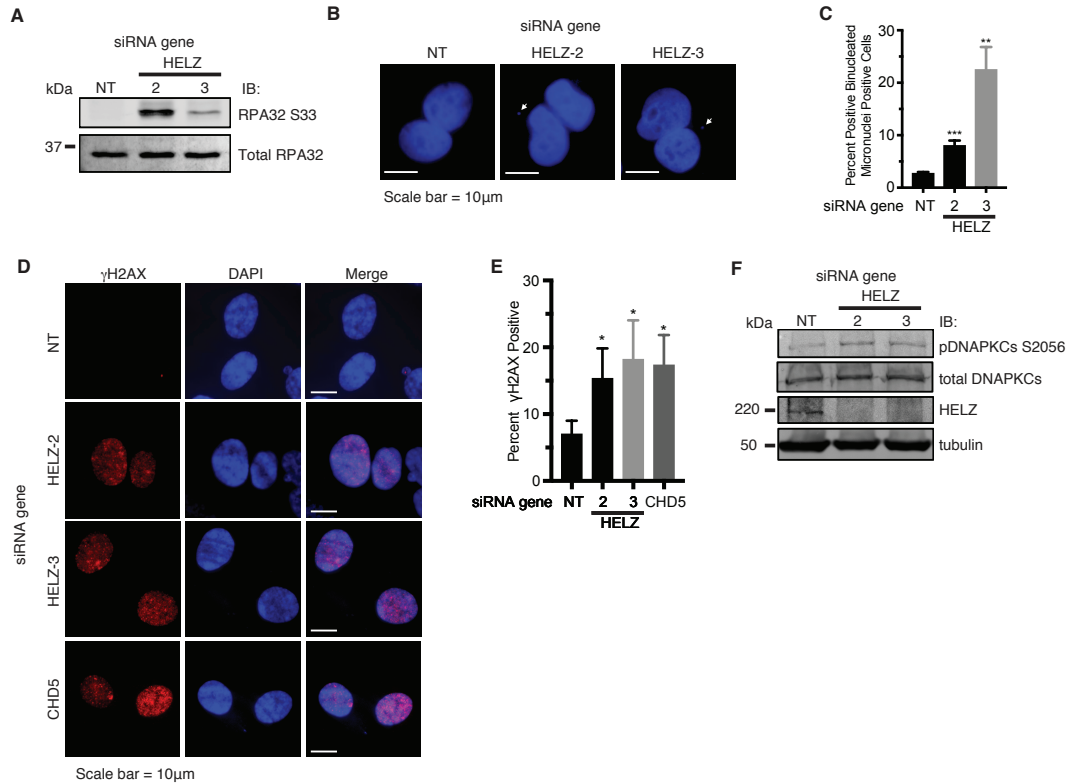


Fig. 3.6. HELZ Promotes Genomic Stability

(A) HELZ knockdown leads to spontaneous induction of DNA replication stress marker pRPA32 S33. Immortalized non-tumorigenic HEK-293T cells were transfected with siRNA, targeting HELZ or a NT control. 72 hours post knockdown, cells were harvested, lysed and run on SDS-PAGE. Western blot analysis was performed and membranes were immunoblotted with the indicated antibodies. (B-C) HELZ knockdown promotes formation of micronuclei in binucleated cells. Cells were transfected with siRNA targeting HELZ or a NT control. 72 hours post knockdown, cells were fixed and stained with DAPI. (B) Representative images of binucleated cells stained with DAPI. The arrow indicates the presence of a micronucleus. (C) Quantification of the percent of binucleated cells that were positive for one or more micronucleus is represented. (D-E) HELZ knockdown promotes the spontaneous formation of γ H2AX foci. Immortalized non-tumorigenic RPE-1 cells

were transfected with siRNA targeting HELZ or a NT control. 72 hours post knockdown, cells were fixed and stained for γ H2AX. **(D)** Representative images of undamaged cells with or without spontaneous γ H2AX foci formation in the nucleus. **(E)** Quantification of percent of cells positive for spontaneous γ H2AX foci. Cells with >5 foci per nucleus with an intensity above background were considered positive. **(F)** HELZ knockdown leads to spontaneous induction of pDNAPKCs S2056. HEK-293T cells were transfected with siRNA targeting HELZ or a NT control. 72 hours post knockdown, cells were harvested, lysed and run on SDS-PAGE. Western blot analysis was performed and membranes were immunoblotted with the indicated antibodies. (For **A** and **F**, a representative blot from 3 independent experiments (n=3) is shown. For **C** and **E**, the mean and standard deviation of three replicas is shown). *** indicates $p < 0.001$. Scale bars represent 10 μ m.

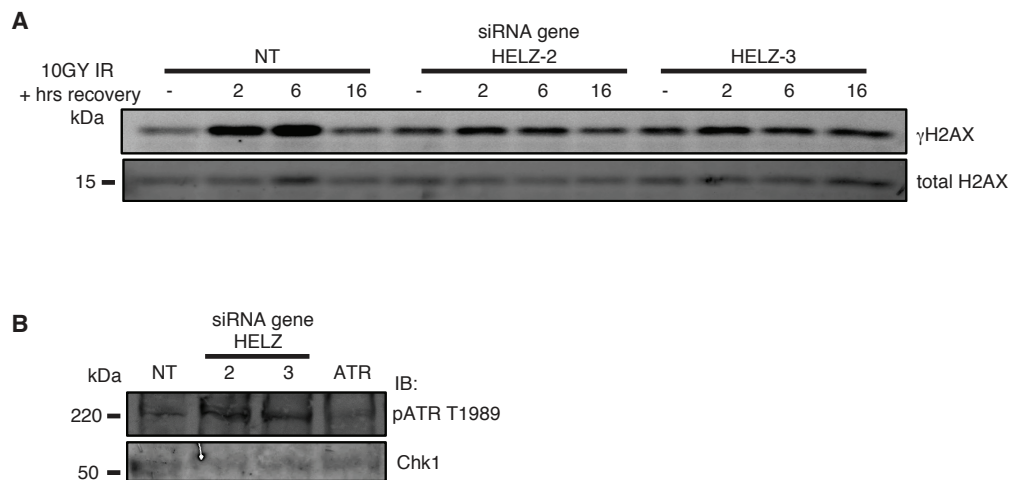


Fig. 3.7. HELZ promotes Genomic Stability, 2

(A) HELZ knockdown leads to spontaneous phosphorylation of γ H2AX. HEK-293T cells were transfected with siRNA targeting HELZ or a NT control. 72 hours post knockdown, cells were irradiated with 10 GY IR and allowed to recover at the indicated time, or left untreated. Cells were harvested, lysed and run on SDS-PAGE. Western blot analysis was performed and membranes were immunoblotted with the indicated antibodies. **(B)** HELZ knockdown leads to spontaneous induction of pATR T1989. HEK-293T cells were transfected with siRNA targeting HELZ or a NT control. 72 hours post knockdown, cells were harvested, lysed and run on SDS-PAGE. Western blot analysis was performed and membranes were immunoblotted with the indicated antibodies. (For **A** and **B**, a representative blot from 3 independent experiments (n=3) is shown).

HELZ interacts with HR proteins PRP19 and DDX1 and promotes DNA-RNA Hybrid Resolution

To more clearly define the mechanism by which HELZ regulates HR and genomic stability, we performed MS analysis of HELZ immunopurified from 293T cells treated with or without etoposide. (**Fig. 3.8 A**). As expected, we found peptide enrichment corresponding to HELZ, as well as EBF3, one of HELZ's interacting proteins identified previously [201]. We also found interaction with HR proteins PRP19, DDX1 and DDX21 (**Fig. 3.8 B**). DDX1 and DDX21 are intriguing because they are also RNA helicases involved in HR. Co-IP of SFB-PRP19 pulled down HA-HELZ (**Fig. 3.8 C**). Furthermore, IP of HA-HELZ pulled down endogenous DDX1 (**Fig. 3.8 D**), validating the interactions identified by MS. PRP19 facilitates NER by catalyzing the ubiquitination of RPA, facilitating its removal from ssDNA overhangs and promoting RAD51 loading there [71]. Furthermore, DDX1, another RNA helicase, has been implicated in HR in resolving DNA-RNA hybrids, which can form at ssDNA overhangs after end resection [72]. We therefore hypothesized that HELZ may similarly function to resolve DNA-RNA hybrids. Depletion of HELZ in CALU-3 cells increased spontaneous hybrid levels and hybrid levels in response to etoposide damage, suggesting that HELZ may be resolving hybrids, possibly through its helicase activity. (**Fig. 3.8 D**). We then asked if HELZ had functionality as a helicase by mutating the conserved residue critical for the function of other helicases (K674N). We examined if helicase dead HELZ was capable of restoring etoposide resistance in SCLC. Interestingly, both wild HELZ and the K674N mutant restored etoposide resistance, but the K674N mutant restored viability to a lesser extent than wild type HELZ (**Fig. 3.8 F**). These data indicate that (1) residue 674 is functional in HELZ where it likely promotes

helicase function, and (2) residue 674 at least in part mediates etoposide resistance in SCLC. Collectively, these data suggest that HELZ regulates DNA-RNA hybrid resolution and etoposide resistance, potentially through its helicase function.

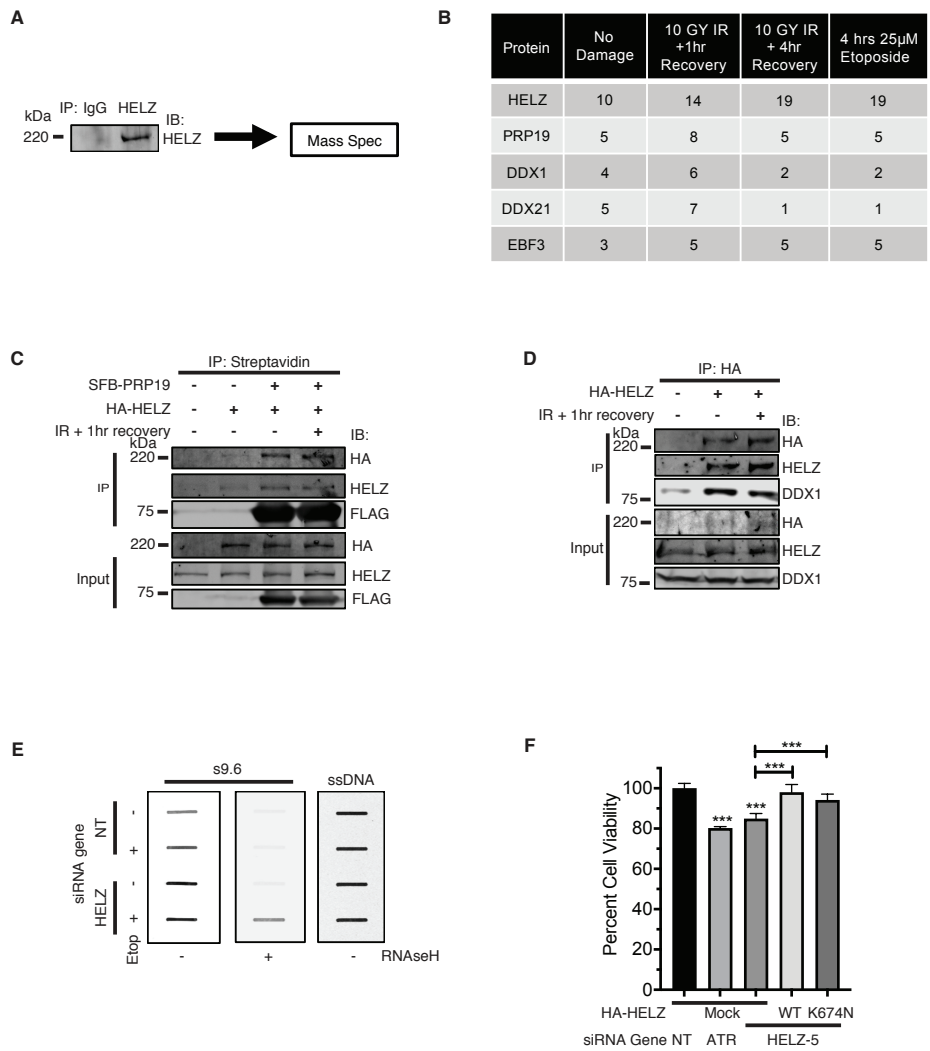


Fig. 3.8. HELZ interacts with HR proteins PRP19 and DDX1 and promotes DNA-RNA Hybrid resolution

(A-B) HEK-293T cells were damaged with 10 GY IR and allowed to recover at the indicated times, treated with etoposide for four hours, or left untreated. Cells were harvested, lysed and immunoprecipitated (IP'd) with HELZ antibody or normal rabbit IgG as a control, using protein A agarose beads. Beads were washed and processed for mass spectrometry (MS) analysis for protein-protein interactions. (B) Summary of IP-MS

results for HELZ. Peptide counts corresponding to proteins of interest enriched for interaction with HELZ are represented, background-subtracted for peptides interacting with IgG at baseline. (C) HEK-293T cells were transfected with HA-HELZ and SFB-PRP19. 48 hours post transfection, groups were damaged with 10 GY IR and allowed 1 hour to recover, or left undamaged. Cells were harvested, lysed and IP'd with streptavidin beads. Samples were run on SDS-PAGE, and immunoblotted with indicated antibodies. (D) HEK-293T cells were transfected with HA-HELZ. 48 hours post transfection, groups were damaged with 10 GY IR and allowed 1 hour to recover, or left undamaged. Cells were harvested, lysed and IP'd with HA conjugated beads. Samples were run on SDS-PAGE, and immunoblotted with indicated antibodies. (E) HELZ promotes DNA-RNA hybrid resolution. Calu-3 cells were transfected with siRNA targeting HELZ or a NT control. 72 hours post knockdown, groups were left untreated or treated with 20 μ M etoposide for five hours. DNA was extracted and either treated with RNaseH or left untreated. Slot blot analysis was performed to assess the presence of DNA-RNA hybrid formation using the S9.6 antibody. The ssDNA signal indicates total DNA loaded per sample. (F) HELZ helicase activity only partially rescues etoposide sensitivity in SCLC. H128 cells were transfected with siRNA targeting the HELZ 5'UTR (HELZ-5) or a NT control. The following day, cells were transfected with HELZ WT, K674N mutant, or mock transfected. 72 hours post knockdown and 48 hours post overexpression, cells were treated with 5 μ M etoposide for 72 hours and subsequently assessed for cell viability. Percent cell viability, normalized to NT control, is represented. (For C-E, representative blots from 3 independent experiments (n=3) is shown. For F, mean and standard deviation of three replicas is shown. *** indicates $p < 0.001$.)

High HELZ Expression is Associated with Poor Outcome in Cancers

Given that HELZ mediates etoposide resistance in SCLC, likely in part through its helicase function, we asked if there were any links to HELZ expression in cancers. Although HELZ expression level or mutational status does not significantly drive any particular cancer, there are associations between HELZ expression level and patient outcome, in both breast and cervical cancer (**Fig. 3.9 A-B**).

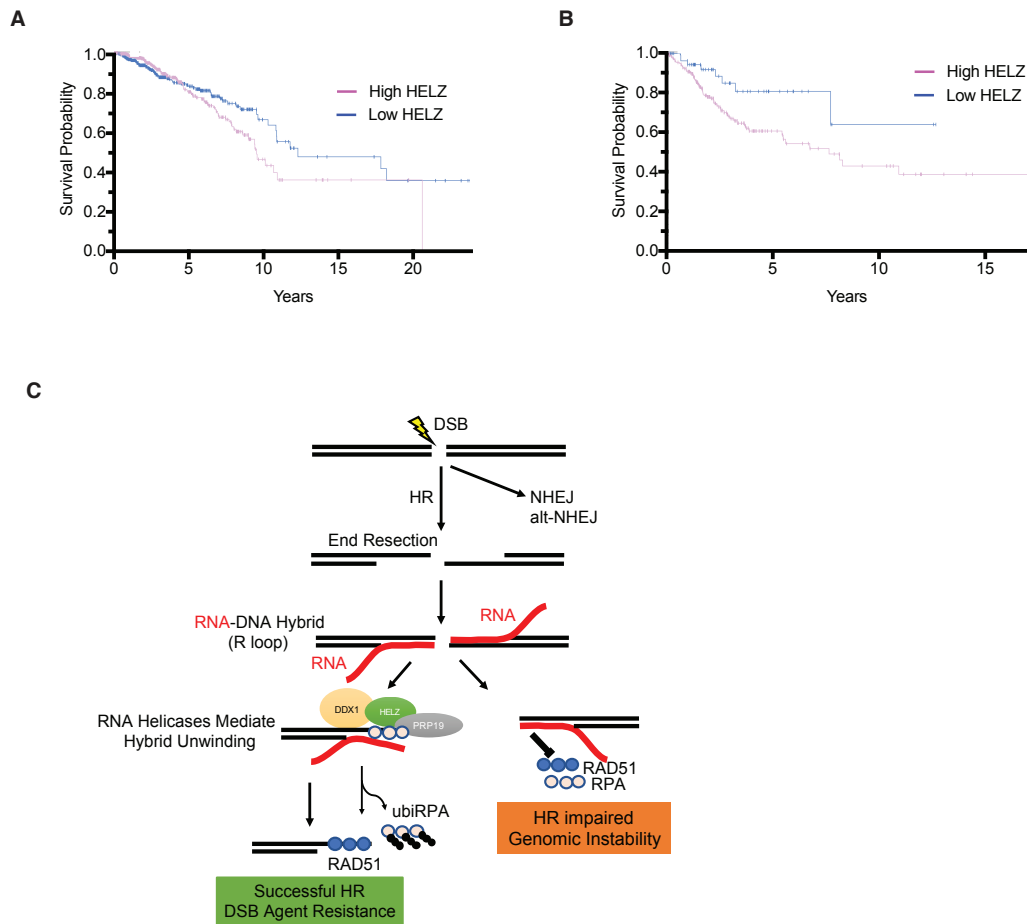


Fig. 3.9. High HELZ Expression is associated with poor outcome in cancers and model for HELZ in HR

(A-B) Kaplan-Meier curves were mined from the Human Protein Atlas database. HELZ expression data was correlated with clinical outcome data. (A) Breast and (B) Cervical cancer patient populations were sorted into high and low HELZ-expressing groups. Survival over time is plotted. (C) Model for HELZ in HR. Following the generation of a DSB, including through etoposide treatment, the homologous recombination pathway activates end resection, exposing 3' ssDNA tails at the site of the break. DNA-RNA hybrids can form at this stage. Together with DDX1, HELZ mediates DNA-RNA hybrid unwinding.

HELZ also interacts with PRP19, which together facilitate the loading of RAD51 on ssDNA and the successful completion of HR. Loss of HELZ prevents DNA-RNA hybrid resolution at 3' ssDNA overhangs, impairment of RAD51 loading on ssDNA, and impairment of homologous recombination overall. Lack of HR can lead to DSB persistence and induction of genomic instability, or activation of apoptosis and the sensitization of cancer to DSB agents such as etoposide.

3.6 Discussion

Our assembled data reveal HELZ as a novel RNA helicase that promotes homologous recombination and helps maintain genomic stability. Using a synthetic lethality screen of a siRNA library biased towards nuclear enzymes, we identified key regulators of etoposide resistance in SCLC cells, including HELZ. We found that depletion of HELZ causes hypersensitivity to DSB inducing agents and that HELZ localizes to DBSs in a PARP dependent manner. There, HELZ promotes DSB repair pathways, including homologous recombination, downstream of DNA end resection, where HELZ depletion impairs proper RAD51 foci formation in response to IR. Furthermore, HELZ depletion induces markers of genomic instability. We found that HELZ interacts with HR proteins PRP19 and DDX1 and helps resolve DNA-RNA hybrids, and that HELZ's helicase function is implicated in mediating etoposide resistance.

Based on our findings, we propose a model where, in response to DSBs, HELZ functions downstream of end resection. It complexes with PRP19, thereby facilitating PRP19 mediated RPA ubiquitination and RAD51 loading on resected ssDNA. Because ssDNA is highly prone to the formation of hybrids with RNA, especially in areas of active transcription, HELZ functions in concert with its interactor, RNA helicase DDX1, where it helps unwind any formed DNA-RNA hybrids and prevent their persistence, thereby ensuring that the HR pathway continues unperturbed. Successful completion of the HR pathway in response to DSBs facilitates DSB agent resistance in cancer. Loss of HELZ results in failure of RAD51 to load onto ssDNA, likely through the blocking of ssDNA via

unresolved DNA-RNA hybrids. Consequently, HR is impaired and DSBs persist, which, if the cell is equipped to survive these changes, leads to genomic instability. **(Fig. 3.9 C)**.

Future work is needed to elucidate the functional link between HELZ, PRP19 and DDX1. It will be of interest to test if HELZ is required for PRP19 mediated RPA ubiquitination. Perhaps HELZ mediated DNA unwinding facilitates PRP19 recruitment to RPA coated ssDNA complexes. Furthermore, it is also unclear as to why HELZ and DDX1, two RNA helicases that each regulate homologous recombination, are interacting. Helicases have been known to act in concert, including in the DDR. For example, XPB and XPD work together in the larger complex of TFIIH, to unwind DNA and promote NER [202]. It will be important to define the functional interplay between DDX1 and HELZ in resolving DNA-RNA hybrids and facilitating HR, including if they are required to function together or are functionally redundant, and, if they work together, whether one helicase functions upstream to regulate the other. Additionally, RNA helicase SETX has been implicated in RAD51 loading on ssDNA to promote HR [115]. SETX was not identified to interact with HELZ in our MS analysis, and recent reports have also indicated that SETX does not interact with DDX1 either. Thus, it may be worth investigating if there is any functional redundancy between HELZ-DDX1 and SETX [72].

It is intriguing that HELZ promotes HR, NHEJ and alt-NHEJ. Most DDR proteins either function in HR or NHEJ, and very few are capable of participating in both pathways. BRCA1 has been shown to promote both HR and NHEJ, although the exact mechanisms are still not fully understood. BRCA1 mediates RAD51 strand transference to promote HR

and negatively regulates end resection to promote NHEJ [203, 204]. Our data indicate that HELZ may be playing individual roles in HR and NHEJ. Interestingly, neither DDX1 nor SETX share this phenotype. Depletion of SETX only mildly impaired HR and SSA, and mildly enhanced NHEJ. Depletion of DDX1 mildly impaired HR, alt-NHEJ and SSA, but also mildly enhanced NHEJ. Thus, HELZ may have a function separate from its interaction with DDX1 in promoting NHEJ.

Our data that HELZ possesses helicase functions needs to be strengthened. HELZ is currently described as a putative RNA helicase in the literature. Our data that HELZ promotes DNA-RNA hybrid resolution, taken together with our data that HELZ is involved in homologous recombination, certainly suggest that HELZ is a functional helicase, as other RNA helicases are heavily involved in these processes as well. Furthermore, we directly tested the putative catalytic function of HELZ by site-directed mutagenesis, altering residue 674 from a lysine to asparagine. While this residue is conserved and important for helicase function in other RNA helicases, our data does not directly show that HELZ's helicase activity is abolished in this mutant. In future work, it will be important to first show that HELZ is functional as a helicase through biochemical assays, and demonstrate that HELZ K674N is indeed helicase dead. Moreover, many RNA helicases also have DNA binding capabilities, providing rationale for the intersection of RNA processing biology with the DNA damage response pathway. The intersection of these pathways is an area of active investigation, and the literature suggests moonlighting roles for transcription modulators in repairing DNA damage at sites of active transcription, and in resolving DNA-RNA hybrids, which generally form when DNA damage occurs in

areas of active transcription. Our data show that HELZ is important for the resolution of DNA-RNA hybrids. Thus, testing if HELZ also possesses DNA binding capabilities is of interest moving forward.

From a clinical standpoint, our data shows that HELZ expression is merely associated with breast and cervical cancer, however, the role of HELZ in driving cancer or in mediating resistance to cancer treatments is worth further investigation, especially since breast and cervical cancer are responsive to DNA damaging agents that induce DSBs. Thus, targeting HELZ in combination with etoposide, radiation or other DSB agents provides an avenue for therapeutic gain. There are currently no HELZ inhibitors in existence. However, helicases have been established as targetable molecules, as small molecules have been identified to successfully impair the function of other helicases [205]. Together, our data provides a rationale for further investigation of HELZ as a therapeutic target for cancers resistant to DSB agents.

3.7 Acknowledgements

The myc-HELZ plasmid was a kind gift from Dr. Roland Wenger (University of Zürich, Switzerland).

3.8 Funding

This work was supported by NIH/NCI [R01CA178999 to D.S.Y., F31CA225119 to A.E.K.] and the Lung Cancer Research Foundation [51347 and 60208 to D.S.Y].

3.9 Conflict of Interest

The authors declare no competing interests.

Chapter 4: Discussion

4.1 Summary of Key Findings and Remaining Questions

In recent years, there has been an increased focus on improving SCLC patient outcomes. The addition of immunotherapy to the approved therapeutic regimen marks the first development in this area in decades. However, the introduction of immunotherapy has only served to marginally shift patient outcomes, with a change in median survival occurring on the order of months. Better options are urgently needed for SCLC. Targeted therapy that is synthetically lethal with the first-line chemotherapeutic regimen of etoposide with platinum is an avenue that, until now, had not been explored. This thesis presents the results of two high throughput screens examining a library of over one thousand nuclear enzymes for the strongest candidates that, when knocked down, re-sensitize chemotherapy-resistant SCLC cells to cisplatin or etoposide, respectively. We identified enriched pathways and characterized the most promising hits, including EZH2, a cisplatin sensitization hit, and HELZ, an etoposide sensitization hit.

EZH2 was the only synthetic lethal candidate overexpressed in SCLC, making it a viable candidate for therapeutic targeting. Moreover, there are a number of inhibitors that already have been developed to target EZH2, including several that are undergoing testing in other clinical trials related to cancer. On the other hand, though HELZ is not amplified or commonly mutated in SCLC, our data suggest that its putative helicase function is important for governing etoposide sensitivity in resistant cells. We provide evidence that HELZ may be important for clearing DNA-RNA hybrids, structures that are capable of

further distorting the genome, which can exacerbate the chemotherapy resistance seen in SCLC.

Current literature describes HELZ as a putative RNA helicase. Collectively, our data that HELZ promotes DNA-RNA hybrid resolution, and our data that HELZ is involved in homologous recombination, certainly suggests that HELZ is a functional helicase, as other RNA helicases are heavily involved at the intersection of these processes. Furthermore, we directly tested the putative catalytic function of HELZ by site directed mutagenesis, altering residue 674 from a lysine to asparagine. While this residue is conserved and important for helicase function in other RNA helicases, our data does not directly show that HELZ helicase activity itself is abolished in this mutant. In future work, it will be important to first show that HELZ is functional as a helicase through biochemical assays, and to demonstrate that the HELZ K674N mutant is indeed helicase dead. Moreover, many RNA helicases also have DNA binding capabilities, providing a rationale for the intersection of RNA processing biology with the DNA damage response pathway. The intersection of these pathways is an area of active investigation, and may explain how DNA damage is preferentially repaired at sites of active transcription. Dual DNA and RNA binding and unwinding roles may also be a key mechanism for resolution of DNA-RNA hybrids, which generally form when DNA damage occurs in areas of active transcription. Our data shows that HELZ is important for the resolution of DNA-RNA hybrids. Thus, testing whether HELZ also possesses DNA binding capabilities is of interest moving forward.

This work also demonstrates a catalytic and PRC2 independent role for EZH2 in NER in promoting the stability of DDB2. Interestingly, parallel discoveries have been made in the TC-NER pathway, where the UVSSA-USP7 complex mediates stability of CSB before it is ubiquitinated. Our work suggests that the stabilization and ubiquitination of lesion detection factors is a unifying mechanism that ensures appropriate lesion recognition in both branches of NER. Our finding that EZH2 plays a role in stabilizing DDB2 in NER is of additional relevance because USP7 has been reported to interact with EZH2 at sites of transcription, where they together stabilize transcription factors involved in neuronal differentiation [186]. Thus, our work may have uncovered an additional mechanistic role for the EZH2-USP7 complex in NER. It is possible that USP7 is functional in both branches of NER, where it can be adapted by EZH2 or UVSSA to regulate DDB2 or CSB stability, respectively. While our work suggests that EZH2 is functioning in GG-NER by stabilizing DDB2, it will be of interest to determine if EZH2 is also capable of promoting the stability of CSB and functioning in TC-NER.

Further experimental work is needed to determine how EZH2 is preventing DDB2 ubiquitination to promote its stability in the context of NER. Perhaps EZH2 is recruiting USP7 to prevent DDB2 ubiquitination. EZH2 may recruit another deubiquitinating enzyme (DUB), as interactions have been reported to occur between DDB2 and USP24 to mediate DDB2 stability [183]. It is also possible that EZH2 may be functioning separately from DUBs, perhaps structurally masking the n-terminal DDB2 autoubiquitination site, which we have defined as the site of EZH2-DDB2 interaction, thereby facilitating DDB2 stabilization.

To date, individual factors that mediate DDB2 stability have been studied, but how these factors function together remains poorly understood. It was reported that PARP1 plays a role in stabilizing DDB2 in NER, where PARP1 interacts with DDB1-DDB2 and parylation of DDB2 functionally opposes ubiquitination of DDB2, thereby promoting DDB2 stability [184]. It may be worth investigating if EZH2 and PARP1 are functioning together to regulate DDB2 stability in NER. Indeed, PARP1 and EZH2 have been reported to function together in other biological processes, including in the DDR [206]. Furthermore, PARP1 and EZH2 are both aberrantly expressed in SCLC, and their common function in stabilizing DDB2 to promote NER may explain the tendency of SCLC to develop resistance to cisplatin.

4.2 The Utility of Phenotypic Screens

High-throughput genetic-based screens are important tools that can be used in an unbiased fashion to understand which genes are responsible for a given phenotype. The rise of next-generation sequencing has made it possible to rapidly screen through the entire genome and better characterize all of its players in specific molecular contexts, where the mechanisms are poorly understood.

Phenotypic screens range in their biological readout, from cell viability to phenotypic abnormalities of embryos or cells [207]. One of the earliest phenotypic screens sought to identify novel genes involved in cell cycle progression in the lung cancer cell line A549.

Using a commercial library of 16,320 small molecules targeting specific protein functions, 139 compounds were identified to affect the endpoint of mitosis [208].

Some of the most interesting advances in the DNA repair field have come from screens. FAN1 was first discovered for its critical role in intrastrand crosslink repair in a shRNA screen for genes conferring resistance to the crosslinking agent MMC in U2OS cells [209]. Now, FAN1 is considered a central nuclease in the Fanconi Anemia pathway for the repair of intrastrand crosslinks. Another proteomic screen identified over 900 potential phosphorylation sites that are substrates of ATM/ATR, with sites occurring on 700 different proteins. The study identified both known and novel ATM and ATR substrates, implicating novel roles for many proteins in the DDR, and/or providing evidence for how ATM and ATR might be connected to other biological processes [210]. These results suggest that there is still much to characterize in both the DDR, and in the interactions occurring between DDR related proteins with other pathways.

Significant advances in cancer therapy have also come from high throughput screens. Chemical screens are particularly useful in identifying compounds targeting molecules that have no existing or useful inhibitors. Notably, Mirin, a potent inhibitor targeting MRE11 was first discovered in a forward chemical genetic screen. [211]. Now Mirin holds promise for use in clinical trials. As with EP resistance in SCLC, gemcitabine resistance poses a challenge for the treatment of pancreatic cancer. One group developed a screen where they stratified pancreatic cancer cells into gemcitabine sensitive and resistant groups and examined differential gene expression between groups to see if patterns in gene expression correlated with gemcitabine sensitivity or resistance. Of note, they found that the pro-

apoptotic factor BNIP3 was an important mediator of gemcitabine sensitivity [212]. BNIP3 status is now routinely examined in pancreatic cancer, particularly in the context of treatment.

Our work demonstrates the power of screens as a tool to discover the molecular roles of understudied factors. There are approximately 20,000 genes in the human genome, many of which are not yet characterized. Our work now provides evidence of a specific function for one of the many poorly characterized genes, HELZ, which has now been linked to the DNA damage response for the first time. In a similar fashion, other papers have used high throughput screens to link novel factors to the DDR. One screen aiming to identify novel DDR factors knocked down a library of genes and examined if cells failed to exhibit damage induced cell cycle arrest in response to IR. This study identified a role for a previously uncharacterized protein, RHINO, in the DDR. The study went on to characterize the specific role of RHINO in the DDR, where it binds to the 9-1-1 complex and promotes Chk1 activation [213].

Screens are also useful because they can help place well-characterized proteins into new molecular contexts. Our identification for a catalytic independent and PRC2 independent role of EZH2 in NER was developed from the results of our cisplatin sensitivity screen, particularly because EPZ6438, an enzymatic inhibitor of EZH2, could not replicate the cisplatin sensitization phenotype identified in our screen, whereas siRNA mediated knockdown and DZNep treatment could, despite the fact that EZH2 is heavily established in its role as a global transcription silencer as a member of the PRC2 complex, which depends on its catalytic activity. Indeed, there are very few roles published on EZH2

outside of the context of its catalytic activity and role in PRC2. Similarly, a homologous recombination screen identified a novel role for RBMX in the DDR, where it had previously been well characterized in its role in alternative splicing. Their screen knocked down a library of siRNAs in cells stably expressing a reporter for homologous recombination (DR-GFP) identifying genes that mediated HR. Their results showed that RBMX has a novel role in facilitating homologous recombination, and further, that this occurs through its regulation of BRCA2 expression. [214] Thus, their work placed RBMX in a context outside of alternative splicing, and further, suggested that there may be functional links between RNA processing and the DDR. Thus, screens are an excellent tool to identify novel roles for genes that have already been characterized, and potentially, to provide evidence of pathway crosstalk.

4.3 Non-Catalytic Roles of DDR Molecules

Beyond our finding that EZH2 has a non-catalytic independent role in promoting NER, catalytic versus non-catalytic functions have been explored elsewhere in the DDR. ATR, a global transmitter in the DDR, is known to function through its kinase activities. In response to RPA coated ssDNA, ATR acts as a kinase to phosphorylate substrates, mainly its effector kinase Chk1. Together, ATR and Chk1 regulate the cell cycle by promoting the stability of stalled replication forks. Interestingly, studies in genetically engineered mouse models have demonstrated that genetic ATR catalytic inhibition significantly differs on a phenotypic level from ATR null mice *in vivo*. Similar findings were also observed when

comparing ATM and DNAPKCs mouse models. In all cases, deletion mouse models differed greatly from enzyme dead knock-in mouse models, with oncogenic phenotypes, especially genomic instability, occurring more intensely in mouse models expressing enzyme dead versions of ATR, ATM and DNAPKCs when compared to mouse models that are null for each kinase [215-217]. These results suggest that catalytic inhibition and depletion of proteins are not equivalent, as they can result in phenotypes that are very different. Moreover, there is evidence that conformational changes that are associated with kinase activation may promote the recruitment of DDR kinases to sites of damage. After their DDR activities are performed, kinases are deactivated, and returned to an inactive conformation, with lower affinity for the site of DNA damage. Competitive, non-depleting enzymatic inhibitors are hypothesized to trap these DDR kinases in their active conformation at sites of DNA damage, thus blocking other DNA processing activities, including essential downstream DNA repair processes. Indeed, if kinases are depleted, they are not capable of being trapped in this way. By extension, this may explain why our data that catalytic inhibition versus depletion of EZH2 result in different phenotypes, both in destabilizing DDB2 and in sensitizing SCLC to cisplatin.

Similar to our findings on a catalytic independent role of EZH2 in NER, another classical histone methyltransferase, SETD1A, which is well-characterized for placing H3K4 methylation marks on chromatin, was found to have a role in the DDR independent of its catalytic activity. A non-catalytic but conserved domain within SETD1A was found to be required for binding Cyclin K and for recruitment of Cyclin K to chromatin to induce gene expression of DNA repair genes during the S phase of the cell cycle, including modulating

the expression of *ATR* and *FANCD2A*. However, the catalytic SET domain of SETD1A was dispensable for this role [218]. Interestingly, a SET domain is also the catalytic domain of EZH2, which was mutated in our work to generate the enzyme dead version of EZH2, H689A, and this mutant was found to be dispensable for EZH2's role in NER.

4.4 Linking RNA Processing to the DDR

Our work further elucidates a functional link between RNA processing and the DDR. We identified a role of HELZ, a putative RNA helicase, in HR. HELZ also has defined roles in RNA biology, where it helps modulate translation and mRNA decay. We also identified and validated an interaction between HELZ and PRP19. PRP19 is a ubiquitin ligase most established in its role in RNA splicing and mRNA export, but it has also been linked to the DNA damage response, participating in both the replication stress response and HR [219]. Downregulation of PRP19 results in the induction of spontaneous DSBs. Moreover, PRP19 participates in HR by (1) regulating BRCA1 levels and (2) binding to RPA coating ssDNA overhangs, where it ubiquitinates RPA, promoting its degradation. PRP19 mediated RPA ubiquitination and degradation facilitates the loading of RAD51 on to ssDNA. Therefore, PRP19 promotes the overall progression of the HR pathway [220]. PRP19 has additional roles in the DDR, where it co-localizes with the PCNA replication clamp, promoting ATRIP recruitment to stalled forks. It also participates in crosslink repair, interacting with DNA helicase WRN to facilitate ICL repair. [221]. Our work shows an association between HELZ and PRP19, and taken together with our data supporting HELZ's role in promoting HR, our work provides yet another link between the RNA processor PRP19 and the DDR.

Our MS analysis also identified an interaction between HELZ and DDX21, another RNA helicase that has been linked to the resolution of genomic R loops. Furthermore, the R loop resolving function prevents the accumulation of DNA damage including DSBs [221]. It will be of interest to investigate if the interaction we found between HELZ and DDX21 exists to promote HR and/or genomic stability. Indeed, it is possible that two helicases can function together in the DDR, as has been seen elsewhere in the literature. For example, XPB and XPD are two DNA helicases that work together, in the larger complex of TFIIH, to unwind DNA and promote NER [202].

Overall, the biological intersection between RNA processing and the DDR is still being defined. Well known RNA processers are increasingly emerging with novel roles in the DDR. Conversely, many DDR proteins have been identified to contain RNA binding motifs and/or possess novel roles in responding to RNA. For example, BRCA1-BARD1 was recently shown to interact with DNA-RNA hybrids, where BRCA2 facilitates the recruitment of RNaseH2 to process hybrids at DSB sites [222]. Interactions between DDR proteins and RNA processing molecules are proving necessary to ensure proper DNA repair.

4.5 Translational Applications

Though this is not the first time targeting EZH2 in small cell lung cancer has been suggested, our work is important because it shows that the function of EZH2 in mediating cisplatin resistance is at least in part due to a non-catalytic role of EZH2. This is important

because most potent EZH2 inhibitors that have come into clinical focus target its catalytic activity. One of the most potent EZH2 inhibitors, EPZ6438, did not have an effect on EZH2's role in NER and did not sensitize our cisplatin-resistant SCLC cell line to cisplatin. DZNep is one of the few EZH2 inhibitors capable of depleting EZH2 itself and therefore, DZNep has the capability of targeting all of EZH2's functions, catalytic or otherwise. Indeed, DZNep targeted EZH2's function in NER and showed much more potent synthetic lethality with cisplatin in a cisplatin resistant SCLC cell line as compared to DZNep.

DZNep is not a direct EZH2 inhibitor, but rather a SAH-hydrolase inhibitor. The increase of the intracellular SAH concentration leads to the degradation of the PRC2 complex by a feedback inhibition mechanism. Studies in DZNep have been limited due to the pleiotropic effects of the inhibitor and lack of specificity for EZH2, the substantial toxicity identified in preclinical models, and its short half-life in blood. Thus, the development of other EZH2 depletion agents is warranted. Of note, a number of chemopreventive phytochemicals, such as green tea extract (EGCG) and curcumin, a natural compound isolated from turmeric, show great promise as EZH2 inhibitors, where they have been found to functionally induce the downregulation of EZH2 [223, 224]. Davidiin, a phytochemical extracted from the medicinal plant *P. capitatum*, is of particular interest, where it functionally promotes the proteasomal degradation of EZH2 [225].

Thus far, most efforts to develop EZH2 inhibitors have focused on those that are specific to EZH2's catalytic activity through competition with its cofactor SAM [226]. The work presented in this dissertation provides rationale for the development and further

optimization of molecules that are specifically capable of depleting EZH2 or promoting its degradation.

Helicases also show promise as therapeutic targets of cancer, given the important roles DNA and RNA helicases play in DNA replication and repair. RNA helicases are most well characterized to be involved in transcription and translation, processes cancer cells also rely on to a greater extent than their normal counterparts due to their rapid division. Thus, actively proliferating cancer cells may have increased reliance on helicases to maintain their proliferative status. Importantly, factors that are relied on for cancer cell viability in this way do not usually harbor mutations or amplifications in cancer, but are still promising targets for therapy. Indeed, targeting non-oncogene addiction has been the basis for the development of several well-known anti-cancer treatments, such as 5-fluorouracil, which generally targets cellular metabolism [227]. 5-FU is actively being investigated to treat cancer in many clinical trials and has also been incorporated into the standard of care in several cancers. Thus, although HELZ (and RNA helicases in general) are not strongly associated with cancers, they can still make excellent targets for therapy.

A number of RNA helicase inhibitors have been developed and investigated in cell lines and preclinical models. Mechanistically, they can function to impair RNA binding by targeting ATP and helicase activity, or by trapping the targeted helicase in complex with its RNA substrate, thus impairing its function. For example, Rocaglates and Flavaglines are well studied eIF4A inhibitors that display potent anticancer activity in solid and hematological malignancies. They function by increasing eIF4A affinity for RNA [228].

RNA helicase inhibitors with proven efficacy in preclinical models warrant evaluation for use in clinical trials. Furthermore, RNA helicases with moonlighting roles in DNA repair may be especially promising therapeutic targets, making it possible to target multiple processes necessary for cancer cell survival within a single molecule.

REFERENCES

- 1 Siegel RL, Miller KD, Jemal A. Cancer statistics, 2020. *CA Cancer J Clin* 2020; 70: 7-30.
- 2 Fruh M, De Ruyscher D, Popat S, Crino L, Peters S, Felip E *et al.* Small-cell lung cancer (SCLC): ESMO Clinical Practice Guidelines for diagnosis, treatment and follow-up. *Ann Oncol* 2013; 24 Suppl 6: vi99-105.
- 3 Subramanian J, Govindan R. Lung cancer in 'Never-smokers': a unique entity. *Oncology (Williston Park)* 2010; 24: 29-35.
- 4 Peifer M, Fernandez-Cuesta L, Sos ML, George J, Seidel D, Kasper LH *et al.* Integrative genome analyses identify key somatic driver mutations of small-cell lung cancer. *Nat Genet* 2012; 44: 1104-1110.
- 5 George J, Lim JS, Jang SJ, Cun Y, Ozretic L, Kong G *et al.* Comprehensive genomic profiles of small cell lung cancer. *Nature* 2015; 524: 47-53.
- 6 Rudin CM, Durinck S, Stawiski EW, Poirier JT, Modrusan Z, Shames DS *et al.* Comprehensive genomic analysis identifies SOX2 as a frequently amplified gene in small-cell lung cancer. *Nat Genet* 2012; 44: 1111-1116.
- 7 Umemura S, Mimaki S, Makinoshima H, Tada S, Ishii G, Ohmatsu H *et al.* Therapeutic priority of the PI3K/AKT/mTOR pathway in small cell lung cancers as revealed by a comprehensive genomic analysis. *J Thorac Oncol* 2014; 9: 1324-1331.
- 8 Ross JS, Wang K, Elkadi OR, Tarasen A, Foulke L, Sheehan CE *et al.* Next-generation sequencing reveals frequent consistent genomic alterations in small cell undifferentiated lung cancer. *J Clin Pathol* 2014; 67: 772-776.
- 9 Umemura S, Tsuchihara K, Goto K. Genomic profiling of small-cell lung cancer: the era of targeted therapies. *Jpn J Clin Oncol* 2015; 45: 513-519.
- 10 Rosell R, Wannesson L. A genetic snapshot of small cell lung cancer. *Cancer Discov* 2012; 2: 769-771.
- 11 Park KS, Liang MC, Raiser DM, Zamponi R, Roach RR, Curtis SJ *et al.* Characterization of the cell of origin for small cell lung cancer. *Cell Cycle* 2011; 10: 2806-2815.
- 12 Bernhardt EB, Jalal SI. Small Cell Lung Cancer. *Cancer Treat Res* 2016; 170: 301-322.

- 13 Lara PN, Jr., Gandara DR, Natale RB. Randomized phase III trial of cisplatin/irinotecan versus cisplatin/etoposide in patients with extensive-stage small-cell lung cancer. *Clin Lung Cancer* 2006; 7: 353-356.
- 14 von Pawel J, Schiller JH, Shepherd FA, Fields SZ, Kleisbauer JP, Chrysos NG *et al.* Topotecan versus cyclophosphamide, doxorubicin, and vincristine for the treatment of recurrent small-cell lung cancer. *J Clin Oncol* 1999; 17: 658-667.
- 15 Horn L, Mansfield AS, Szczesna A, Havel L, Krzakowski M, Hochmair MJ *et al.* First-Line Atezolizumab plus Chemotherapy in Extensive-Stage Small-Cell Lung Cancer. *N Engl J Med* 2018; 379: 2220-2229.
- 16 Yang S, Zhang Z, Wang Q. Emerging therapies for small cell lung cancer. *J Hematol Oncol* 2019; 12: 47.
- 17 Morgensztern D, Besse B, Greillier L, Santana-Davila R, Ready N, Hann CL *et al.* Efficacy and Safety of Rovalpituzumab Tesirine in Third-Line and Beyond Patients with DLL3-Expressing, Relapsed/Refractory Small-Cell Lung Cancer: Results From the Phase II TRINITY Study. *Clin Cancer Res* 2019; 25: 6958-6966.
- 18 Karachaliou N, Rosell R, Viteri S. The role of SOX2 in small cell lung cancer, lung adenocarcinoma and squamous cell carcinoma of the lung. *Transl Lung Cancer Res* 2013; 2: 172-179.
- 19 Rudin CM, Poirier JT, Byers LA, Dive C, Dowlati A, George J *et al.* Molecular subtypes of small cell lung cancer: a synthesis of human and mouse model data. *Nat Rev Cancer* 2019; 19: 289-297.
- 20 McClelland SE. Role of chromosomal instability in cancer progression. *Endocr Relat Cancer* 2017; 24: T23-T31.
- 21 Eastman A. The formation, isolation and characterization of DNA adducts produced by anticancer platinum complexes. *Pharmacol Ther* 1987; 34: 155-166.
- 22 Jamieson ER, Lippard SJ. Structure, Recognition, and Processing of Cisplatin-DNA Adducts. *Chem Rev* 1999; 99: 2467-2498.
- 23 Gillet LC, Scharer OD. Molecular mechanisms of mammalian global genome nucleotide excision repair. *Chem Rev* 2006; 106: 253-276.
- 24 Rodriguez A, D'Andrea A. Fanconi anemia pathway. *Curr Biol* 2017; 27: R986-R988.

- 25 Rocha CRR, Silva MM, Quinet A, Cabral-Neto JB, Menck CFM. DNA repair pathways and cisplatin resistance: an intimate relationship. *Clinics (Sao Paulo)* 2018; 73: e478s.
- 26 Lehmann AR. Translesion synthesis in mammalian cells. *Exp Cell Res* 2006; 312: 2673-2676.
- 27 Su WP, Hsu SH, Wu CK, Chang SB, Lin YJ, Yang WB *et al.* Chronic treatment with cisplatin induces replication-dependent sister chromatid recombination to confer cisplatin-resistant phenotype in nasopharyngeal carcinoma. *Oncotarget* 2014; 5: 6323-6337.
- 28 Bi X. Mechanism of DNA damage tolerance. *World J Biol Chem* 2015; 6: 48-56.
- 29 Shen DW, Pouliot LM, Hall MD, Gottesman MM. Cisplatin resistance: a cellular self-defense mechanism resulting from multiple epigenetic and genetic changes. *Pharmacol Rev* 2012; 64: 706-721.
- 30 McClendon AK, Osheroff N. DNA topoisomerase II, genotoxicity, and cancer. *Mutat Res* 2007; 623: 83-97.
- 31 Montecucco A, Zanetta F, Biamonti G. Molecular mechanisms of etoposide. *EXCLI J* 2015; 14: 95-108.
- 32 Sander M, Hsieh T. Double strand DNA cleavage by type II DNA topoisomerase from *Drosophila melanogaster*. *J Biol Chem* 1983; 258: 8421-8428.
- 33 Baldwin EL, Osheroff N. Etoposide, topoisomerase II and cancer. *Curr Med Chem Anticancer Agents* 2005; 5: 363-372.
- 34 Podhorecka M, Skladanowski A, Bozko P. H2AX Phosphorylation: Its Role in DNA Damage Response and Cancer Therapy. *J Nucleic Acids* 2010; 2010.
- 35 Lamarche BJ, Orazio NI, Weitzman MD. The MRN complex in double-strand break repair and telomere maintenance. *FEBS Lett* 2010; 584: 3682-3695.
- 36 Niida H, Nakanishi M. DNA damage checkpoints in mammals. *Mutagenesis* 2006; 21: 3-9.
- 37 Yi C, He C. DNA repair by reversal of DNA damage. *Cold Spring Harb Perspect Biol* 2013; 5: a012575.
- 38 Li GM. Mechanisms and functions of DNA mismatch repair. *Cell Res* 2008; 18: 85-98.

- 39 Krokan HE, Bjoras M. Base excision repair. *Cold Spring Harb Perspect Biol* 2013; 5: a012583.
- 40 Marteijn JA, Lans H, Vermeulen W, Hoeijmakers JH. Understanding nucleotide excision repair and its roles in cancer and ageing. *Nat Rev Mol Cell Biol* 2014; 15: 465-481.
- 41 Sonoda E, Sasaki MS, Morrison C, Yamaguchi-Iwai Y, Takata M, Takeda S. Sister chromatid exchanges are mediated by homologous recombination in vertebrate cells. *Mol Cell Biol* 1999; 19: 5166-5169.
- 42 Jackson SP, Bartek J. The DNA-damage response in human biology and disease. *Nature* 2009; 461: 1071-1078.
- 43 Abraham RT. Cell cycle checkpoint signaling through the ATM and ATR kinases. *Genes Dev* 2001; 15: 2177-2196.
- 44 Knox RJ, Lydall DA, Friedlos F, Basham C, Roberts JJ. The effect of monofunctional or difunctional platinum adducts and of various other associated DNA damage on the expression of transfected DNA in mammalian cell lines sensitive or resistant to difunctional agents. *Biochim Biophys Acta* 1987; 908: 214-223.
- 45 Huang JC, Svoboda DL, Reardon JT, Sancar A. Human nucleotide excision nuclease removes thymine dimers from DNA by incising the 2'nd phosphodiester bond 5' and the 6th phosphodiester bond 3' to the photodimer. *Proc Natl Acad Sci U S A* 1992; 89: 3664-3668.
- 46 Kraemer KH, Patronas NJ, Schiffmann R, Brooks BP, Tamura D, DiGiovanna JJ. Xeroderma pigmentosum, trichothiodystrophy and Cockayne syndrome: a complex genotype-phenotype relationship. *Neuroscience* 2007; 145: 1388-1396.
- 47 Bohr VA, Smith CA, Okumoto DS, Hanawalt PC. DNA repair in an active gene: removal of pyrimidine dimers from the DHFR gene of CHO cells is much more efficient than in the genome overall. *Cell* 1985; 40: 359-369.
- 48 Sigurdsson S, Dirac-Svejstrup AB, Svejstrup JQ. Evidence that transcript cleavage is essential for RNA polymerase II transcription and cell viability. *Mol Cell* 2010; 38: 202-210.
- 49 Ruthemann P, Balbo Pogliano C, Naegeli H. Global-genome Nucleotide Excision Repair Controlled by Ubiquitin/Sumo Modifiers. *Front Genet* 2016; 7: 68.
- 50 Scrima A, Konickova R, Czyzewski BK, Kawasaki Y, Jeffrey PD, Groisman R *et al.* Structural basis of UV DNA-damage recognition by the DDB1-DDB2 complex. *Cell* 2008; 135: 1213-1223.

- 51 Wakasugi M, Kawashima A, Morioka H, Linn S, Sancar A, Mori T *et al.* DDB accumulates at DNA damage sites immediately after UV irradiation and directly stimulates nucleotide excision repair. *J Biol Chem* 2002; 277: 1637-1640.
- 52 Sugasawa K, Okuda Y, Saijo M, Nishi R, Matsuda N, Chu G *et al.* UV-induced ubiquitylation of XPC protein mediated by UV-DDB-ubiquitin ligase complex. *Cell* 2005; 121: 387-400.
- 53 Kapetanaki MG, Guerrero-Santoro J, Bisi DC, Hsieh CL, Ropic-Otrin V, Levine AS. The DDB1-CUL4ADDB2 ubiquitin ligase is deficient in xeroderma pigmentosum group E and targets histone H2A at UV-damaged DNA sites. *Proc Natl Acad Sci U S A* 2006; 103: 2588-2593.
- 54 Wang H, Zhai L, Xu J, Joo HY, Jackson S, Erdjument-Bromage H *et al.* Histone H3 and H4 ubiquitylation by the CUL4-DDB-ROC1 ubiquitin ligase facilitates cellular response to DNA damage. *Mol Cell* 2006; 22: 383-394.
- 55 Tang JY, Hwang BJ, Ford JM, Hanawalt PC, Chu G. Xeroderma pigmentosum p48 gene enhances global genomic repair and suppresses UV-induced mutagenesis. *Mol Cell* 2000; 5: 737-744.
- 56 Fitch ME, Nakajima S, Yasui A, Ford JM. In vivo recruitment of XPC to UV-induced cyclobutane pyrimidine dimers by the DDB2 gene product. *J Biol Chem* 2003; 278: 46906-46910.
- 57 Coin F, Oksenysh V, Mocquet V, Groh S, Blattner C, Egly JM. Nucleotide excision repair driven by the dissociation of CAK from TFIIH. *Mol Cell* 2008; 31: 9-20.
- 58 Missura M, Buterin T, Hindges R, Hubscher U, Kasparikova J, Brabec V *et al.* Double-check probing of DNA bending and unwinding by XPA-RPA: an architectural function in DNA repair. *EMBO J* 2001; 20: 3554-3564.
- 59 O'Donovan A, Davies AA, Moggs JG, West SC, Wood RD. XPG endonuclease makes the 3' incision in human DNA nucleotide excision repair. *Nature* 1994; 371: 432-435.
- 60 Sijbers AM, de Laat WL, Ariza RR, Biggerstaff M, Wei YF, Moggs JG *et al.* Xeroderma pigmentosum group F caused by a defect in a structure-specific DNA repair endonuclease. *Cell* 1996; 86: 811-822.
- 61 Shivji MK, Podust VN, Hubscher U, Wood RD. Nucleotide excision repair DNA synthesis by DNA polymerase epsilon in the presence of PCNA, RFC, and RPA. *Biochemistry* 1995; 34: 5011-5017.

- 62 Ogi T, Limsirichaikul S, Overmeer RM, Volker M, Takenaka K, Cloney R *et al.* Three DNA polymerases, recruited by different mechanisms, carry out NER repair synthesis in human cells. *Mol Cell* 2010; 37: 714-727.
- 63 Araujo SJ, Tirode F, Coin F, Pospiech H, Syvaioja JE, Stucki M *et al.* Nucleotide excision repair of DNA with recombinant human proteins: definition of the minimal set of factors, active forms of TFIIH, and modulation by CAK. *Genes Dev* 2000; 14: 349-359.
- 64 Lord CJ, Tutt AN, Ashworth A. Synthetic lethality and cancer therapy: lessons learned from the development of PARP inhibitors. *Annu Rev Med* 2015; 66: 455-470.
- 65 Takata M, Sasaki MS, Sonoda E, Morrison C, Hashimoto M, Utsumi H *et al.* Homologous recombination and non-homologous end-joining pathways of DNA double-strand break repair have overlapping roles in the maintenance of chromosomal integrity in vertebrate cells. *EMBO J* 1998; 17: 5497-5508.
- 66 Shao Z, Davis AJ, Fattah KR, So S, Sun J, Lee KJ *et al.* Persistently bound Ku at DNA ends attenuates DNA end resection and homologous recombination. *DNA Repair (Amst)* 2012; 11: 310-316.
- 67 Sartori AA, Lukas C, Coates J, Mistrik M, Fu S, Bartek J *et al.* Human CtIP promotes DNA end resection. *Nature* 2007; 450: 509-514.
- 68 Budd ME, Campbell JL. Interplay of Mre11 nuclease with Dna2 plus Sgs1 in Rad51-dependent recombinational repair. *PLoS One* 2009; 4: e4267.
- 69 Gravel S, Chapman JR, Magill C, Jackson SP. DNA helicases Sgs1 and BLM promote DNA double-strand break resection. *Genes Dev* 2008; 22: 2767-2772.
- 70 Prakash R, Zhang Y, Feng W, Jasin M. Homologous recombination and human health: the roles of BRCA1, BRCA2, and associated proteins. *Cold Spring Harb Perspect Biol* 2015; 7: a016600.
- 71 Dubois JC, Yates M, Gaudreau-Lapierre A, Clement G, Cappadocia L, Gaudreau L *et al.* A phosphorylation-and-ubiquitylation circuitry driving ATR activation and homologous recombination. *Nucleic Acids Res* 2017; 45: 8859-8872.
- 72 Li L, Germain DR, Poon HY, Hildebrandt MR, Monckton EA, McDonald D *et al.* DEAD Box 1 Facilitates Removal of RNA and Homologous Recombination at DNA Double-Strand Breaks. *Mol Cell Biol* 2016; 36: 2794-2810.
- 73 Scully R, Panday A, Elango R, Willis NA. DNA double-strand break repair-pathway choice in somatic mammalian cells. *Nat Rev Mol Cell Biol* 2019; 20: 698-714.

- 74 May WA, Lessnick SL, Braun BS, Klemsz M, Lewis BC, Lunsford LB *et al.* The Ewing's sarcoma EWS/FLI-1 fusion gene encodes a more potent transcriptional activator and is a more powerful transforming gene than FLI-1. *Mol Cell Biol* 1993; 13: 7393-7398.
- 75 Ren R. Mechanisms of BCR-ABL in the pathogenesis of chronic myelogenous leukaemia. *Nat Rev Cancer* 2005; 5: 172-183.
- 76 Gorodetska I, Kozeretska I, Dubrovskaya A. BRCA Genes: The Role in Genome Stability, Cancer Stemness and Therapy Resistance. *J Cancer* 2019; 10: 2109-2127.
- 77 Zeman MK, Cimprich KA. Causes and consequences of replication stress. *Nat Cell Biol* 2014; 16: 2-9.
- 78 Moon JJ, Lu A, Moon C. Role of genomic instability in human carcinogenesis. *Exp Biol Med (Maywood)* 2019; 244: 227-240.
- 79 Gan W, Guan Z, Liu J, Gui T, Shen K, Manley JL *et al.* R-loop-mediated genomic instability is caused by impairment of replication fork progression. *Genes Dev* 2011; 25: 2041-2056.
- 80 Deb G, Singh AK, Gupta S. EZH2: not EZHY (easy) to deal. *Mol Cancer Res* 2014; 12: 639-653.
- 81 Margueron R, Justin N, Ohno K, Sharpe ML, Son J, Drury WJ, 3rd *et al.* Role of the polycomb protein EED in the propagation of repressive histone marks. *Nature* 2009; 461: 762-767.
- 82 Cao R, Zhang Y. SUZ12 is required for both the histone methyltransferase activity and the silencing function of the EED-EZH2 complex. *Mol Cell* 2004; 15: 57-67.
- 83 Shi Y, Wang XX, Zhuang YW, Jiang Y, Melcher K, Xu HE. Structure of the PRC2 complex and application to drug discovery. *Acta Pharmacol Sin* 2017; 38: 963-976.
- 84 Jacobs SA, Harp JM, Devarakonda S, Kim Y, Rastinejad F, Khorasanizadeh S. The active site of the SET domain is constructed on a knot. *Nat Struct Biol* 2002; 9: 833-838.
- 85 Kuzmichev A, Nishioka K, Erdjument-Bromage H, Tempst P, Reinberg D. Histone methyltransferase activity associated with a human multiprotein complex containing the Enhancer of Zeste protein. *Genes Dev* 2002; 16: 2893-2905.

- 86 Tan JZ, Yan Y, Wang XX, Jiang Y, Xu HE. EZH2: biology, disease, and structure-based drug discovery. *Acta Pharmacol Sin* 2014; 35: 161-174.
- 87 Wan L, Xu K, Wei Y, Zhang J, Han T, Fry C *et al.* Phosphorylation of EZH2 by AMPK Suppresses PRC2 Methyltransferase Activity and Oncogenic Function. *Mol Cell* 2018; 69: 279-291 e275.
- 88 Pinter SF, Sadreyev RI, Yildirim E, Jeon Y, Ohsumi TK, Borowsky M *et al.* Spreading of X chromosome inactivation via a hierarchy of defined Polycomb stations. *Genome Res* 2012; 22: 1864-1876.
- 89 Lee TI, Jenner RG, Boyer LA, Guenther MG, Levine SS, Kumar RM *et al.* Control of developmental regulators by Polycomb in human embryonic stem cells. *Cell* 2006; 125: 301-313.
- 90 Wang L, Jin Q, Lee JE, Su IH, Ge K. Histone H3K27 methyltransferase Ezh2 represses Wnt genes to facilitate adipogenesis. *Proc Natl Acad Sci U S A* 2010; 107: 7317-7322.
- 91 Kim KH, Roberts CW. Targeting EZH2 in cancer. *Nat Med* 2016; 22: 128-134.
- 92 Kim E, Kim M, Woo DH, Shin Y, Shin J, Chang N *et al.* Phosphorylation of EZH2 activates STAT3 signaling via STAT3 methylation and promotes tumorigenicity of glioblastoma stem-like cells. *Cancer Cell* 2013; 23: 839-852.
- 93 Xu K, Wu ZJ, Groner AC, He HH, Cai C, Lis RT *et al.* EZH2 oncogenic activity in castration-resistant prostate cancer cells is Polycomb-independent. *Science* 2012; 338: 1465-1469.
- 94 Gonzalez ME, Moore HM, Li X, Toy KA, Huang W, Sabel MS *et al.* EZH2 expands breast stem cells through activation of NOTCH1 signaling. *Proc Natl Acad Sci U S A* 2014; 111: 3098-3103.
- 95 Bracken AP, Pasini D, Capra M, Prosperini E, Colli E, Helin K. EZH2 is downstream of the pRB-E2F pathway, essential for proliferation and amplified in cancer. *EMBO J* 2003; 22: 5323-5335.
- 96 Morin RD, Johnson NA, Severson TM, Mungall AJ, An J, Goya R *et al.* Somatic mutations altering EZH2 (Tyr641) in follicular and diffuse large B-cell lymphomas of germinal-center origin. *Nat Genet* 2010; 42: 181-185.
- 97 Kleer CG, Cao Q, Varambally S, Shen R, Ota I, Tomlins SA *et al.* EZH2 is a marker of aggressive breast cancer and promotes neoplastic transformation of breast epithelial cells. *Proc Natl Acad Sci U S A* 2003; 100: 11606-11611.

- 98 Varambally S, Dhanasekaran SM, Zhou M, Barrette TR, Kumar-Sinha C, Sanda MG *et al.* The polycomb group protein EZH2 is involved in progression of prostate cancer. *Nature* 2002; 419: 624-629.
- 99 Bachmann IM, Halvorsen OJ, Collett K, Stefansson IM, Straume O, Haukaas SA *et al.* EZH2 expression is associated with high proliferation rate and aggressive tumor subgroups in cutaneous melanoma and cancers of the endometrium, prostate, and breast. *J Clin Oncol* 2006; 24: 268-273.
- 100 Gan L, Xu M, Hua R, Tan C, Zhang J, Gong Y *et al.* The polycomb group protein EZH2 induces epithelial-mesenchymal transition and pluripotent phenotype of gastric cancer cells by binding to PTEN promoter. *J Hematol Oncol* 2018; 11: 9.
- 101 Yamagishi M, Nakano K, Miyake A, Yamochi T, Kagami Y, Tsutsumi A *et al.* Polycomb-mediated loss of miR-31 activates NIK-dependent NF-kappaB pathway in adult T cell leukemia and other cancers. *Cancer Cell* 2012; 21: 121-135.
- 102 O'Hagan HM, Mohammad HP, Baylin SB. Double strand breaks can initiate gene silencing and SIRT1-dependent onset of DNA methylation in an exogenous promoter CpG island. *PLoS Genet* 2008; 4: e1000155.
- 103 Yang Q, Nair S, Laknaur A, Ismail N, Diamond MP, Al-Hendy A. The Polycomb Group Protein EZH2 Impairs DNA Damage Repair Gene Expression in Human Uterine Fibroids. *Biol Reprod* 2016; 94: 69.
- 104 Zeidler M, Varambally S, Cao Q, Chinnaiyan AM, Ferguson DO, Merajver SD *et al.* The Polycomb group protein EZH2 impairs DNA repair in breast epithelial cells. *Neoplasia* 2005; 7: 1011-1019.
- 105 Gonzalez ME, DuPrie ML, Krueger H, Merajver SD, Ventura AC, Toy KA *et al.* Histone methyltransferase EZH2 induces Akt-dependent genomic instability and BRCA1 inhibition in breast cancer. *Cancer Res* 2011; 71: 2360-2370.
- 106 Rondinelli B, Gogola E, Yucel H, Duarte AA, van de Ven M, van der Sluijs R *et al.* EZH2 promotes degradation of stalled replication forks by recruiting MUS81 through histone H3 trimethylation. *Nat Cell Biol* 2017; 19: 1371-1378.
- 107 Wu Z, Lee ST, Qiao Y, Li Z, Lee PL, Lee YJ *et al.* Polycomb protein EZH2 regulates cancer cell fate decision in response to DNA damage. *Cell Death Differ* 2011; 18: 1771-1779.
- 108 Gardner EE, Lok BH, Schneeberger VE, Desmeules P, Miles LA, Arnold PK *et al.* Chemosensitive Relapse in Small Cell Lung Cancer Proceeds through an EZH2-SLFN11 Axis. *Cancer Cell* 2017; 31: 286-299.

- 109 Yamaguchi H, Du Y, Nakai K, Ding M, Chang SS, Hsu JL *et al.* EZH2 contributes to the response to PARP inhibitors through its PARP-mediated poly-ADP ribosylation in breast cancer. *Oncogene* 2018; 37: 208-217.
- 110 Xia H, Yu CH, Zhang Y, Yu J, Li J, Zhang W *et al.* EZH2 silencing with RNAi enhances irradiation-induced inhibition of human lung cancer growth in vitro and in vivo. *Oncol Lett* 2012; 4: 135-140.
- 111 Xu L, Tang H, Wang K, Zheng Y, Feng J, Dong H *et al.* Pharmacological inhibition of EZH2 combined with DNAdamaging agents interferes with the DNA damage response in MM cells. *Mol Med Rep* 2019; 19: 4249-4255.
- 112 Bleichert F, Baserga SJ. The long unwinding road of RNA helicases. *Mol Cell* 2007; 27: 339-352.
- 113 Ohle C, Tesorero R, Schermann G, Dobrev N, Sinning I, Fischer T. Transient RNA-DNA Hybrids Are Required for Efficient Double-Strand Break Repair. *Cell* 2016; 167: 1001-1013 e1007.
- 114 Britton S, Dernoncourt E, Delteil C, Froment C, Schiltz O, Salles B *et al.* DNA damage triggers SAF-A and RNA biogenesis factors exclusion from chromatin coupled to R-loops removal. *Nucleic Acids Res* 2014; 42: 9047-9062.
- 115 Cohen S, Puget N, Lin YL, Clouaire T, Aguirrebengoa M, Rocher V *et al.* Senataxin resolves RNA:DNA hybrids forming at DNA double-strand breaks to prevent translocations. *Nat Commun* 2018; 9: 533.
- 116 Hasgall PA, Hoogewijs D, Faza MB, Panse VG, Wenger RH, Camenisch G. The putative RNA helicase HELZ promotes cell proliferation, translation initiation and ribosomal protein S6 phosphorylation. *PLoS One* 2011; 6: e22107.
- 117 Hanet A, Rasch F, Weber R, Ruscica V, Fauser M, Raisch T *et al.* HELZ directly interacts with CCR4-NOT and causes decay of bound mRNAs. *Life Sci Alliance* 2019; 2.
- 118 Nagai H, Yabe A, Mine N, Mikami I, Fujiwara H, Terada Y *et al.* Down-regulation in human cancers of DRHC, a novel helicase-like gene from 17q25.1 that inhibits cell growth. *Cancer Lett* 2003; 193: 41-47.
- 119 SEER Program (National Cancer Institute (U.S.)), National Center for Health Statistics (U.S.), National Cancer Institute (U.S.). Surveillance Program., National Cancer Institute (U.S.). Cancer Statistics Branch., National Cancer Institute (U.S.). Cancer Control Research Program. SEER cancer statistics review. *NIH publication*. U.S. Dept. of Health and Human Services, Public Health Service, National Institutes of Health, National Cancer Institute: Bethesda, Md., 1993, p volumes.

- 120 Chute JP, Chen T, Feigal E, Simon R, Johnson BE. Twenty years of phase III trials for patients with extensive-stage small-cell lung cancer: perceptible progress. *J Clin Oncol* 1999; 17: 1794-1801.
- 121 Horita N, Yamamoto M, Sato T, Tsukahara T, Nagakura H, Tashiro K *et al.* Topotecan for Relapsed Small-cell Lung Cancer: Systematic Review and Meta-Analysis of 1347 Patients. *Sci Rep* 2015; 5: 15437.
- 122 Keeney S, Chang GJ, Linn S. Characterization of a human DNA damage binding protein implicated in xeroderma pigmentosum E. *J Biol Chem* 1993; 268: 21293-21300.
- 123 Chen X, Zhang Y, Douglas L, Zhou P. UV-damaged DNA-binding proteins are targets of CUL-4A-mediated ubiquitination and degradation. *J Biol Chem* 2001; 276: 48175-48182.
- 124 Fischer ES, Scrima A, Bohm K, Matsumoto S, Lingaraju GM, Faty M *et al.* The molecular basis of CRL4DDB2/CSA ubiquitin ligase architecture, targeting, and activation. *Cell* 2011; 147: 1024-1039.
- 125 Puppe J, Opdam M, Schouten PC, Jozwiak K, Lips E, Severson T *et al.* EZH2 Is Overexpressed in BRCA1-like Breast Tumors and Predictive for Sensitivity to High-Dose Platinum-Based Chemotherapy. *Clin Cancer Res* 2019; 25: 4351-4362.
- 126 Byers LA, Wang J, Nilsson MB, Fujimoto J, Saintigny P, Yordy J *et al.* Proteomic profiling identifies dysregulated pathways in small cell lung cancer and novel therapeutic targets including PARP1. *Cancer Discov* 2012; 2: 798-811.
- 127 Sato T, Kaneda A, Tsuji S, Isagawa T, Yamamoto S, Fujita T *et al.* PRC2 overexpression and PRC2-target gene repression relating to poorer prognosis in small cell lung cancer. *Sci Rep* 2013; 3: 1911.
- 128 Nienstedt JC, Schroeder C, Clauditz T, Simon R, Sauter G, Muenscher A *et al.* EZH2 overexpression in head and neck cancer is related to lymph node metastasis. *J Oral Pathol Med* 2018; 47: 240-245.
- 129 Coe BP, Thu KL, Aviel-Ronen S, Vucic EA, Gazdar AF, Lam S *et al.* Genomic deregulation of the E2F/Rb pathway leads to activation of the oncogene EZH2 in small cell lung cancer. *PLoS One* 2013; 8: e71670.
- 130 Hubaux R, Thu KL, Coe BP, MacAulay C, Lam S, Lam WL. EZH2 promotes E2F-driven SCLC tumorigenesis through modulation of apoptosis and cell-cycle regulation. *J Thorac Oncol* 2013; 8: 1102-1106.

- 131 Xie H, Peng C, Huang J, Li BE, Kim W, Smith EC *et al.* Chronic Myelogenous Leukemia- Initiating Cells Require Polycomb Group Protein EZH2. *Cancer Discov* 2016; 6: 1237-1247.
- 132 Li H, Cai Q, Godwin AK, Zhang R. Enhancer of zeste homolog 2 promotes the proliferation and invasion of epithelial ovarian cancer cells. *Mol Cancer Res* 2010; 8: 1610-1618.
- 133 Rao ZY, Cai MY, Yang GF, He LR, Mai SJ, Hua WF *et al.* EZH2 supports ovarian carcinoma cell invasion and/or metastasis via regulation of TGF-beta1 and is a predictor of outcome in ovarian carcinoma patients. *Carcinogenesis* 2010; 31: 1576-1583.
- 134 Murai F, Koinuma D, Shinozaki-Ushiku A, Fukayama M, Miyaozono K, Ehata S. EZH2 promotes progression of small cell lung cancer by suppressing the TGF-beta-Smad-ASCL1 pathway. *Cell Discov* 2015; 1: 15026.
- 135 Jiang FZ, He YY, Wang HH, Zhang HL, Zhang J, Yan XF *et al.* Mutant p53 induces EZH2 expression and promotes epithelial-mesenchymal transition by disrupting p68-Drosha complex assembly and attenuating miR-26a processing. *Oncotarget* 2015; 6: 44660-44674.
- 136 Knutson SK, Kawano S, Minoshima Y, Warholic NM, Huang KC, Xiao Y *et al.* Selective inhibition of EZH2 by EPZ-6438 leads to potent antitumor activity in EZH2-mutant non-Hodgkin lymphoma. *Mol Cancer Ther* 2014; 13: 842-854.
- 137 Miranda TB, Cortez CC, Yoo CB, Liang G, Abe M, Kelly TK *et al.* DZNep is a global histone methylation inhibitor that reactivates developmental genes not silenced by DNA methylation. *Mol Cancer Ther* 2009; 8: 1579-1588.
- 138 Chen YT, Zhu F, Lin WR, Ying RB, Yang YP, Zeng LH. The novel EZH2 inhibitor, GSK126, suppresses cell migration and angiogenesis via down-regulating VEGF-A. *Cancer Chemother Pharmacol* 2016; 77: 757-765.
- 139 Qi W, Chan H, Teng L, Li L, Chuai S, Zhang R *et al.* Selective inhibition of Ezh2 by a small molecule inhibitor blocks tumor cells proliferation. *Proc Natl Acad Sci U S A* 2012; 109: 21360-21365.
- 140 McCabe MT, Ott HM, Ganji G, Korenchuk S, Thompson C, Van Aller GS *et al.* EZH2 inhibition as a therapeutic strategy for lymphoma with EZH2-activating mutations. *Nature* 2012; 492: 108-112.
- 141 Vaswani RG, Gehling VS, Dakin LA, Cook AS, Nasveschuk CG, Duplessis M *et al.* Identification of (R)-N-((4-Methoxy-6-methyl-2-oxo-1,2-dihydropyridin-3-yl)methyl)-2-methyl-1-(1-(1-(2,2,2-trifluoroethyl)piperidin-4-yl)ethyl)-1H-indole-3-carboxamide (CPI-1205), a Potent and Selective Inhibitor of Histone

- Methyltransferase EZH2, Suitable for Phase I Clinical Trials for B-Cell Lymphomas. *J Med Chem* 2016; 59: 9928-9941.
- 142 He A, Shen X, Ma Q, Cao J, von Gise A, Zhou P *et al.* PRC2 directly methylates GATA4 and represses its transcriptional activity. *Genes Dev* 2012; 26: 37-42.
- 143 Sanulli S, Justin N, Teissandier A, Ancelin K, Portoso M, Caron M *et al.* Jarid2 Methylation via the PRC2 Complex Regulates H3K27me3 Deposition during Cell Differentiation. *Mol Cell* 2015; 57: 769-783.
- 144 Vasanthakumar A, Xu D, Lun AT, Kueh AJ, van Gisbergen KP, Iannarella N *et al.* A non-canonical function of Ezh2 preserves immune homeostasis. *EMBO Rep* 2017; 18: 619-631.
- 145 Yan J, Li B, Lin B, Lee PT, Chung TH, Tan J *et al.* EZH2 phosphorylation by JAK3 mediates a switch to noncanonical function in natural killer/T-cell lymphoma. *Blood* 2016; 128: 948-958.
- 146 Kim J, Lee Y, Lu X, Song B, Fong KW, Cao Q *et al.* Polycomb- and Methylation-Independent Roles of EZH2 as a Transcription Activator. *Cell Rep* 2018; 25: 2808-2820 e2804.
- 147 Lee JM, Lee JS, Kim H, Kim K, Park H, Kim JY *et al.* EZH2 generates a methyl degron that is recognized by the DCAF1/DDB1/CUL4 E3 ubiquitin ligase complex. *Mol Cell* 2012; 48: 572-586.
- 148 Hu S, Yu L, Li Z, Shen Y, Wang J, Cai J *et al.* Overexpression of EZH2 contributes to acquired cisplatin resistance in ovarian cancer cells in vitro and in vivo. *Cancer Biol Ther* 2010; 10: 788-795.
- 149 Sun S, Zhao S, Yang Q, Wang W, Cai E, Wen Y *et al.* Enhancer of zeste homolog 2 promotes cisplatin resistance by reducing cellular platinum accumulation. *Cancer Sci* 2018; 109: 1853-1864.
- 150 Chang JW, Gwak SY, Shim GA, Liu L, Lim YC, Kim JM *et al.* EZH2 is associated with poor prognosis in head-and-neck squamous cell carcinoma via regulating the epithelial-to-mesenchymal transition and chemosensitivity. *Oral Oncol* 2016; 52: 66-74.
- 151 Liu H, Li W, Yu X, Gao F, Duan Z, Ma X *et al.* EZH2-mediated Puma gene repression regulates non-small cell lung cancer cell proliferation and cisplatin-induced apoptosis. *Oncotarget* 2016; 7: 56338-56354.
- 152 Campbell S, Ismail IH, Young LC, Poirier GG, Hendzel MJ. Polycomb repressive complex 2 contributes to DNA double-strand break repair. *Cell Cycle* 2013; 12: 2675-2683.

- 153 Chou DM, Adamson B, Dephore NE, Tan X, Nottke AC, Hurov KE *et al.* A chromatin localization screen reveals poly (ADP ribose)-regulated recruitment of the repressive polycomb and NuRD complexes to sites of DNA damage. *Proc Natl Acad Sci U S A* 2010; 107: 18475-18480.
- 154 Owonikoko TK, Zhang G, Deng X, Rossi MR, Switchenko JM, Doho GH *et al.* Poly (ADP) ribose polymerase enzyme inhibitor, veliparib, potentiates chemotherapy and radiation in vitro and in vivo in small cell lung cancer. *Cancer Med* 2014; 3: 1579-1594.
- 155 Yap DB, Chu J, Berg T, Schapira M, Cheng SW, Moradian A *et al.* Somatic mutations at EZH2 Y641 act dominantly through a mechanism of selectively altered PRC2 catalytic activity, to increase H3K27 trimethylation. *Blood* 2011; 117: 2451-2459.
- 156 Head PE, Zhang H, Bastien AJ, Koyen AE, Withers AE, Daddacha WB *et al.* Sirtuin 2 mutations in human cancers impair its function in genome maintenance. *J Biol Chem* 2017; 292: 9919-9931.
- 157 Shannon P, Markiel A, Ozier O, Baliga NS, Wang JT, Ramage D *et al.* Cytoscape: a software environment for integrated models of biomolecular interaction networks. *Genome Res* 2003; 13: 2498-2504.
- 158 Wu G, Dawson E, Duong A, Haw R, Stein L. ReactomeFIViz: a Cytoscape app for pathway and network-based data analysis. *F1000Res* 2014; 3: 146.
- 159 Bindea G, Mlecnik B, Hackl H, Charoentong P, Tosolini M, Kirilovsky A *et al.* ClueGO: a Cytoscape plug-in to decipher functionally grouped gene ontology and pathway annotation networks. *Bioinformatics* 2009; 25: 1091-1093.
- 160 Zhang H, Head PE, Daddacha W, Park SH, Li X, Pan Y *et al.* ATRIP Deacetylation by SIRT2 Drives ATR Checkpoint Activation by Promoting Binding to RPA-ssDNA. *Cell Rep* 2016; 14: 1435-1447.
- 161 Zhang H, Park SH, Pantazides BG, Karpiuk O, Warren MD, Hardy CW *et al.* SIRT2 directs the replication stress response through CDK9 deacetylation. *Proc Natl Acad Sci U S A* 2013; 110: 13546-13551.
- 162 Daddacha W, Koyen AE, Bastien AJ, Head PE, Dhere VR, Nabeta GN *et al.* SAMHD1 Promotes DNA End Resection to Facilitate DNA Repair by Homologous Recombination. *Cell Rep* 2017; 20: 1921-1935.
- 163 Guerrero-Santoro J, Kapetanaki MG, Hsieh CL, Gorbachinsky I, Levine AS, Raptic-Otrin V. The cullin 4B-based UV-damaged DNA-binding protein ligase

- binds to UV-damaged chromatin and ubiquitinates histone H2A. *Cancer Res* 2008; 68: 5014-5022.
- 164 Nagel ZD, Margulies CM, Chaim IA, McRee SK, Mazzucato P, Ahmad A *et al.* Multiplexed DNA repair assays for multiple lesions and multiple doses via transcription inhibition and transcriptional mutagenesis. *Proc Natl Acad Sci U S A* 2014; 111: E1823-1832.
- 165 Perez-Riverol Y, Csordas A, Bai J, Bernal-Llinares M, Hewapathirana S, Kundu DJ *et al.* The PRIDE database and related tools and resources in 2019: improving support for quantification data. *Nucleic Acids Res* 2019; 47: D442-D450.
- 166 Smith SC, Petrova AV, Madden MZ, Wang H, Pan Y, Warren MD *et al.* A gemcitabine sensitivity screen identifies a role for NEK9 in the replication stress response. *Nucleic Acids Res* 2014; 42: 11517-11527.
- 167 Colbert LE, Petrova AV, Fisher SB, Pantazides BG, Madden MZ, Hardy CW *et al.* CHD7 expression predicts survival outcomes in patients with resected pancreatic cancer. *Cancer Res* 2014; 74: 2677-2687.
- 168 Bhattacharjee A, Richards WG, Staunton J, Li C, Monti S, Vasa P *et al.* Classification of human lung carcinomas by mRNA expression profiling reveals distinct adenocarcinoma subclasses. *Proc Natl Acad Sci U S A* 2001; 98: 13790-13795.
- 169 Garber ME, Troyanskaya OG, Schluens K, Petersen S, Thaesler Z, Pacyna-Gengelbach M *et al.* Diversity of gene expression in adenocarcinoma of the lung. *Proc Natl Acad Sci U S A* 2001; 98: 13784-13789.
- 170 Fei J, Kaczmarek N, Luch A, Glas A, Carell T, Naegeli H. Regulation of nucleotide excision repair by UV-DDB: prioritization of damage recognition to internucleosomal DNA. *PLoS Biol* 2011; 9: e1001183.
- 171 Stoyanova T, Roy N, Kopanja D, Bagchi S, Raychaudhuri P. DDB2 decides cell fate following DNA damage. *Proc Natl Acad Sci U S A* 2009; 106: 10690-10695.
- 172 Stoyanova T, Yoon T, Kopanja D, Mokyr MB, Raychaudhuri P. The xeroderma pigmentosum group E gene product DDB2 activates nucleotide excision repair by regulating the level of p21Waf1/Cip1. *Mol Cell Biol* 2008; 28: 177-187.
- 173 Crea F, Hurt EM, Mathews LA, Cabarcas SM, Sun L, Marquez VE *et al.* Pharmacologic disruption of Polycomb Repressive Complex 2 inhibits tumorigenicity and tumor progression in prostate cancer. *Mol Cancer* 2011; 10: 40.

- 174 Li Z, Wang Y, Qiu J, Li Q, Yuan C, Zhang W *et al.* The polycomb group protein EZH2 is a novel therapeutic target in tongue cancer. *Oncotarget* 2013; 4: 2532-2549.
- 175 Matsumoto S, Fischer ES, Yasuda T, Dohmae N, Iwai S, Mori T *et al.* Functional regulation of the DNA damage-recognition factor DDB2 by ubiquitination and interaction with xeroderma pigmentosum group C protein. *Nucleic Acids Res* 2015; 43: 1700-1713.
- 176 Huang Y, Wang X, Niu X, Wang X, Jiang R, Xu T *et al.* EZH2 suppresses the nucleotide excision repair in nasopharyngeal carcinoma by silencing XPA gene. *Mol Carcinog* 2017; 56: 447-463.
- 177 Barckhausen C, Roos WP, Naumann SC, Kaina B. Malignant melanoma cells acquire resistance to DNA interstrand cross-linking chemotherapeutics by p53-triggered upregulation of DDB2/XPC-mediated DNA repair. *Oncogene* 2014; 33: 1964-1974.
- 178 Barakat BM, Wang QE, Han C, Milum K, Yin DT, Zhao Q *et al.* Overexpression of DDB2 enhances the sensitivity of human ovarian cancer cells to cisplatin by augmenting cellular apoptosis. *Int J Cancer* 2010; 127: 977-988.
- 179 El-Mahdy MA, Zhu Q, Wang QE, Wani G, Praetorius-Ibba M, Wani AA. Cullin 4A-mediated proteolysis of DDB2 protein at DNA damage sites regulates in vivo lesion recognition by XPC. *J Biol Chem* 2006; 281: 13404-13411.
- 180 Zhao R, Cui T, Han C, Zhang X, He J, Srivastava AK *et al.* DDB2 modulates TGF-beta signal transduction in human ovarian cancer cells by downregulating NEDD4L. *Nucleic Acids Res* 2015; 43: 7838-7849.
- 181 Huang S, Fantini D, Merrill BJ, Bagchi S, Guzman G, Raychaudhuri P. DDB2 Is a Novel Regulator of Wnt Signaling in Colon Cancer. *Cancer Res* 2017; 77: 6562-6575.
- 182 Takedachi A, Saijo M, Tanaka K. DDB2 complex-mediated ubiquitylation around DNA damage is oppositely regulated by XPC and Ku and contributes to the recruitment of XPA. *Mol Cell Biol* 2010; 30: 2708-2723.
- 183 Zhang L, Lubin A, Chen H, Sun Z, Gong F. The deubiquitinating protein USP24 interacts with DDB2 and regulates DDB2 stability. *Cell Cycle* 2012; 11: 4378-4384.
- 184 Pines A, Vrouwe MG, Marteijn JA, Typas D, Luijsterburg MS, Cansoy M *et al.* PARP1 promotes nucleotide excision repair through DDB2 stabilization and recruitment of ALC1. *J Cell Biol* 2012; 199: 235-249.

- 185 Groisman R, Polanowska J, Kuraoka I, Sawada J, Saijo M, Drapkin R *et al.* The ubiquitin ligase activity in the DDB2 and CSA complexes is differentially regulated by the COP9 signalosome in response to DNA damage. *Cell* 2003; 113: 357-367.
- 186 Lei A, Chen L, Zhang M, Yang X, Xu L, Cao N *et al.* EZH2 Regulates Protein Stability via Recruiting USP7 to Mediate Neuronal Gene Expression in Cancer Cells. *Front Genet* 2019; 10: 422.
- 187 Jansson M, Durant ST, Cho EC, Sheahan S, Edelmann M, Kessler B *et al.* Arginine methylation regulates the p53 response. *Nat Cell Biol* 2008; 10: 1431-1439.
- 188 Byrski T, Gronwald J, Huzarski T, Grzybowska E, Budryk M, Stawicka M *et al.* Response to neo-adjuvant chemotherapy in women with BRCA1-positive breast cancers. *Breast Cancer Res Treat* 2008; 108: 289-296.
- 189 Byrski T, Huzarski T, Dent R, Marczyk E, Jasiowka M, Gronwald J *et al.* Pathologic complete response to neoadjuvant cisplatin in BRCA1-positive breast cancer patients. *Breast Cancer Res Treat* 2014; 147: 401-405.
- 190 Stefansson OA, Villanueva A, Vidal A, Marti L, Esteller M. BRCA1 epigenetic inactivation predicts sensitivity to platinum-based chemotherapy in breast and ovarian cancer. *Epigenetics* 2012; 7: 1225-1229.
- 191 Ceccaldi R, Liu JC, Amunugama R, Hajdu I, Primack B, Petalcorin MI *et al.* Homologous-recombination-deficient tumours are dependent on Poltheta-mediated repair. *Nature* 2015; 518: 258-262.
- 192 Wang QE, Praetorius-Ibba M, Zhu Q, El-Mahdy MA, Wani G, Zhao Q *et al.* Ubiquitylation-independent degradation of Xeroderma pigmentosum group C protein is required for efficient nucleotide excision repair. *Nucleic Acids Res* 2007; 35: 5338-5350.
- 193 Hamperl S, Cimprich KA. The contribution of co-transcriptional RNA:DNA hybrid structures to DNA damage and genome instability. *DNA Repair (Amst)* 2014; 19: 84-94.
- 194 Ponten F, Jirstrom K, Uhlen M. The Human Protein Atlas--a tool for pathology. *J Pathol* 2008; 216: 387-393.
- 195 Liu WM, Oakley PR, Joel SP. Exposure to low concentrations of etoposide reduces the apoptotic capability of leukaemic cell lines. *Leukemia* 2002; 16: 1705-1712.

- 196 Kolas NK, Chapman JR, Nakada S, Ylanko J, Chahwan R, Sweeney FD *et al.* Orchestration of the DNA-damage response by the RNF8 ubiquitin ligase. *Science* 2007; 318: 1637-1640.
- 197 Kollarovic G, Topping CE, Shaw EP, Chambers AL. The human HELLS chromatin remodelling protein promotes end resection to facilitate homologous recombination and contributes to DSB repair within heterochromatin. *Nucleic Acids Res* 2020; 48: 1872-1885.
- 198 Ray Chaudhuri A, Nussenzweig A. The multifaceted roles of PARP1 in DNA repair and chromatin remodelling. *Nat Rev Mol Cell Biol* 2017; 18: 610-621.
- 199 Patel DS, Misenko SM, Her J, Bunting SF. BLM helicase regulates DNA repair by counteracting RAD51 loading at DNA double-strand break sites. *J Cell Biol* 2017; 216: 3521-3534.
- 200 Ashley AK, Shrivastav M, Nie J, Amerin C, Troksa K, Glanzer JG *et al.* DNA-PK phosphorylation of RPA32 Ser4/Ser8 regulates replication stress checkpoint activation, fork restart, homologous recombination and mitotic catastrophe. *DNA Repair (Amst)* 2014; 21: 131-139.
- 201 Boldt K, van Reeuwijk J, Lu Q, Koutroumpas K, Nguyen TM, Texier Y *et al.* An organelle-specific protein landscape identifies novel diseases and molecular mechanisms. *Nat Commun* 2016; 7: 11491.
- 202 Fuss JO, Tainer JA. XPB and XPD helicases in TFIIH orchestrate DNA duplex opening and damage verification to coordinate repair with transcription and cell cycle via CAK kinase. *DNA Repair (Amst)* 2011; 10: 697-713.
- 203 Saha J, Davis AJ. Unsolved mystery: the role of BRCA1 in DNA end-joining. *J Radiat Res* 2016; 57 Suppl 1: i18-i24.
- 204 Shrivastav M, De Haro LP, Nickoloff JA. Regulation of DNA double-strand break repair pathway choice. *Cell Res* 2008; 18: 134-147.
- 205 Datta A, Brosh RM, Jr. New Insights Into DNA Helicases as Druggable Targets for Cancer Therapy. *Front Mol Biosci* 2018; 5: 59.
- 206 Caruso LB, Martin KA, Lauretto E, Hulse M, Siciliano M, Lupey-Green LN *et al.* Poly(ADP-ribose) Polymerase 1, PARP1, modifies EZH2 and inhibits EZH2 histone methyltransferase activity after DNA damage. *Oncotarget* 2018; 9: 10585-10605.
- 207 Etzion Y, Muslin AJ. The application of phenotypic high-throughput screening techniques to cardiovascular research. *Trends Cardiovasc Med* 2009; 19: 207-212.

- 208 Mayer TU, Kapoor TM, Haggarty SJ, King RW, Schreiber SL, Mitchison TJ. Small molecule inhibitor of mitotic spindle bipolarity identified in a phenotype-based screen. *Science* 1999; 286: 971-974.
- 209 Smogorzewska A, Desetty R, Saito TT, Schlabach M, Lach FP, Sowa ME *et al.* A genetic screen identifies FAN1, a Fanconi anemia-associated nuclease necessary for DNA interstrand crosslink repair. *Mol Cell* 2010; 39: 36-47.
- 210 Matsuoka S, Ballif BA, Smogorzewska A, McDonald ER, 3rd, Hurov KE, Luo J *et al.* ATM and ATR substrate analysis reveals extensive protein networks responsive to DNA damage. *Science* 2007; 316: 1160-1166.
- 211 Dupre A, Boyer-Chatenet L, Sattler RM, Modi AP, Lee JH, Nicolette ML *et al.* A forward chemical genetic screen reveals an inhibitor of the Mre11-Rad50-Nbs1 complex. *Nat Chem Biol* 2008; 4: 119-125.
- 212 Akada M, Crnogorac-Jurcevic T, Lattimore S, Mahon P, Lopes R, Sunamura M *et al.* Intrinsic chemoresistance to gemcitabine is associated with decreased expression of BNIP3 in pancreatic cancer. *Clin Cancer Res* 2005; 11: 3094-3101.
- 213 Cotta-Ramusino C, McDonald ER, 3rd, Hurov K, Sowa ME, Harper JW, Elledge SJ. A DNA damage response screen identifies RHINO, a 9-1-1 and TopBP1 interacting protein required for ATR signaling. *Science* 2011; 332: 1313-1317.
- 214 Adamson B, Smogorzewska A, Sigoillot FD, King RW, Elledge SJ. A genome-wide homologous recombination screen identifies the RNA-binding protein RBMX as a component of the DNA-damage response. *Nat Cell Biol* 2012; 14: 318-328.
- 215 Yamamoto K, Wang Y, Jiang W, Liu X, Dubois RL, Lin CS *et al.* Kinase-dead ATM protein causes genomic instability and early embryonic lethality in mice. *J Cell Biol* 2012; 198: 305-313.
- 216 Jiang W, Crowe JL, Liu X, Nakajima S, Wang Y, Li C *et al.* Differential phosphorylation of DNA-PKcs regulates the interplay between end-processing and end-ligation during nonhomologous end-joining. *Mol Cell* 2015; 58: 172-185.
- 217 Menolfi D, Jiang W, Lee BJ, Moiseeva T, Shao Z, Estes V *et al.* Kinase-dead ATR differs from ATR loss by limiting the dynamic exchange of ATR and RPA. *Nat Commun* 2018; 9: 5351.
- 218 Hoshii T, Cifani P, Feng Z, Huang CH, Koche R, Chen CW *et al.* A Non-catalytic Function of SETD1A Regulates Cyclin K and the DNA Damage Response. *Cell* 2018; 172: 1007-1021 e1017.

- 219 Abbas M, Shanmugam I, Bsaili M, Hromas R, Shaheen M. The role of the human psoralen 4 (hPso4) protein complex in replication stress and homologous recombination. *J Biol Chem* 2014; 289: 14009-14019.
- 220 Marechal A, Li JM, Ji XY, Wu CS, Yazinski SA, Nguyen HD *et al.* PRP19 transforms into a sensor of RPA-ssDNA after DNA damage and drives ATR activation via a ubiquitin-mediated circuitry. *Mol Cell* 2014; 53: 235-246.
- 221 Zhang N, Kaur R, Lu X, Shen X, Li L, Legerski RJ. The Pso4 mRNA splicing and DNA repair complex interacts with WRN for processing of DNA interstrand cross-links. *J Biol Chem* 2005; 280: 40559-40567.
- 222 D'Alessandro G, Whelan DR, Howard SM, Vitelli V, Renaudin X, Adamowicz M *et al.* BRCA2 controls DNA:RNA hybrid level at DSBs by mediating RNase H2 recruitment. *Nat Commun* 2018; 9: 5376.
- 223 Choudhury SR, Balasubramanian S, Chew YC, Han B, Marquez VE, Eckert RL. (-)-Epigallocatechin-3-gallate and DZNep reduce polycomb protein level via a proteasome-dependent mechanism in skin cancer cells. *Carcinogenesis* 2011; 32: 1525-1532.
- 224 Hua WF, Fu YS, Liao YJ, Xia WJ, Chen YC, Zeng YX *et al.* Curcumin induces down-regulation of EZH2 expression through the MAPK pathway in MDA-MB-435 human breast cancer cells. *Eur J Pharmacol* 2010; 637: 16-21.
- 225 Wang Y, Ma J, Chow SC, Li CH, Xiao Z, Feng R *et al.* A potential antitumor ellagitannin, davidiin, inhibited hepatocellular tumor growth by targeting EZH2. *Tumour Biol* 2014; 35: 205-212.
- 226 Morera L, Lubbert M, Jung M. Targeting histone methyltransferases and demethylases in clinical trials for cancer therapy. *Clin Epigenetics* 2016; 8: 57.
- 227 Luo J, Solimini NL, Elledge SJ. Principles of cancer therapy: oncogene and non-oncogene addiction. *Cell* 2009; 136: 823-837.
- 228 Heerma van Voss MR, van Diest PJ, Raman V. Targeting RNA helicases in cancer: The translation trap. *Biochim Biophys Acta Rev Cancer* 2017; 1868: 510-520.